



BNXXXX-v0.0
September 16, 2022

Measurement of inclusive $B \rightarrow \Lambda_c$ branching fractions using Belle data and hadronic Full Event Interpretation

Leonardo Benjamin Rizzuto¹.

¹*Institute Jožef Stefan, Ljubljana, Slovenia*

Abstract

Inclusive $B \rightarrow \Lambda_c$ branching fractions were measured most recently by BaBar collaboration. However, the measurement still presented a poor accuracy. A more precise measurement of inclusive $B \rightarrow \Lambda_c$ branching fraction could be useful to gain a better confidence on B meson weak decays treatment. With help of the Full Event Interpretation algorith, it is possible to perform a more precise measurment of inclusive $B \rightarrow \Lambda_c$ branching fractions using Belle data set.

Contents

1	Introduction	1
1.1	Analysis Setup	1
1.2	Datasets	1
2	Event selection and reconstruction	2
2.1	B_{tag} reconstruction	2
2.2	Λ_c reconstruction	2
2.3	Wrongly reconstructed B_{tag} candidates	3
3	Signal selection optimization	3
4	$B^- \rightarrow \Lambda_c^+$ decays	6
4.1	Probability Density Functions (PDFs) for the two dimensional fit	11
4.2	Two dimensional fit	23
4.3	Probability Density Functions (PDFs) for the B_{tag}	27
4.4	B_{tag} fit	29
4.5	Λ_c and FEI efficiency	30
4.6	Studies of Systematic Effects	31
4.7	Continuum background modeling	31
4.8	Crossfeed background modeling	33
4.9	Crossfeed ratio	33
4.10	Efficiencies	34
4.11	Fit biases	34
4.12	Measured $B^+ \rightarrow \bar{\Lambda}_c^- X$ inclusive Branching Fraction	34
5	$B^- \rightarrow D^0$ control decay	36
5.1	Dataset used	36
5.2	Event selection and reconstruction	36
5.3	Signal selection optimization	36
5.4	Probability Density Functions (PDFs) for two dimensional fit	37
5.5	2D Fit on Monte Carlo simulated data	40
5.6	2D Fit on data	41
5.7	Probability Density Functions (PDFs) for the B_{tag}	43
5.8	B_{tag} Fit on Monte Carlo simulated data	44
5.9	B_{tag} Fit on data	46
5.10	PID efficiency correction	47
5.11	D^0 and FEI efficiency	47
5.12	Measured $B^+ \rightarrow \bar{D}^0 X$ inclusive Branching Fraction	48

6	$B^- \rightarrow \bar{\Lambda}_c^-$ decays	50
6.1	Probability Density Functions (PDFs) for the two dimensional fit	50
6.2	Two dimensional fit	56
6.3	Probability Density Functions (PDFs) for the B_{tag}	60
6.4	B_{tag} fit	62
6.5	Λ_c and FEI efficiency	63
6.6	Studies of Systematic Effects	64
6.7	Continuum background modeling	64
6.8	Crossfeed background modeling	66
6.9	Crossfeed ratio	66
6.10	Efficiencies	67
6.11	Fit biases	67
6.12	Measured $B^+ \rightarrow \Lambda_c^+$ inclusive Branching Fraction	67
Appendix		68
.1	$B^- \rightarrow \Lambda_c^+$ decays: additional plots	68
.2	$B^- \rightarrow D^0$ decays: additional plots	72
.3	$B^- \rightarrow \bar{\Lambda}_c^-$ decays: additional plots	76

¹ 1 Introduction

² Inclusive B meson baryonic decays with a Λ_c baryon in the final state are the most
³ abundant, due to a relatively large V_{cb} element of the CKM matrix. The *BaBar* experiment
⁴ measured their branching fractions to be around the percent level (see ref. [?]). However, the
⁵ branching fractions were determined with big uncertainties: nearly 50% on the measured
⁶ values or, in the case of the $B^0 \rightarrow \Lambda_c^+$ decay, only an upper limit could be established.
⁷ A more precise measurement of inclusive $B \rightarrow \Lambda_c$ branching fractions may shed light on
⁸ the appropriateness of B meson weak decays treatment, particularly of strong interaction
⁹ effects modelling. Predictions for inclusive branching fractions are given, for example, in
¹⁰ ref. [?].

¹¹ Exploiting the Full Event Interpretation (FEI) algorithm, developed for the Belle
¹² II experiment, it may be possible to perform a more precise measurement of inclusive
¹³ $B \rightarrow \Lambda_c$ branching fractions, using the full Belle data set. A more precise measurement
¹⁴ may also trigger further research on currently scarce theory predictions for B meson decays
¹⁵ to charm baryons.

¹⁶ 1.1 Analysis Setup

¹⁷ The reconstruction is performed with BASF2 release 05-02-03 together with the `b2bii`
¹⁸ package in order to convert the *Belle* MDST files (BASF data format) to *Belle II* MDST files
¹⁹ (`BASF2` data format). The FEI version used is `FEI_B2BII_light-2012-minos`.

²⁰ 1.2 Datasets

²¹ The Belle detector acquired a dataset of about $L_0 \approx 710 fb^{-1}$ of integrated luminosity in
²² its lifetime at the $\Upsilon(4S)$ energy of 10.58 GeV, which corresponds to about $771 \times 10^6 B\bar{B}$
²³ meson pairs. Additionally, several streams of Monte-Carlo (MC) samples were produced,
²⁴ where each stream of MC corresponds to the same amount of data that was taken with
²⁵ the detector. No specific signal MC was used: instead of producing dedicated signal MC
²⁶ samples, the samples were obtained by filtering the decays of interest from the generic
²⁷ on-resonance MC samples. The following samples were used in this analysis:

- ²⁸ • data
- ²⁹ • MC - 10 streams of B^+B^- and $B^0\bar{B}^0$ (denoted as `charged` and `mixed`) for signal
³⁰ decays and backgrounds.
 - ³¹ - 6 streams of $q\bar{q}$ produced at $\Upsilon(4S)$ resonance energy
 - ³² - 6 streams of $q\bar{q}$ produced at 60 MeV below $\Upsilon(4S)$ resonance energy, where each
³³ stream corresponds to $1/10 \times L_0$.

³⁵ 2 Event selection and reconstruction

³⁶ In this chapter the procedure for reconstruction of the events where one B meson decays
³⁷ inclusively to a Λ_c baryon and the accompanying B meson decays hadronically.

³⁸ 2.1 B_{tag} reconstruction

³⁹ The FEI is an exclusive tagging algorithm that uses machine learning to reconstruct
⁴⁰ B meson decay chains and calculates the probability that these decay chains correctly
⁴¹ describe the true process. In this analysis only hadronically reconstructed decay chains are
⁴² considered. The training called `FEI_B2BII_light-2012-minos` is used. Tag-side B meson
⁴³ candidates are required to have a beam-constrained mass greater than $5.22 \text{ GeV}/c^2$ and
⁴⁴ $-0.15 < \Delta E < 0.07 \text{ GeV}$.

⁴⁵ In the case of multiple candidates in the same event, the candidate with the highest
⁴⁶ `SignalProbability` (the signal probability calculated by FEI using FastBDT) is chosen. To
⁴⁷ suppress the background consisting of B^0 events misreconstructed as B^+ (and vice-versa)
⁴⁸ from neutral (charged) decays also a B^0 (B^+) candidate is reconstructed with FEI and if
⁴⁹ its `SignalProbability` is higher than the charged (neutral) reconstructed B meson, the event
⁵⁰ is discarded. This constitutes a sort of crossfeed-veto, rejecting part of events belonging
⁵¹ to the other typology of decays of interest: for example in the case one is interested
⁵² in reconstructing $B^{+/-}$ decays and the event actually contains B^0/\bar{B}^0 decays, the FEI
⁵³ reconstructed neutral B meson candidate most likely presents a higher `SignalProbability`
⁵⁴ than the charged FEI reconstructed candidate.

⁵⁵ 2.2 Λ_c reconstruction

⁵⁶ In the *rest of event* (ROE) of the reconstructed B_{tag} meson, to select $\Lambda_c \rightarrow pK\pi$ signal
⁵⁷ candidates, the following event selection criteria are applied. Charged tracks with the
⁵⁸ impact parameters perpendicular to and along the nominal interaction point (IP) are
⁵⁹ required to be less than 2 cm and 4 cm respectively ($dr < 2 \text{ cm}$ and $|dz| < 4 \text{ cm}$).

⁶⁰ The pion tracks are required to be identified with $\frac{\mathcal{L}_\pi}{\mathcal{L}_K + \mathcal{L}_\pi} > 0.6$. The kaon tracks are
⁶¹ required to be identified with $\frac{\mathcal{L}_K}{\mathcal{L}_K + \mathcal{L}_\pi} > 0.6$, and the proton/anti-proton tracks are
⁶² required to be identified with $\frac{\mathcal{L}_{p/\bar{p}}}{\mathcal{L}_K + \mathcal{L}_{p/\bar{p}}} > 0.6$ and $\frac{\mathcal{L}_{p/\bar{p}}}{\mathcal{L}_\pi + \mathcal{L}_{p/\bar{p}}} > 0.6$, where the $\mathcal{L}_{\pi,K,p/\bar{p}}$ are the
⁶³ likelihoods for pion, kaon, proton/anti-proton, respectively, determined using the ratio of
⁶⁴ the energy deposit in the ECL to the momentum measured in the SVD and CDC, the
⁶⁵ shower shape in the ECL, the matching between the position of charged track trajectory
⁶⁶ and the cluster position in the ECL, the hit information from the ACC and the dE/dx
⁶⁷ information in the CDC.

⁶⁸ For the Λ_c candidates a vertex fit is performed with `TreeFitter`, requiring it to converge.
⁶⁹ If there are more than one Λ_c combination, then the best candidate based on the χ^2
⁷⁰ probability is chosen. The Λ_c signal region is defined to be $|M_{\Lambda_c} - m_{\Lambda_c}| < 20 \text{ MeV}/c^2$ (\sim
⁷¹ 3σ), here m_{Λ_c} is the nominal mass of m_{Λ_c} .

⁷²



73 2.3 Wrongly reconstructed B_{tag} candidates

74 In the case of the signal sample the distributions for the beam-constrained mass M_{bc} and
 75 for the correctly reconstructed Λ_c candidates, look like in Fig. 1. If one then investigates
 76 the M_{bc} distribution of the B_{tag} candidates reconstructed with FEI, it can be seen that
 77 there is a peaking structure for wrongly reconstructed B mesons (as in Fig. 2), according
 78 to the BASF2 internal truth matching variable **isSignal**. It is obvious from this that the
 79 BASF2 internal truth matching variable cannot be used to separate properly the signal
 80 events in correctly and wrongly reconstructed B mesons. In the study BELLE2-NOTE-TE-
 81 2021-026 <https://docs.belle2.org/record/2711/files/BELLE2-NOTE-TE-2021-026.pdf>
 82 a possible solution was found developing new variables that can be used for an
 83 improved truth matching for the FEI (those variables were added to a newer BASF2
 84 release than the one used for this study). In the present study instead a more "traditional"
 85 approach was adopted: fitting the M_{bc} distribution with a sum of PDFs that account for
 86 the flat (background) component and the peaking (signal) component. To validate this
 87 method a control decay study was performed on the flavor correlated $B^+ \rightarrow \bar{D}^0$ channel.

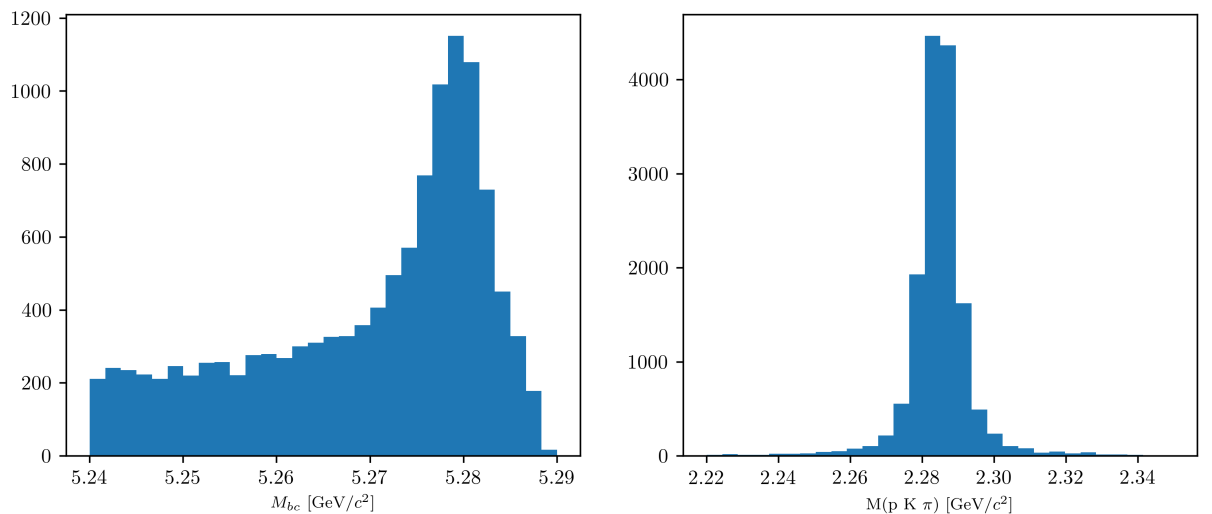


Figure (1) M_{bc} and $M(pK\pi)$ distributions of B_{tag} and Λ_c candidates reconstructed in the signal sample.

88 3 Signal selection optimization

89 To further enhance the purity of the signal decays, an optimization procedure is adopted
 90 to determine optimal cuts for a set of variables for each decay mode under investigation
 91 by this study. The cuts on the following variables are optimized:

- 92 • *foxWolframR2*: the event based ratio of the 2-nd to the 0-th order Fox-Wolfram
 93 moments

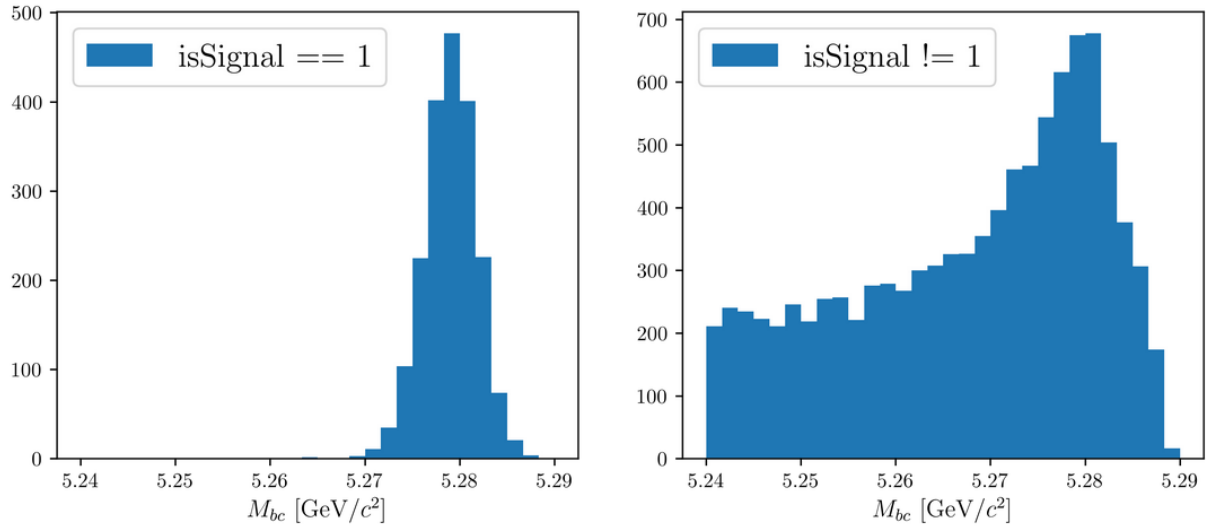


Figure (2) M_{bc} distribution of B_{tag} candidates reconstructed in the signal sample, truth-matched (on the left) and not (on the right).

- 94 • SignalProbability: the already mentioned signal probability calculated by FEI using
95 FastBDT
- 96 • $p_{CMS}^{\Lambda_c}$: momentum of the Λ_c candidates in the center of mass system
- 97 The optimization is based on the Figure Of Merit (FOM): $\text{FOM} = \frac{S}{\sqrt{S+B}}$
98 Where S and B are respectively signal and background events in the signal region:
99 $M_{bc} > 5.27 \text{ GeV}/c^2$, $2.2665 < M(pK\pi) < 2.3065 \text{ GeV}/c^2$.
- 100 Due to the issue reported in Sec. 2.3, to separate signal events that peak in M_{bc} from
101 the ones that are not (which are then categorized as background events), the events
102 reconstructed in the signal sample are fitted with a sum of Crystal Ball function and
103 Argus for each cut value on the corresponding variable to optimize (as in Fig. 3).

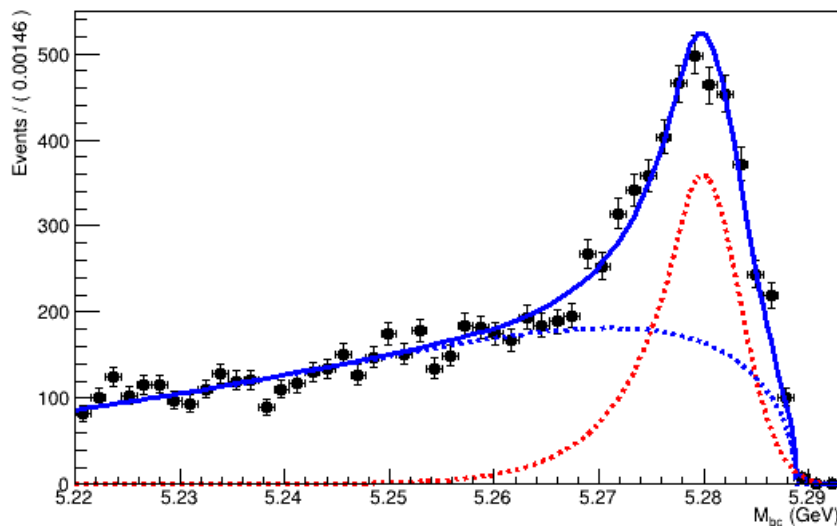


Figure (3) Example of a fit used to separate the correctly reconstructed B mesons (described by the red dotted Crystal Ball function) from the wrongly reconstructed ones (described by the blue dotted Argus function).

¹⁰⁴ **4 $B^- \rightarrow \Lambda_c^+ \text{ decays}$**

¹⁰⁵ First, in order to suppress the continuum background the cut on *foxWolframR2* is
¹⁰⁶ optimized. Fig. 4 shows the *foxWolframR2* distributions for signal and continuum
events.

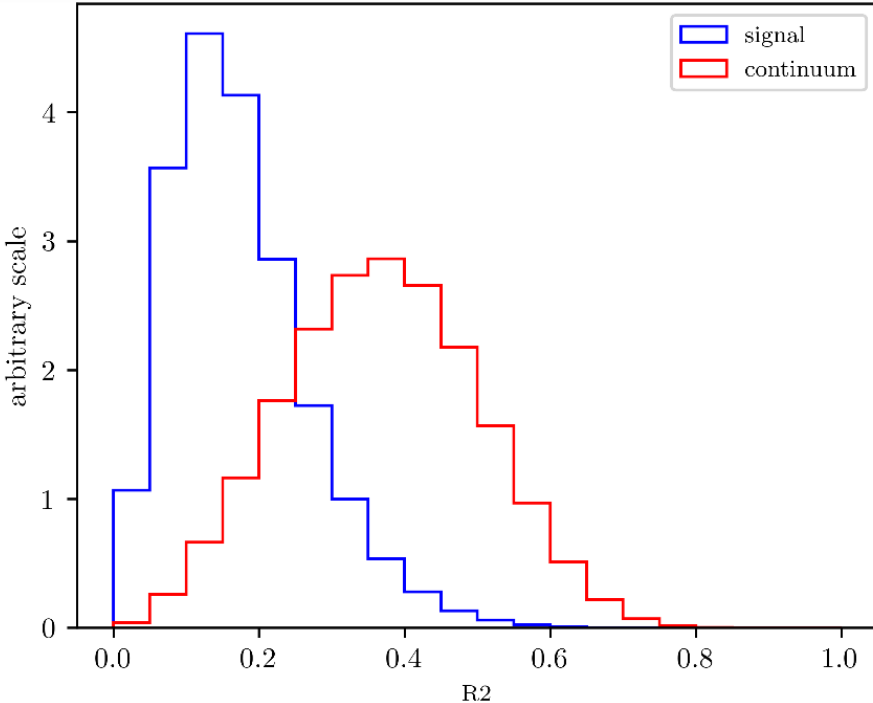


Figure (4) Distribution of the *foxWolframR2* variable for signal and continuum background events.

¹⁰⁷
¹⁰⁸ With the optimized cut $\text{foxWolframR2} < 0.27$, the cut on SignalProbability is
¹⁰⁹ optimized in the same way (see Fig. 7).

¹¹⁰ With the optimized cut SignalProbability > 0.01 , the cut on *foxWolframR2* variable is
¹¹¹ rechecked (Fig. 8). Being the maximum values fluctuating around *foxWolframR2* < 0.3 ,
¹¹² this cut is the one finally chosen for this variable.

¹¹³ With the optimized cuts on SignalProbability and *foxWolframR2* variable, the cut
¹¹⁴ on $p_{CMS}^{\Lambda_c}$ is optimized

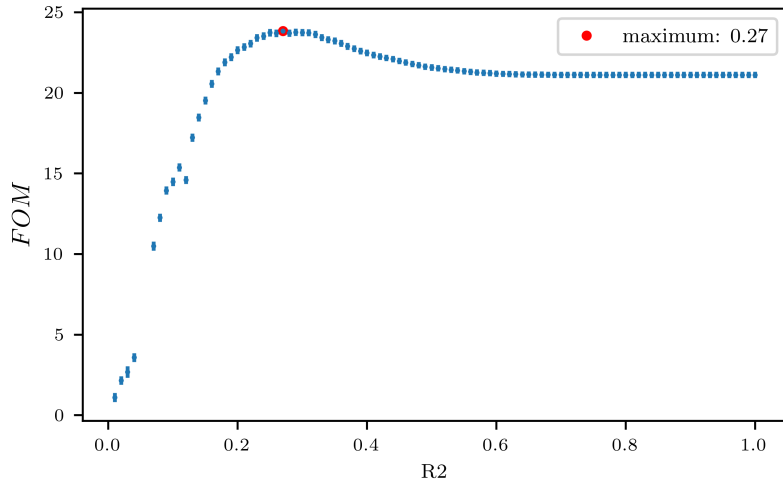


Figure (5) Figure of Merit values calculated at several cuts on the *foxWolframR2* variable

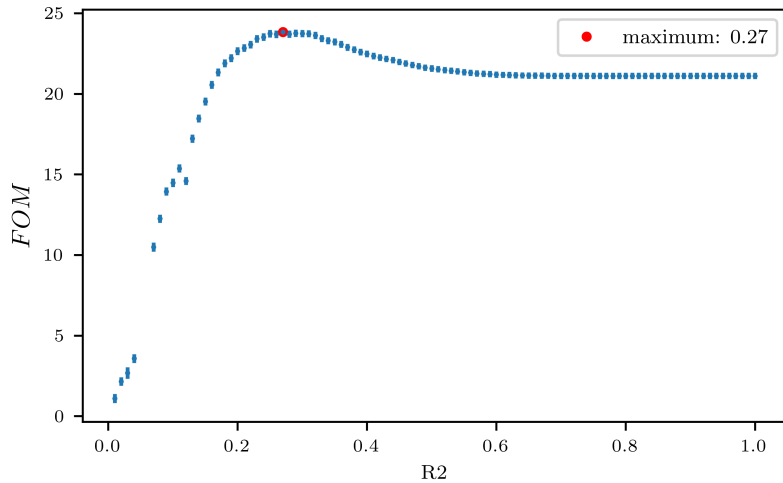


Figure (6) Figure of Merit values calculated at several cuts on the *foxWolframR2* variable

From Fig. 9 one can see that with values of the cut above $p_{CMS}^{\Lambda_c} < 1.8 \text{ GeV}/c^2$ a plateau of maximum FOM values is reached. But such a cut would still be useful to reject some background events as one can see from Fig. 10.

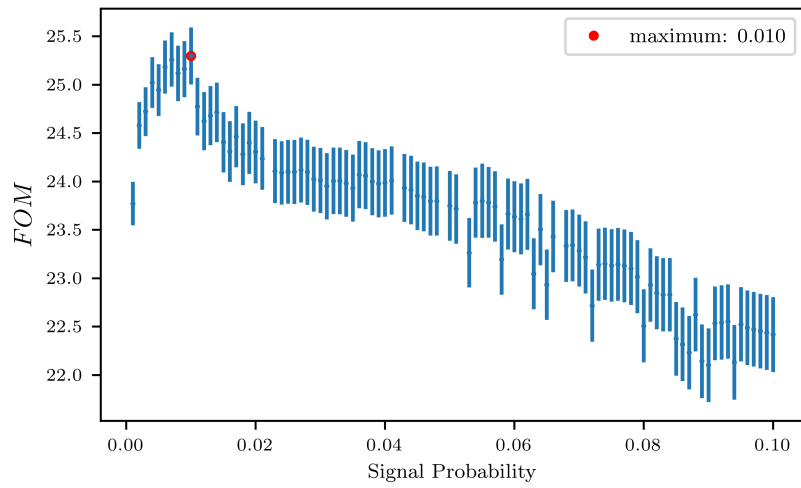


Figure (7) Figure of Merit values calculated at several cuts on the SignalProbability variable

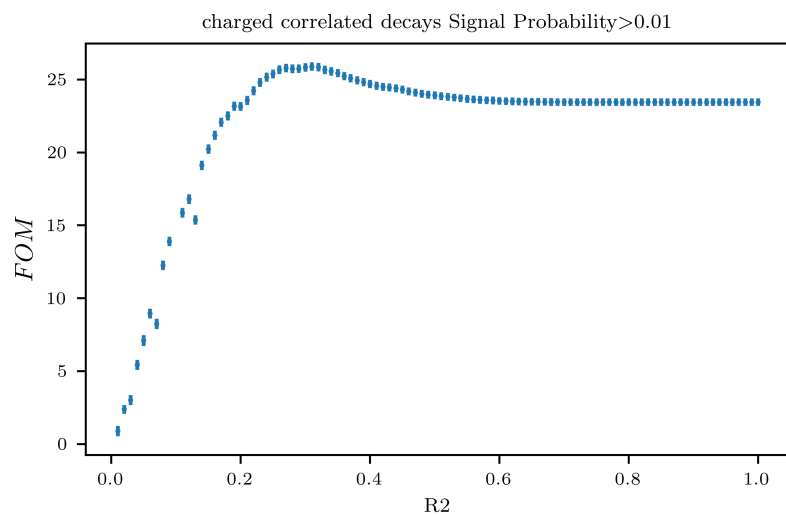


Figure (8) Figure of Merit values calculated at several cuts on the *foxWolframR2* variable

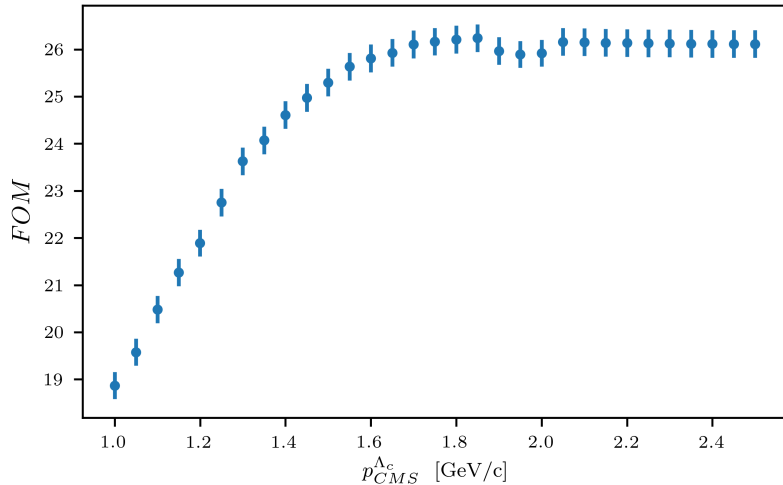


Figure (9) Figure of Merit values calculated at several cuts on the momentum of the Λ_c candidates in the center of mass system

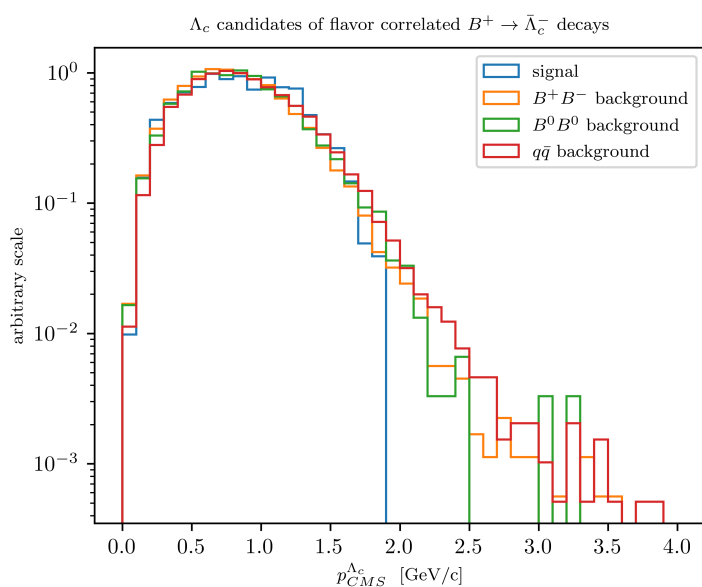


Figure (10) Distribution of Λ_c candidates momenta in the center of mass system

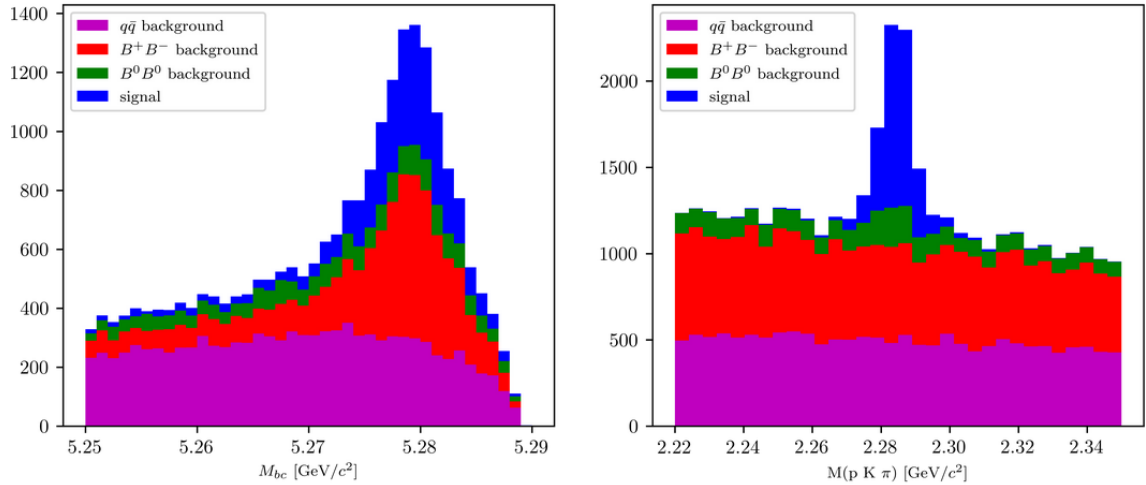


Figure (11) Distribution of M_{bc} (left) and invariant mass of charged correlated Λ_c candidates (right), in the signal region after the above mentioned selection cuts.

121

122

123 To measure the inclusive branching fraction of $B^- \rightarrow \Lambda_c^+ X$ the following quantities
124 need to be known:

$$Br(B^- \rightarrow \Lambda_c^+ X) = \frac{N_{tag,\Lambda_c} \cdot \epsilon_{FEI}^+}{N_{tag} \cdot Br(\Lambda_c^+ \rightarrow pK^-\pi^+) \epsilon_{\Lambda_c} \epsilon_{FEI,sig}^+} \quad (1)$$

125

Where

- 126 • N_{tag,Λ_c} is the reconstructed signal yield obtained from a two dimensional fit of M_{bc}
127 and $M(pK\pi)$ in the final sample.
- 128 • N_{tag} is the reconstructed signal yield obtained from the M_{bc} fit of all the tagged B
129 mesons in the final sample.
- 130 • ϵ_{Λ_c} is the Λ_c reconstruction efficiency.
- 131 • ϵ_{FEI}^+ represents the hadronic tag-side efficiency for generic B^+B^- events.
- 132 • $\epsilon_{FEI,sig}^+$ represents the hadronic tag-side efficiency for B^+B^- events where the tagged
133 B meson decays hadronically and the accompanying meson decays inclusively into
134 the studied signal channel.
- 135 • $Br(\Lambda_c^+ \rightarrow pK^-\pi^+)$: the branching fraction of the decay mode used to reconstruct
136 the Λ_c baryon.

137 The final samples contain both signal and background candidates from various sources
138 and in order to extract N_{tag,Λ_c} and N_{tag} unbinned extended maximum-likelihood fits are

139 performed.

140 In the next sections the methods used to determine the above mentioned quantities are
 141 described. First the fit model that accurately describes the distributions in the $B_{tag} + \Lambda_c$
 142 final sample will be described.

143 **4.1 Probability Density Functions (PDFs) for the two dimensional fit**

145 The PDFs used to describe the signal distributions are discussed first. The final sample
 146 of total signal events presents a peak around the expected B meson mass and a tail at
 147 low M_{bc} values. The peaking component represents the correctly reconstructed signal
 148 events in M_{bc} and therefore denoted from now on as **reconstructed signal**. The flat
 149 component on the left side from the peak represents the combinatorial background, i.e. B
 150 mesons that were mis-reconstructed, and therefore those events are denoted from now on
 151 as **misreconstructed signal**.

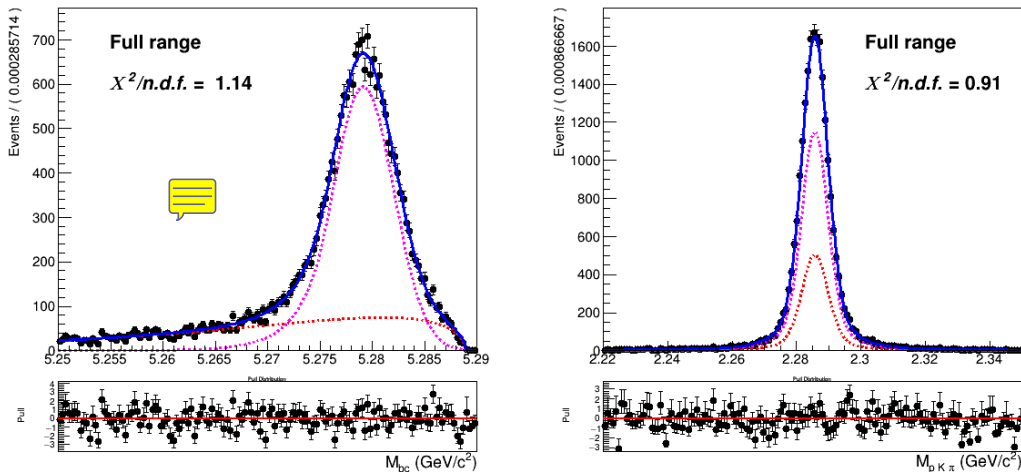


Figure (12) Two dimensional fit of total signal events in M_{bc} and $M(pK\pi)$

152 The 2D fit shown in Fig. 12¹⁴³ performed with a sum of the following probability
 153 density functions:

$$P_{B,\Lambda_c}^{recSig}(M_{bc}, M(pK\pi)) = \Gamma_{CB}(M_{bc}) \times \rho_G(M(pK\pi)) \quad (2)$$

154

$$P_{B,\Lambda_c}^{misSig}(M_{bc}, M(pK\pi)) = \Gamma_{ARG}(M_{bc}) \times \rho_G(M(pK\pi)) \quad (3)$$

155

156 The first is used to fit the reconstructed signal and $\Gamma_{CB}(M_{bc})$ is a Crystal Ball function.
 157 The second is used to model the misreconstructed signal and $\Gamma_{ARG}(M_{bc})$ is an Argus

function. In both cases a sum of three Gaussian functions $\rho_G(M(pK\pi))$ describes the mass of the Λ_c baryon.

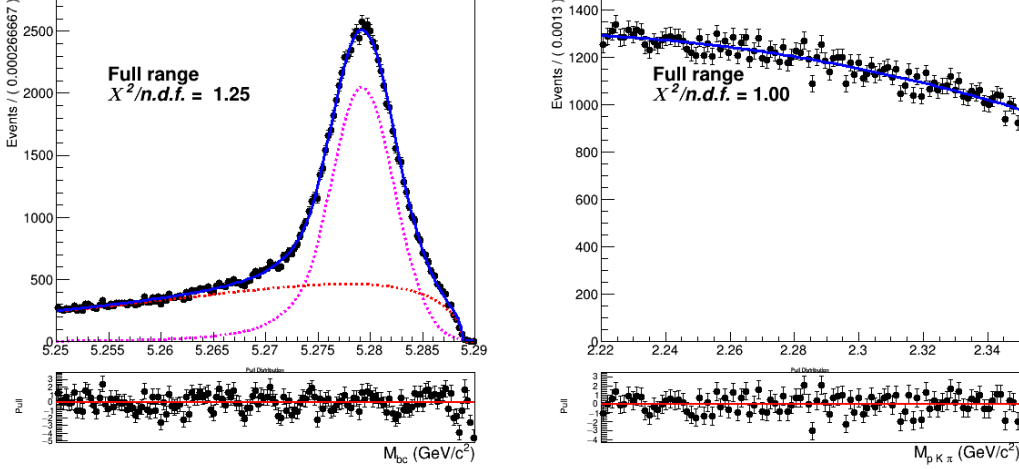


Figure (13) Two dimensional fit of generic (B^+B^-) events in M_{bc} and $M(pK\pi)$.

The generic background deriving from other B^+B^- events presents a similar shape of the distribution in M_{bc} (see Fig. 13): the probability density functions used for it are again a Crystal Ball and an Argus. Instead, the flat background in $M(pK\pi)$ can be described with a second order Chebychev polynomial function. The two dimensional PDF in this case is given by:

$$P_{B,\Lambda_c}^{GenBkg}(M_{bc}, M(pK\pi)) = [\Gamma_{CB}(M_{bc}) + \Gamma_{ARG}(M_{bc})] \times \rho_{Cheb2}(M(pK\pi)) \quad (4)$$

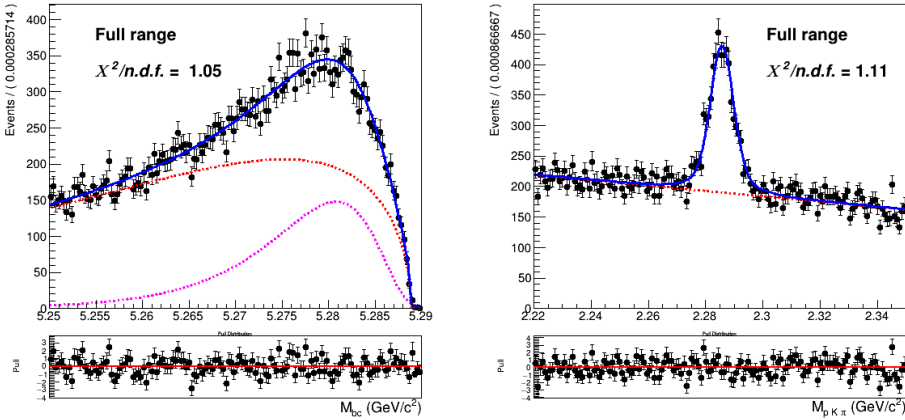


Figure (14) Two dimensional fit of crossfeed ($B^0\bar{B}^0$) events in M_{bc} and $M(pK\pi)$.

The contamination of misreconstructed B^0 events in the B^+ signal (and vice-versa) induces a background which peaks near the B meson mass, as one can see in Fig. 14.

168 Since among the misreconstructed B^0 events there are also $B^0 \rightarrow \Lambda_c$ decays (peaking
 169 at the Λ_c mass), this background contribution is also named "crossfeed background".
 170 The M_{bc} is modelled with a sum of Novosibirsk (colored in magenta) and Argus
 171 function (colored in red). Whereas the $M(pK\pi)$ distribution is described by the
 172 sum of a first order Chebychev polynomial and the peak by the same sum of three
 173 Gaussian functions used to describe the signal peak. In fact the latter is the result
 174 of the reconstruction of crossfeed events $B^0 \rightarrow \Lambda_c$. Therefore the 2D PDF can be written as:
 175

$$P_{B,\Lambda_c}^{CrossBkg}(M_{bc}, M(pK\pi)) = [\Gamma_{Nov}(M_{bc}) + \Gamma_{ARG}(M_{bc})] \times [\rho_{Cheb1}(M(pK\pi)) + \rho_G(M(pK\pi))] \quad (5)$$

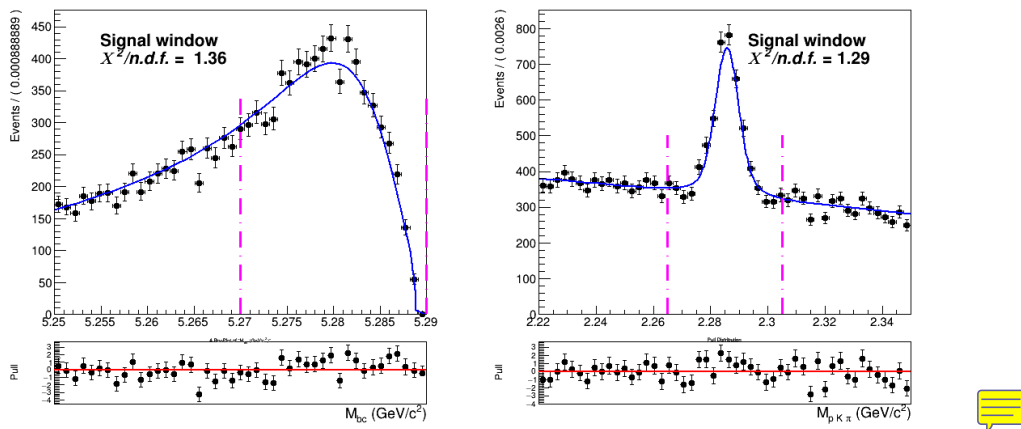


Figure (15) Signal region projections in M_{bc} and $M(pK\pi)$.

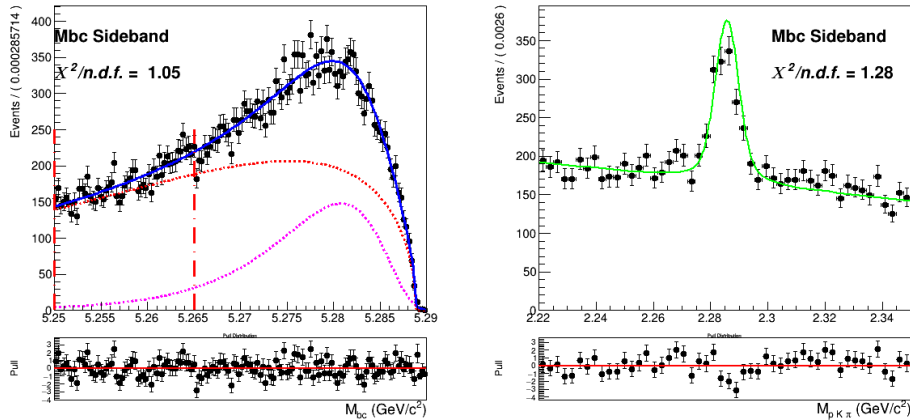


Figure (16) M_{bc} sideband region projection.

176 From the projections plotted in Fig. 14 the distributions appear to be well described
 177 by the PDF discussed above. Though the agreement in the Λ_c invariant mass is not fully

178 respected when different regions of M_{bc} are considered, as one can see from Fig. 15 and
 179 Fig. 16. The fraction of the amount of peaking events is not uniform among different M_{bc}
 180 regions. Since this background typology is peaking in both the observables of the fit, the
 181 potential correlation between them could have an impact on the signal yield extraction in
 182 the total fit.

183 To minimize this effect, and to avoid possible biases deriving from this feature, a
 184 correction is attempted. The M_{bc} is divided in 5 different regions. As shown in Figures
 185 ??-18e, for each of these regions a fit on the projected Λ_c invariant mass is performed to
 186 extract 5 values of the fraction of peaking events in those regions (all other parameters are
 187 fixed). Those values are then used for a parametrization of this parameter as a function of
 188 M_{bc} . From the plot shown in Fig. 17 one can see that it is possible to describe the trend
 189 with a linear dependence with a good approximation.

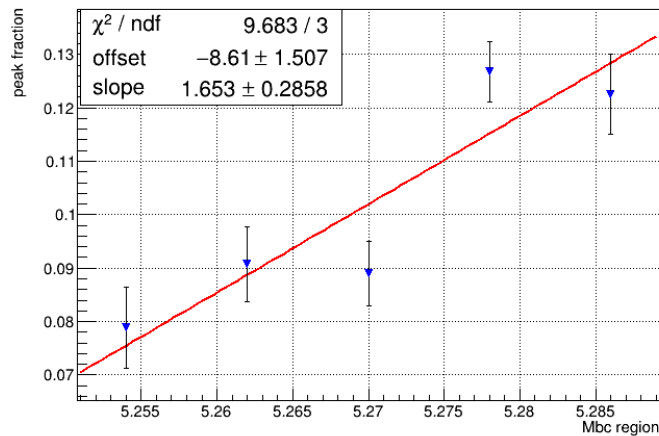


Figure (17) Invariant mass peak fraction as a function of M_{bc} .

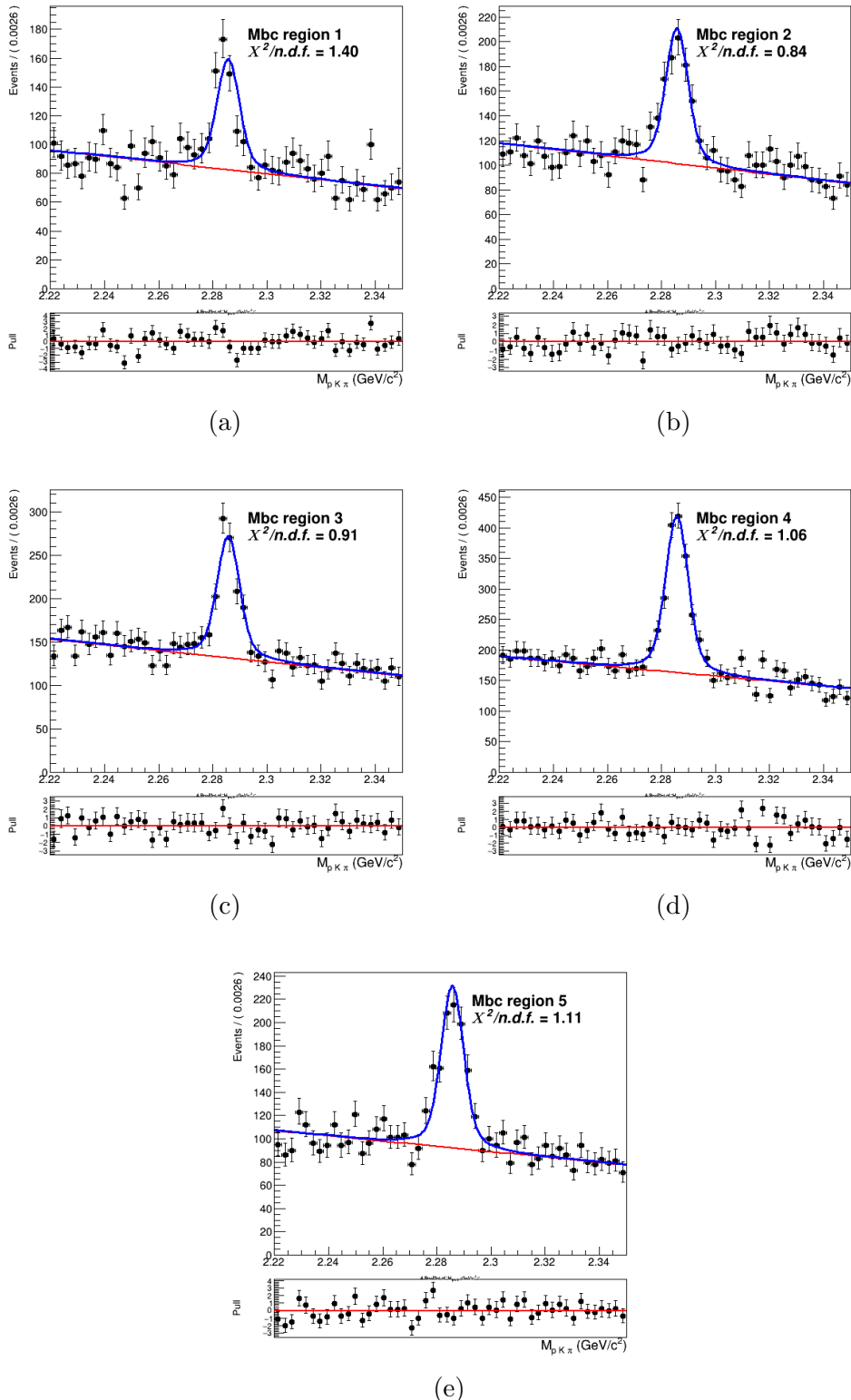


Figure (18) Fits of $M(pK\pi)$ in 5 different regions of M_{bc} : $5.25 < M_{bc} < 5.258 \text{ GeV}/c^2$, $5.258 < M_{bc} < 5.266 \text{ GeV}/c^2$, $5.266 < M_{bc} < 5.274 \text{ GeV}/c^2$, $5.274 < M_{bc} < 5.282 \text{ GeV}/c^2$, $5.282 < M_{bc} < 5.29 \text{ GeV}/c^2$.

190 The 2D PDF describing the crossfeed background is consequently modified:

191

$$P_{B,\Lambda_c}^{CrossBkg}(M_{bc}, M(pK\pi)) = [\Gamma_{Nov}(M_{bc}) + \Gamma_{ARG}(M_{bc})] \times [F(M(pK\pi)|M_{bc})]$$

193

194 where the conditional PDF $F(M(pK\pi)|M_{bc})$ describing the invariant mass is still a
 195 sum of $\rho_{Cheb1}(M(pK\pi))$ and $\rho_G(M(pK\pi))$, but their fraction is now parametrized as a
 196 function of M_{bc} .

197 In Figures 19- 20 one can appreciate the improvement obtained with this correction.

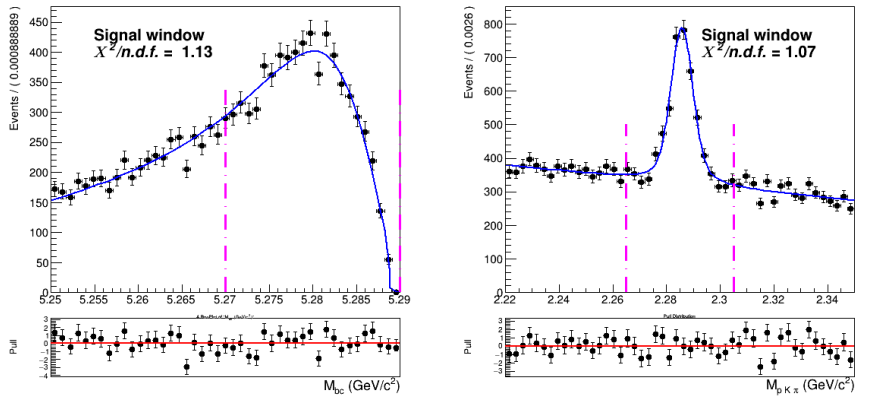


Figure (19) Signal region projections in M_{bc} and $M(pK\pi)$ after the parametrization.

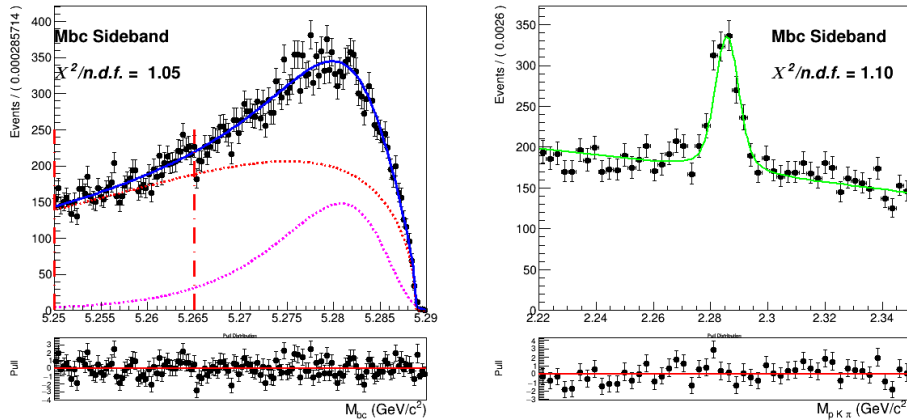


Figure (20) M_{bc} sideband region projection after the parametrization.

198 Besides the dataset recorded at the energy of the $\Upsilon(4S)$ resonance ($E_{CMS}^{on-res} = 10.58$
 199 GeV), the *Belle* experiment recorded a sample of 89.4 fb^{-1} at an energy 60 MeV below
 200 the nominal $\Upsilon(4S)$ resonance ($E_{CMS}^{off-res} = 10.52 \text{ GeV}$). The dataset allows to check for
 201 an appropriate modeling of the continuum MC simulation. Using the official tables (<https://belle.kek.jp/secured/nbb/nbb.html>) the off-resonance sample is scaled by
 202

$$\frac{\mathcal{L}^{on-res}}{\mathcal{L}^{off-res}} \left(\frac{E_{CMS}^{off-res}}{E_{CMS}^{on-res}} \right)^2 \quad (6)$$

203 taking into account the difference in luminosity and in E_{CMS} (Energy in center of mass
 204 system).
 205

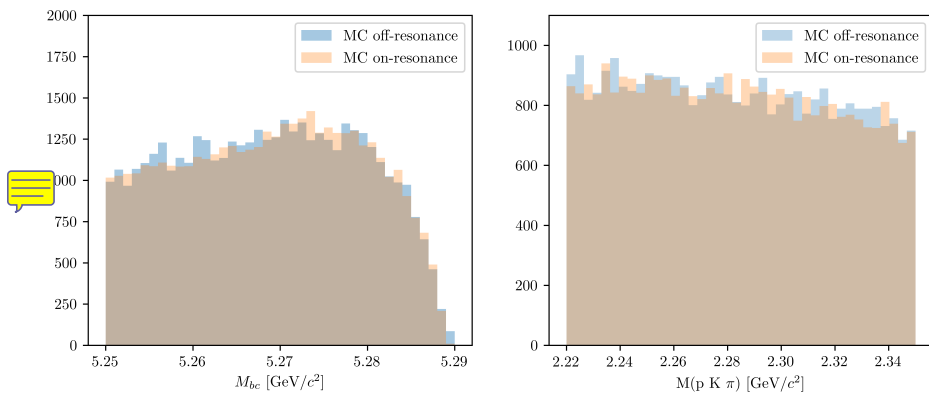


Figure (21) M_{bc} and $M(pK\pi)$ comparison between on-/off-resonance (scaled) Monte Carlo simulated continuum.

206 The plot in Fig.21 shows the M_{bc} and $M(pK\pi)$ distributions in the MC on-/off-resonance
 207 continuum after the scaling¹.
 208

Ideally, provided that there's a good agreement between MC and data for the off-resonance sample and also between the MC on-/off-resonance continuum after the scaling, one could directly use the scaled off-resonance data to describe the continuum background in the fit on data. Since the off-resonance MC (and data) present very low statistics (Fig. 22 shows the Λ_c invariant mass in off-resonance data), scaling them with all the applied selection cuts would cause the PDF describing the continuum to be very much affected by statistical fluctuations. Additionally, since the B meson candidates are reconstructed in both on-resonance and off-resonance events for values of $M_{bc} \geq 5.22 \text{ GeV}/c^2$, but the E_{CMS} differs, there can be effects of correlations between the applied *SignalProbability* cut and the M_{bc} variable that one needs to take into account. This effects on the M_{bc} are carefully studied in the analysis of the control sample. In Fig. 24 one can notice some discrepancy in the shapes, apart from the not negligible statistical fluctuations

¹it is obtained with the MC off-resonance sample being composed of 6 streams: the total amount is normalized

220 in the (scaled) off-resonance distribution. In the Λ_c invariant mass one doesn't expect
 221 correlation effects, but nevertheless there can be differences due to the limited statistics of
 222 the off-resonance sample. In fact, in the case of on-resonance MC some events in which Λ_c
 223 candidates survive nominal selection cuts are visible and can be described with a small
 224 Gaussian on the top of the flat background (Fig.27a). On the contrary in the off-resonance
 225 sample doesn't show anything beside the flat background (the Fig.27b shows a 5 streams
 226 statistics).

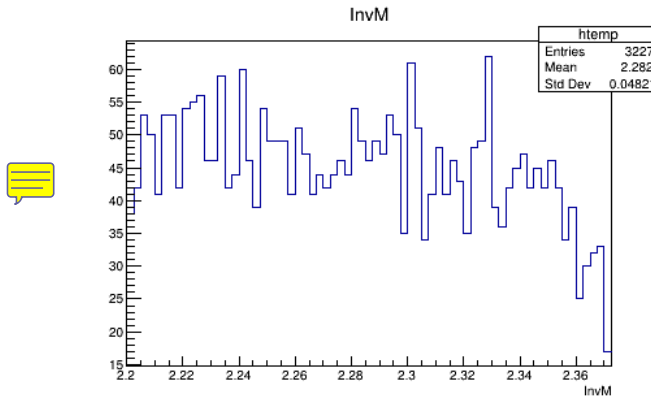


Figure (22) Λ_c invariant mass in off-resonance data (all cuts applied).

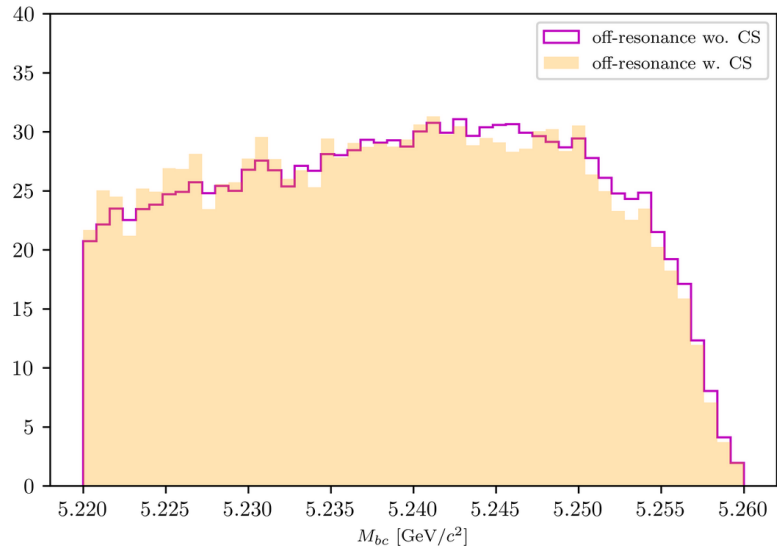
227 To obtain the shape that can describe the continuum background M_{bc} distribution on
 228 data the continuum suppression is not applied on the off-resonance continuum sample,
 229 in order to acquire more statistics. Then it has to be scaled (according to Eq. 4.1)
 230 and corrected for the *SignalProbability* correlated effects. This procedure is validated
 231 first on MC samples. This method works if the shape of the M_{bc} distribution doesn't
 232 change significantly removing the continuum suppression cut. Figures 23a - 23b show the
 233 agreement between the distributions with and without continuum suppression on MC and
 234 data respectively.

235 The scaling and bin-correction procedure was carried out on a sample of 5 streams of on-
 236 and off-resonance MC. From a ratio plot, like the one in Fig. 25a, showing the continuum
 237 on-resonance distribution in M_{bc} and the scaled continuum on-resonance distribution
 238 without the continuum suppression applied, the bin-correction is obtained to correct the
 239 off-resonance data in the scaling procedure. The validity of this procedure is first tested on
 240 a sixth independent MC sample: Fig. 25b shows the scaled and bin-corrected off-resonance
 241 continuum histogram compared with the continuum on-resonance distribution of the
 242 independent stream.

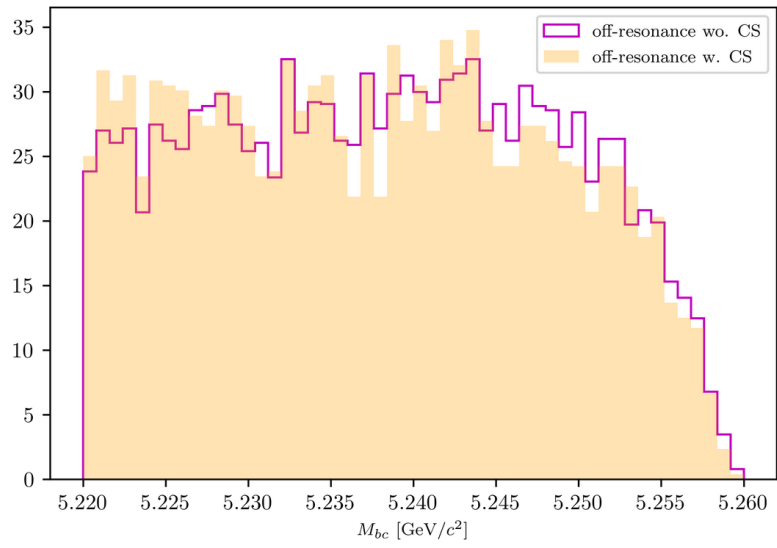
243 One can see that with this method the scaled simulated off-resonance events agree
 244 at reasonable level with the simulated on-resonance continuum. If the on-/off-resonance
 245 continuum events are correctly modelled the described method is able to provide a PDF
 246 that models continuum events in M_{bc} on data applying it on the off-resonance sample.

247 The obtained distribution can be then fitted (see Fig. 26), i.e. with a Novosibirsk
 248 function.





(a)



(b)

Figure (23) Above: M_{bc} distributions of the MC off-resonance sample (5 streams) with and without continuum suppression. Below: M_{bc} distributions on data with and without continuum suppression.

249 This is the procedure which can be then applied on the off-resonance data to obtain the
 250 M_{bc} shape describing the continuum background in data.

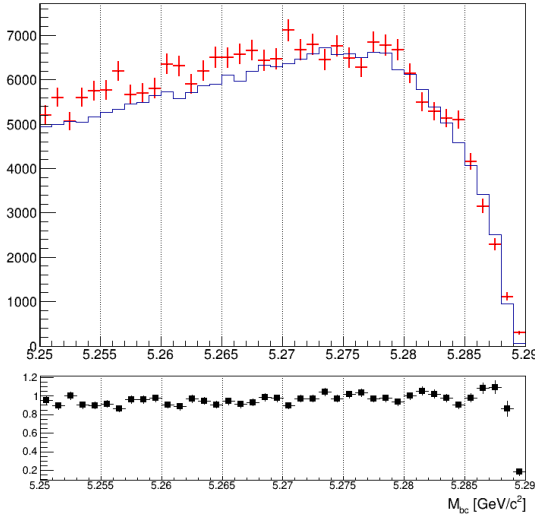


Figure (24) M_{bc} distributions of the MC (scaled) off-resonance sample (in red) and on-resonance (in blue) using 5 streams statistics and all nominal selection cuts applied.

251 The shape describing the Λ_c invariant mass is obtained from the simulated on-resonance
252 continuum, again using 5 streams statistics (see Fig. ??).

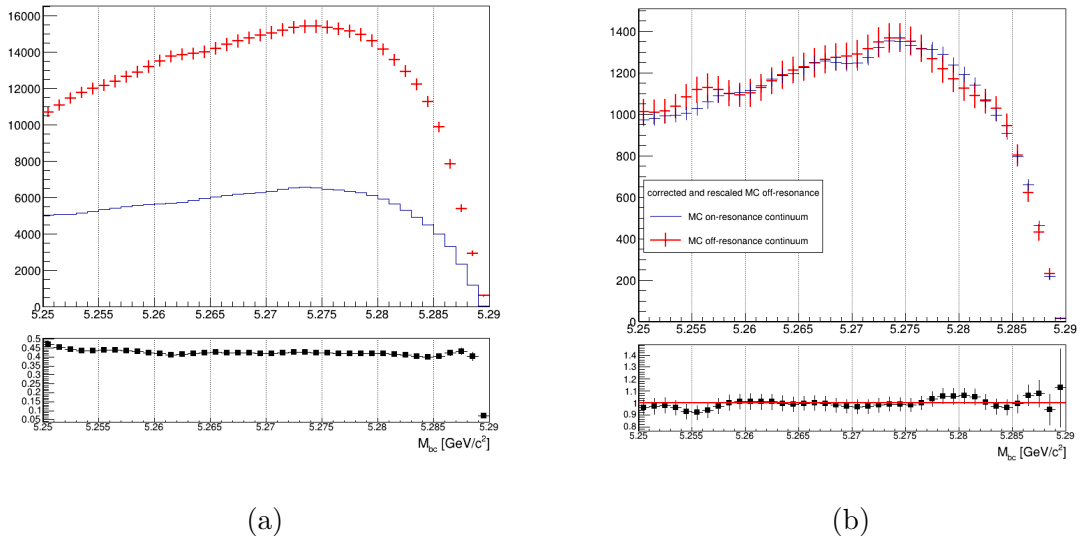


Figure (25) On the left: M_{bc} distributions of the MC off-resonance sample without continuum suppression and the MC continuum sample with applied continuum suppression. On the right: M_{bc} distributions of the corrected scaled MC off-resonance and on-resonance MC continuum.

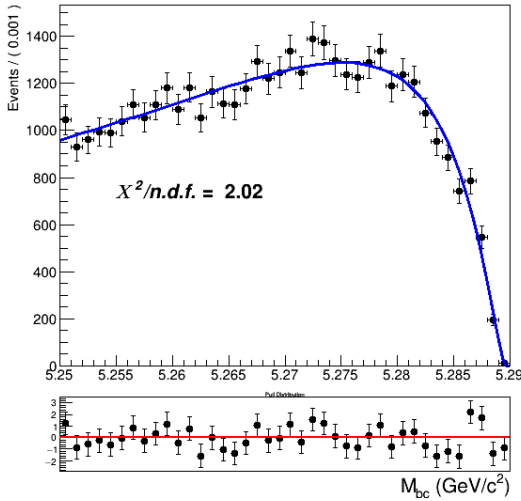


Figure (26) Fit of the M_{bc} distribution MC (scaled) off-resonance continuum (one stream).

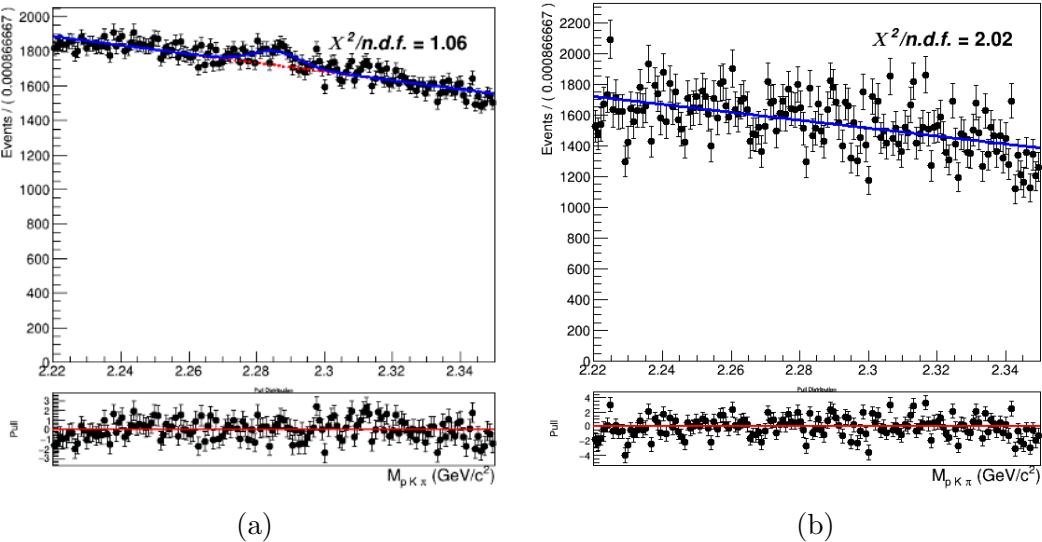


Figure (27) Comparison between 5 streams of MC on-resonance continuum 27a) and off-resonance (scaled) continuum in $M(pK\pi)$ (27b).

Finally, it is possible to examine the validity of the whole procedure on the independent stream. Fig. 29 shows the M_{bc} , $M(pK\pi)$ projections of the two dimensional fit with the one-dimensional PDFs obtained with the above described procedure. The 2D PDF used can be written as:

$$P_{B,\Lambda_c}^{Continuum}(M_{bc}, M(pK\pi)) = \Gamma_{Nov}(M_{bc}) \times [\rho_{Cheb1}(M(pK\pi)) + \rho_G(M(pK\pi))]$$

258

where, as already anticipated, the invariant mass is described by a sum of a first order

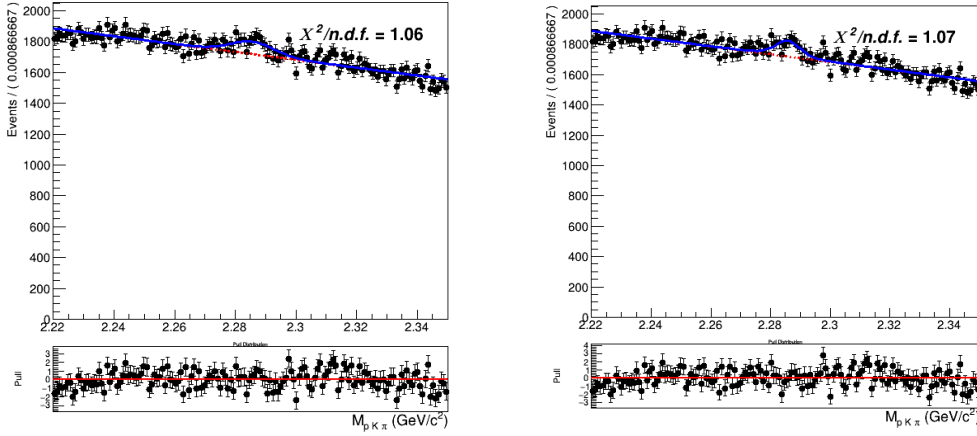


Figure (28) On the left: fit of the Λ_c invariant mass of on-resonance continuum using the one Gaussian description (all nominal cuts applied). On the right: fit of the Λ_c invariant mass of on-resonance continuum using the same three gaussian PDF to describe the peak in the signal invariant mass (all nominal cuts applied).

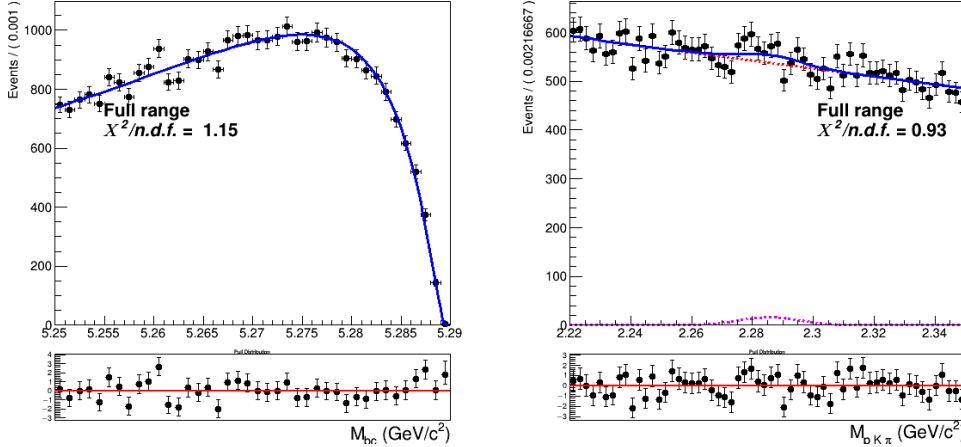


Figure (29) Two dimensional fit of continuum events (one stream).

260 Chebychev polynomial and the peak by a single Gaussian function.

261 It was then also investigated to alternatively use the same triple Gaussian PDF to
262 describe the peak, as it is shown in Fig. ???. The two descriptions seem to be equivalent.
263 The final fits described in Sec. 4.2 were performed with the one Gaussian description, but
264 it was also tried with the alternative three Gaussian description: no significant difference
265 was noticed and the signal yields differ by only about 10% of the statistical uncertainties.
266 For consistency reasons, on data the second description will be applied.



267 4.2 Two dimensional fit

268 All the already discussed PDFs describing the various categories of events were constructed
 269 using five streams. Then an independent stream is used to test if the total PDF enables
 270 to extract the signal yield in an unbiased way. In order to test this a total of six fits are
 271 performed on six different streams of generic MC. Exemplary, the distributions of stream
 272 0 overlaid by the fitted PDF are depicted in Fig. 30 (see Appendix .1 for the projections
 273 in signal and sideband regions). In all six fits all the shaping parameters are kept fixed,
 274 except:

- 275
- σ_{G1} : the width of the wider of the three Gaussian functions in $\rho_G(M(pK\pi))$
 - σ_{CB} parameter for the Crystal Ball describing the signal 

277 In the M_{bc} distribution the σ_{CB} parameter for the Crystal Ball describing the generic
 278 background is expressed as function of the signal σ_{CB} with a ratio fixed from the MC. For
 279 the crossfeed background the ratio between its contribution and misreconstructed signal is
 280 fixed from the MC.

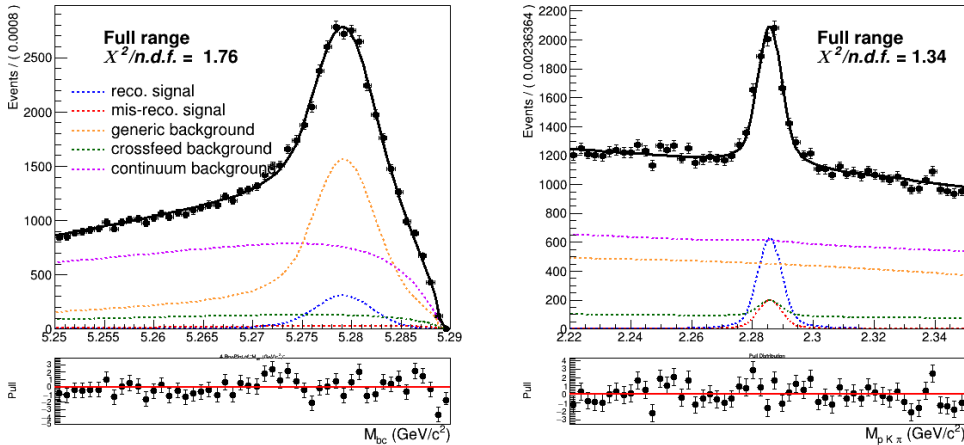


Figure (30) Two dimensional fit on stream 0 Monte Carlo simulated data.

281 The normalizations of mis-/reconstructed signal events and generic background events are
 282 floated in the two dimensional unbinned maximum likelihood fits.

283 In Table 1 the signal yields of the fits (**Reconstructed Signal**) to the two dimensional
 284 distributions for the six streams of $B^- \rightarrow \Lambda_c^+$ flavor-correlated decays are listed and
 285 compared to the yields obtained from fits of signal distributions of each individual stream.
 286 The latter are the "expected" yields of reconstructed signal from a fit to the total signal
 287 events in the individual stream as the one plotted on Fig. 31 where all the parameters of
 288 the PDFs described in Sec. 4.1 are kept fixed and the corresponding yields are extracted
 289 from the fit.

290 Except for stream 3, the fits present slightly higher values of reconstructed signal than
 291 expected ones, although always within the 1σ uncertainties (as shown in Fig. 32). The

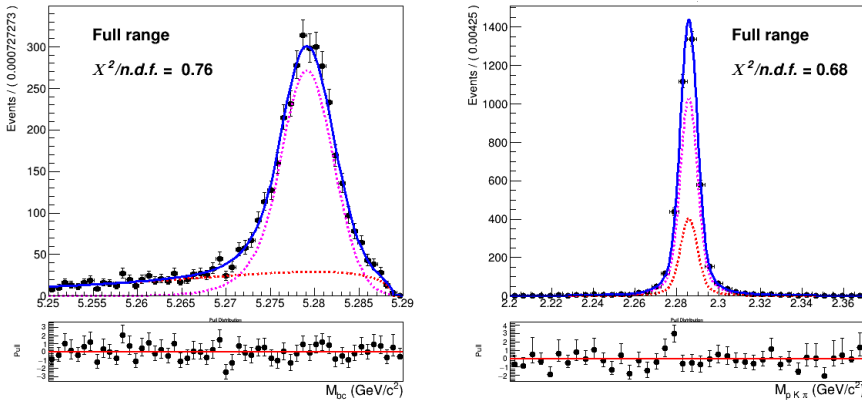


Figure (31) Two dimensional fit of Total Signal of stream 0 used to extract the expected reconstructed (corresponding to the PDF colored in magenta) and expected misreconstructed yields (corresponding to the PDF colored in red).

	Reconstructed Signal		Total Signal			
	fit	expected	fit	MC truth	fit - MC truth	
stream 0	3058 ± 123	2928 ± 66	4037 ± 121	4061	-24	-0.6%
stream 1	3047 ± 127	2956 ± 66	4098 ± 126	4084	14	0.3%
stream 2	3100 ± 126	3038 ± 68	4189 ± 125	4267	-78	-1.8%
stream 3	3124 ± 126	3156 ± 68	4377 ± 125	4337	40	0.9%
stream 4	3125 ± 128	3048 ± 67	4054 ± 125	4169	-115	-2.8%
stream 5	2909 ± 127	2816 ± 65	4080 ± 129	4001	79	2.0%
sum	18363	17942	24844	24919	-75	-0.3%

Table (1) Comparison of fitted and expected signal yields, fitted and truth-matched total signal for six streams of Belle generic MC when fitting the two dimensional distributions of M_{bc} and $M(pK\pi)$.

table also reports the fitted and truth-matched number of total signal (sum of reconstructed and misreconstructed signal) events. The values show that deviations are within statistical expectations, which indicates that this sum doesn't present biases. Nevertheless the fact that the reconstructed signal is not fluctuating around zero can be seen as an evidence of a small bias. Fig. 33 shows the differences between fitted and expected values of reconstructed signal with associated uncertainties (calculated as sum of quadrature of both uncertainties on the results from the fits and the expected values). The performed linear fit shows that, taken together, the six fits present an overall, small but not negligible, bias, which has to be taken into account while fitting the data.

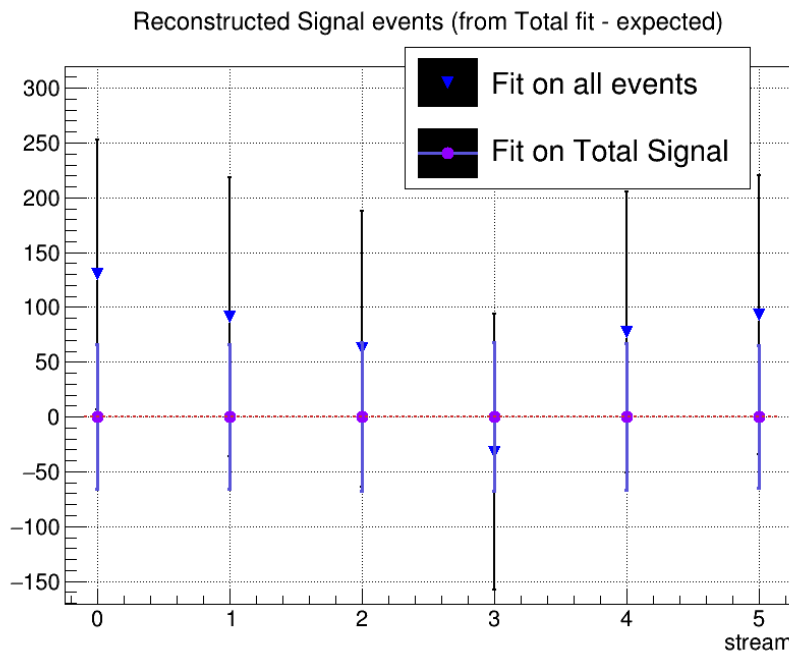


Figure (32) Differences between results from the fits and "expected" values for signal yields as reported in the first columns on Table1 .

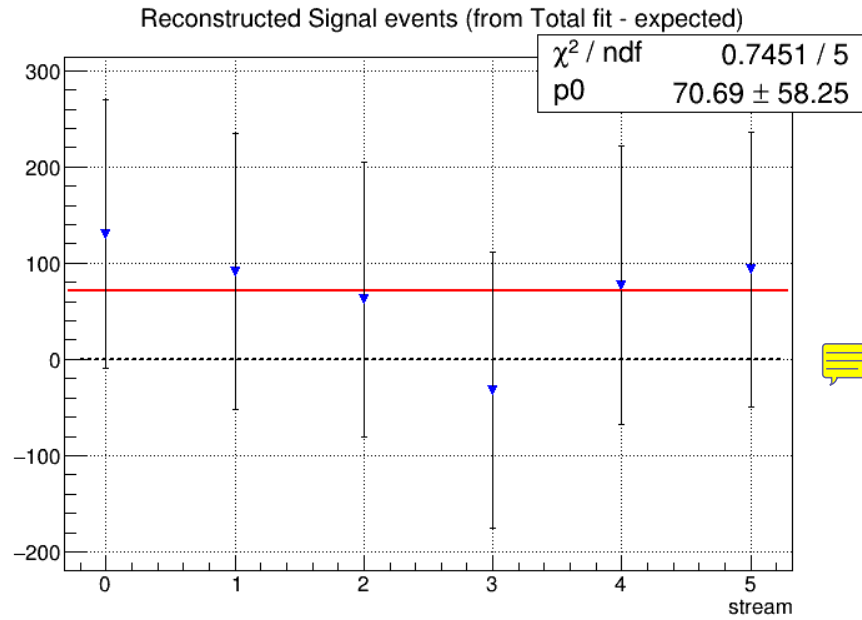


Figure (33) Fitted-expectation subtracted values for reconstructed signal yields with associated uncertainties summed in quadrature.

301 Additionally, one can investigate the behaviour for different signal-to-background ratio.

302 Thus, a second test of the fit model is performed. Using four independent streams the
 303 amount of total signal is varied between 25% and 100% of the nominal values. The
 304 amount of background varies according to poissonian fluctuations, as it is taken from
 305 four independent streams. The plot in Fig. 34 shows the values of reconstructed signal
 306 obtained in the total fits versus those expected by the fits on total signal events. One can
 307 see that the values distribute according to a linear dependence. The linear fit suggests
 308 a compatibility with a 1:1 relation: the red and the blue dotted lines don't overlap, but
 309 the values of the fitted line are compatible within the uncertainties with the identity line.
 310 Though also in this second test we see a slight tendency of overshooting the expected
 311 values.

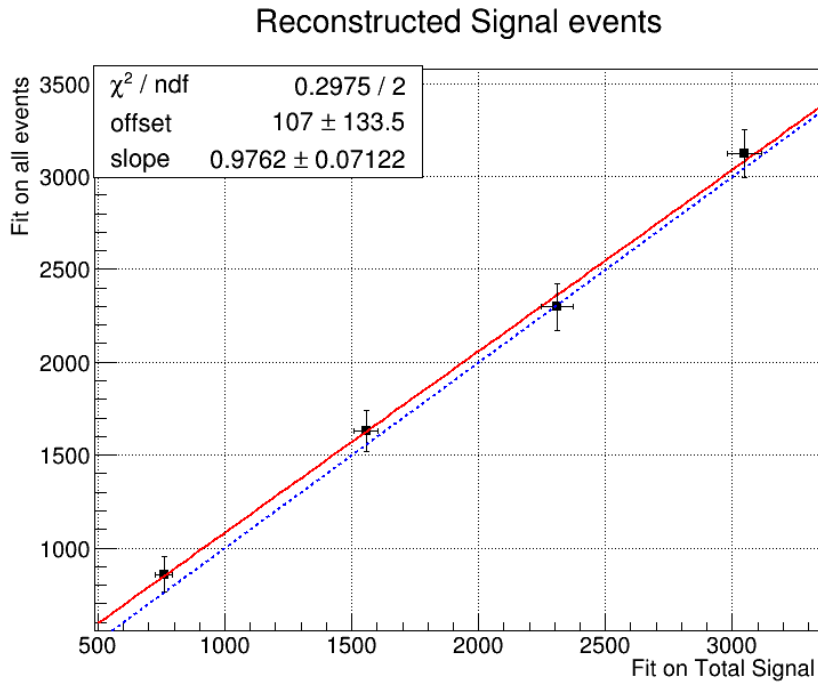


Figure (34) Linearity test: on the x-axis the obtained reconstructed signal yields from fits on different amounts of total signal; on y-axis the yields of reconstructed signal obtained fitting all events (as in Fig. 30). The values are fitted with a red continuous line, whereas the blue dotted line corresponds to a 1:1 linear dependence.

312 For the fit model also toy MC pseudo-experiments were performed in order to confirm
 313 the behavior of the fit setup. With toy MC experiments the yields, errors and the pulls
 314 of the fit are studied by generating our own pseudo-datasets, according to the MC (see
 315 Appendix). 3×10^3 pseudo-datasets are constructed, where each dataset was generated
 316 with the expected amount of events, distributed according to the Poisson distribution.



317 4.3 Probability Density Functions (PDFs) for the B_{tag}

318 The M_{bc} distribution of the tagged B mesons is fitted with a Crystal Ball as for the
 319 "peaking" component and the "flat" component is fitted with a Novosibirsk function (Fig.
 320 35). The crossfeed background, consisting of neutral B mesons tagged as charged B , is
 321 fitted instead with a sum of a Novosibirsk and an asymmetric Gaussian PDF (Fig. 36).

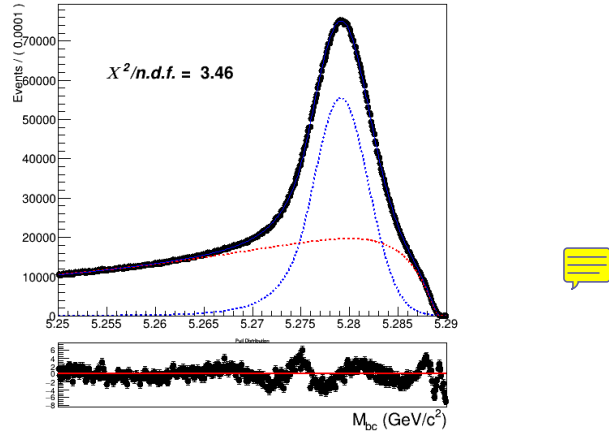


Figure (35) Fitted distribution of tagged charged B mesons: reconstructed signal events are described by the blue dotted PDF, the misreconstructed with a Novosibirsk function (red dotted).

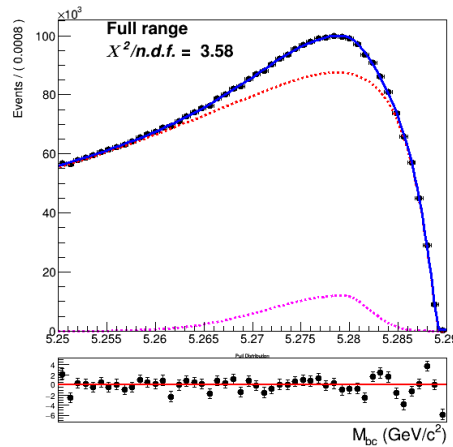


Figure (36) Crossfeed distribution fitted with a sum of Novosibirsk (red) and asymmetric Gaussian PDF (magenta)

322 As for the continuum background, a similar procedure as the one described already for
 323 the two dimensional fit was adopted:

- 324 • first the off-resonance sample is scaled accordingly

- 325 • the ratio between the scaled off-resonance and the on-resonance in MC is calculated
 326 in each bin (see Fig.37a)
- 327 • the bin-correction is applied on an independent stream and the scaled and bin-
 328 corrected M_{bc} distribution is compared with the on-resonance distribution as shown
 329 in Fig.37b

330 As for the B_{tag} continuum background the statistics is much larger than in the 2D sample,
 331 there's no need to remove the continuum suppression cut on the off-resonance sample.

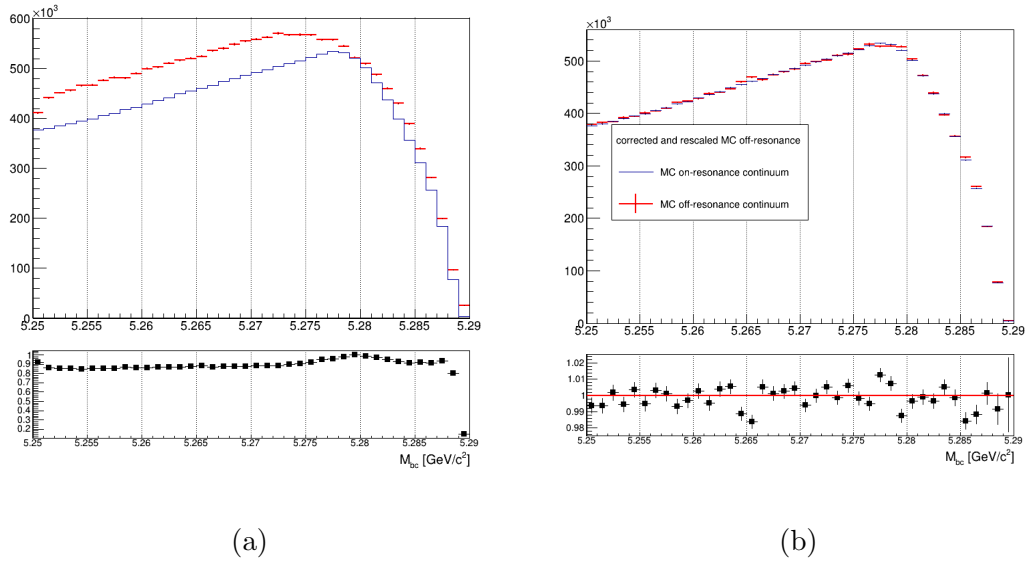


Figure (37) On the left: M_{bc} distributions of the MC off-resonance sample and the MC continuum sample with applied continuum suppression. On the right: M_{bc} distributions of the corrected scaled MC off-resonance and on-resonance MC continuum.



332 **4.4 B_{tag} fit**

333 An independent Monte Carlo stream was used to test the total fit model on tagged B meson
 334 candidates. As in the 2D fit, the parameter for the width, σ_{CB} , of the Crystal Ball is floated
 335 and the ratio between expected crossfeed background events and misreconstructed signal
 336 events is fixed from the MC. The Novosibirsk function describing the misreconstructed
 337 signal is also not fully constrained: the parameter describing the tail is free. To avoid
 338 introducing significant systematic uncertainties in the fit deriving from the M_{bc} endpoint
 339 region, where one has a smearing effect due to variations of the beam energy at the MeV
 340 level, the range for the fit is restricted to values between 5.250 and 5.287 GeV/c². Yields
 341 for the reconstructed and misreconstructed signal are obtained from the fit:

342

343

NrecSig	$4.2681 \cdot 10^6 \pm 5871$
NmisSig	$5.8787 \cdot 10^6 \pm 5128$

344 The Total Signal (the sum NrecSig+NmisSig) is 10146748 ± 4380 (to be compared
 345 with 10158571 from the Monte Carlo). This reflects a $\sim 2.5\sigma$ discrepancy between the true
 346 MC value and the result from the fit. This can produce some systematic effect, however
 347 the normalization does not influence the branching fraction result significantly.

348 To check the stability of the fit model a toy MC study was performed with 3×10^3
 349 pseudo-datasets (as it was done for the two-dimensional fit model). No evidence for
 350 possible biases in the reconstructed signal yields was found (see Appendix).

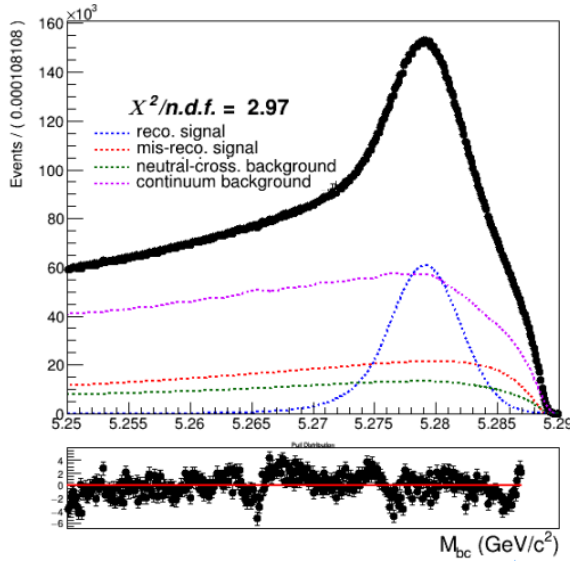


Figure (38) Total fit of tagged B mesons on Monte Carlo simulated data.

351 **4.5 Λ_c and FEI efficiency**

352 The efficiency in reconstructing the Λ_c baryon after correctly tagging the charged B
 353 meson, can be estimated from Monte Carlo simulated data as the fraction of correctly
 354 reconstructed signal events that have a correctly reconstructed B_{tag} companion, i.e.:

$$\frac{N_{recSig}(B_{tag}, \Lambda_c)}{N_{recSig}(B_{tag}^{sig})} \quad (7)$$

355 where $N_{recSig}(B_{tag}, \Lambda_c)$ are the yields of reconstructed signal from the two dimensional
 356 fits (reported in Table 1) and $N_{recSig}(B_{tag}^{sig})$ are the yields of correctly reconstructed signal
 357 in a fit of B mesons tagged in events where one of the two mesons decayed hadronically
 358 and inclusively into a Λ_c baryon (see Fig 39). To minimize statistical uncertainties, in
 359 the efficiency calculation the results from all the two dimensional fits were used and six
 360 streams of B_{tag} candidates reconstructed in signal events were used for the M_{bc} shown
 361 below.

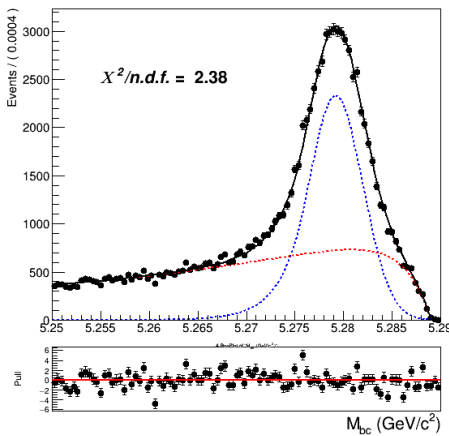


Figure (39) Fit of tagged B mesons in the "signal events" sample

362 From this and the results listed in sec. 4.2 the efficiency to reconstruct Λ_c is obtained :

363 $\epsilon_{\Lambda_c} = \frac{N_{recSig}(B_{tag}, \Lambda_c)}{N_{recSig}(B_{tag}^{sig})} = 44.83 \pm 0.32\%$

365 The yields from the fit shown in (Fig. 39) can be used also to calculate the FEI tag-side
 366 efficiency for signal events, i.e. the efficiency to tag the B meson accompanying a B_{sig}
 367 decaying into a Λ_c on the signal side. Whereas results from the fit of charged B_{tag} shown
 368 in Fig. 35 can be used to calculate the hadronic tag-side efficiency in the generic B^+B^-
 369 events case.

370 The ratio between the two efficiencies is calculated: $\frac{\epsilon_{FEI,sig}^+}{\epsilon_{FEI}^+} = 0.908 \pm 0.017$

372 4.6 Studies of Systematic Effects

373 In Table 2 the systematic uncertainties of the various considered sources are summarized.
 374 Their individual calculation is outlined in the subsequent subsections

source	%
Continuum modeling	0.07
Crossfeed PDFs	0.02
Crossfeed fraction	0.04
$\epsilon_{FEI,sig}^+/\epsilon_{FEI}^+$	0.06
ϵ_{Λ_c}	0.02
Fit bias	0.06
Total	0.12

Table (2) Systematic uncertainties in the determination of the $B^+ \rightarrow \bar{\Lambda}_c^- X$ branching fractions in %.

375 4.7 Continuum background modeling

376 Regarding this source of systematics, one has to take into account two different types.
 377 First of all, the continuum background PDFs were obtained based on the limited Monte
 378 Carlo statistics.  The statistical uncertainties are reflected in the uncertainties on the
 379 PDF parameters. Therefore, to estimate this type of uncertainty two-dimensional fits
 380 with varied parameters' values by their uncertainties (a fit with +err and -err) were
 381 performed. Whereas, the estimation of statistical uncertainty in the case of the B_{tag} should
 382 be estimated in principle varying each bin content of its error. On first approximation this
 383 is equivalent to vary the nominal number of events described with the histogram PDF by
 384 Poissonian variation. Exemplary, fits used to estimate the impact of these uncertainties
 385 are shown here in Figures 40 - 41. The yields obtained from those fits for benchmark
 386 stream5 results are then compared with the ones already reported previously and a mean
 387 deviation value is obtained for both the two-dimensional fit and the B_{tag} fit.

Fit	$-\sigma$	$+\sigma$	$\pm\bar{\sigma}$
2D	87	53	70
B_{tag}	10218	10620	10419

Table (3) Offsets on the signal yields obtained in the two dimensional and B_{tag} fit and mean deviations reported in the last column.

388 The estimated systematic uncertainty on Br value from this source is 0.07%.
 389 The other type of systematic uncertainty in modeling the continuum is originated
 390 by the continuum suppression cut. In fact, when comparing the distribution of the
 391 *foxWolframR2* variable in off-resonance MC and data a slight shift is visible (see Fig.
 392 42). Because of this shift the cut applied on this variable could have a different impact



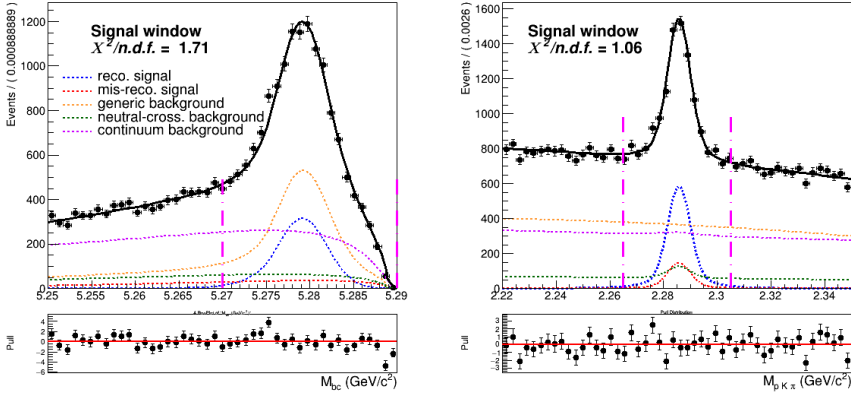


Figure (40) Signal window projections of a two dimensional fit on Monte Carlo simulated data where the shaping parameters were varied of their uncertainties.

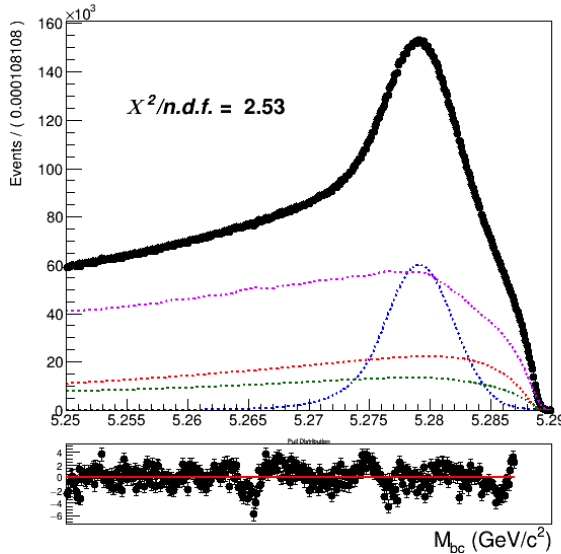


Figure (41) Fit of tagged B meson candidates on Monte Carlo simulated data where the amount of continuum was varied according to poissonian fluctuations.

393 on data, in terms of rejected continuum background. It is found to reject about 60% of
 394 the continuum background in data, whereas it rejects 55% of the continuum background
 395 in MC (56% in on-resonance MC). The conclusion is that in data one can expect about
 396 2.25% less continuum background events. This discrepancy can be then taken into account
 397 when fitting the data sample, applying a simple correction to the number of events.
 398 However, the statistical uncertainty on this fraction of events can also be taken into
 399 account as systematics. Being the number of events in the off-resonance data sample
 400 without the continuum suppression applied is very small (less than 10^4), the uncertainty
 401 in the mentioned fraction of events is negligible compared to the statistical uncertainty on

402 the on-resonance continuum background events in MC: it would account for 0.002% on
 403 the BR value. Therefore, this second source of uncertainty is not taken into account.

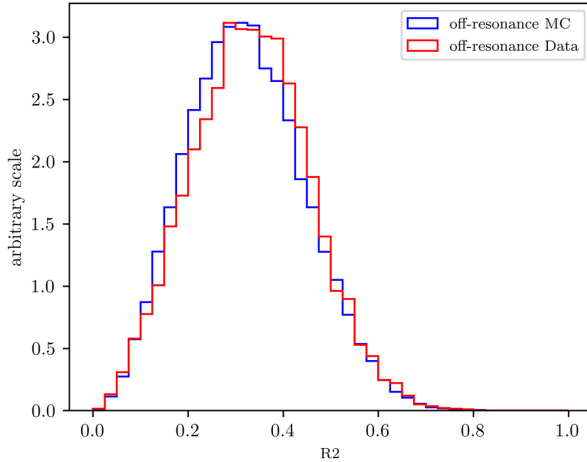


Figure (42) Distributions of variable $foxWolframR2$ in off-resonance MC and data.

404 4.8 Crossfeed background modeling

405 Since also the shapes of the PDFs describing the crossfeed background are fully fixed to the
 406 ones determined with the limited Monte Carlo statistics, also their statistical uncertainties
 407 need to be taken into account as possible source of systematics. The procedure to estimate
 408 this source of systematic uncertainty is the same described in the previous section regarding
 409 the continuum background. In the table below the signal yields' offsets are listed changing
 410 the parameters within their uncertainties, and the mean offsets value used to calculate the
 411 expected uncertainty on the BR value. The resulting absolute systematic uncertainty is
 412 about 0.02% on the BR value.



Fit	$-\sigma$	$+\sigma$	$\pm\bar{\sigma}$
2D	27	8	18
B_{tag}	5400	5700	5550

Table (4) Offsets on the signal yields obtained varying the parameters of crossfeed background PDFs within their uncertainties in the two dimensional and B_{tag} fit and mean deviations reported in the last column.

413 4.9 Crossfeed ratio

414 The systematic uncertainty on the crossfeed/misreconstructed events' ratio is studied
 415 investigating the impact on the yields when considering a plausible discrepancy up to 20%
 416 between Monte Carlo and data.

417 For the two-dimensional fit the ratio was artificially set to consider scenarios of $\pm 20\%$
 418 difference in the ratio, whereas in the case of the B_{tag} fit the number of crossfeed events
 419 were varied artificially in order to have $\pm 20\%$ different ratio, keeping the previously
 420 determined Monte Carlo ratio fixed.

Fit	$-\sigma$	$+\sigma$	$\pm\bar{\sigma}$
2D	24	48	36
B_{tag}	2807	3940	3374

Table (5) Offsets on the signal yields obtained varying of $\pm 20\%$ the cross-feed/misreconstructed in the two dimensional and B_{tag} fit and mean deviations reported in the last column.



421 The estimated systematic uncertainty on Br value from this source is 0.04%.

422 4.10 Efficiencies

423 The ratio between the two FEI efficiencies is: $\frac{\epsilon_{FEI,sig}^+}{\epsilon_{FEI}^+} = 0.908 \pm 0.017$

424 The uncertainty on this value originates a systematic uncertainty of 0.06% on the Br
 425 value. The Λ_c reconstruction efficiency is determined to be $\epsilon_{\Lambda_c} = 44.83 \pm 0.32\%$. The
 426 systematic uncertainty originated by its uncertainty is 0.02% on the Br value.



427 4.11 Fit biases

428 The small bias on the reconstructed signal seen in the two-dimensional fit model (see Fig.
 429 33) has to be corrected when fitting data, but the uncertainty on it has to be taken into
 430 account in the systematics. Also the discrepancy in the total signal fit result observed in
 431 the B_{tag} (Sec. 4.4) needs to be included in the systematic effects. Propagating the two
 432 sources of systematics in the branching fraction calculation results in an additional 0.06%
 433 uncertainty on the branching fraction value.

434 4.12 Measured $B^+ \rightarrow \bar{\Lambda}_c^- X$ inclusive Branching Fraction

435 As the measurement is performed considering only the $\Lambda_c \rightarrow pK\pi$ decays, to evaluate
 436 the inclusive $B^+ \rightarrow \bar{\Lambda}_c^- X$ Branching Ratio on Monte Carlo simulated data one needs
 437 to take into account the value set for the Λ_c Branching Ratio to the specific decay into
 438 that particular final state. The total $Br(\Lambda_c^+ \rightarrow pK^-\pi^+) = 5.53\%$ in Belle Generic MC
 439 (including resonant decays). Using the results from the two dimensional fit performed on
 440 stream 5 and with all the needed factors known, it's possible to examine the agreement
 441 between the expected inclusive $B^+ \rightarrow \bar{\Lambda}_c^- X$ Branching Fraction.

442 Using the expected yields for the two-dimensional fit on stream5 and the B_{tag} fit
443 performed only on signal events, the measured value is $(2.85 \pm 0.07^{stat.})\%$.

444 Instead from the fit result on stream5 for the two-dimensional fit and the result for the
445 B_{tag} fit shown in Fig. 38, the measured value is $(3.03 \pm 0.13^{stat.} \pm 0.12^{syst.})\%$. 

446 The two measured values using Monte Carlo simulated data agree with each other
447 within statistical uncertainties. Moreover they also show agreement within statistical
448 uncertainties with the value set in the Belle MC (which can be determined by counting
449 method): 2.92%.

450 Comparing the obtained values with the branching fraction measured by BaBar exper-
451 iment (see [?]), the uncertainties appear substantially reduced (statistical uncertainties
452 almost by factor four).

453 **5 $B^- \rightarrow D^0$ control decay**

454 To monitor the analysis steps, which are applied to both measured and simulated data, a
455 control decay of the form

456

457
$$B^+ \rightarrow D^0 X, D^0 \rightarrow K^+ \pi^-$$

458 which is much more abundant, is used.

459 **5.1 Dataset used**

460 For this analysis the amount of data and Monte Carlo simulated data used was restricted
461 to the SVD2 period: experiments ranging from 31 to 65. This choice was made to save
462 processing time, anyway most of the $B\bar{B}$ meson pairs were produced in this range of
463 experiments (620×10^6 out of almost 800×10^6).

464 **5.2 Event selection and reconstruction**

465 The approach used for the inclusive decays reconstruction is the same as for the $B \rightarrow \Lambda_c$
466 analysis. The same FEI training was used, though excluding the signal decay $D^0 \rightarrow K^+ \pi^-$
467 from the decay chains used by the FEI to reconstruct the B_{tag} . Same preliminary selection
468 criteria were applied to the tag-side B meson candidates as well.

469 In the *rest of event* (ROE) of the reconstructed B_{tag} meson, to select $D^0 \rightarrow K^+ \pi^-$ signal
470 candidates, the following event selection criteria are applied:

- 471 • $dr < 2$ cm and $|dz| < 4$ cm
472 • $\frac{\mathcal{L}_K}{\mathcal{L}_K + \mathcal{L}_\pi} > 0.6$

473 For the D^0 candidates a vertex fit is performed with `TreeFitter`, requiring it to converge.
474 If there are more than one D^0 combination, then the best candidate based on the χ^2
475 probability is chosen. The D^0 signal region is defined to be $|M_{D^0} - m_{D^0}| < 30$ MeV/ c^2
476 ($\sim 3\sigma$), here m_{D^0} is the nominal mass of D^0 .

477

478 **5.3 Signal selection optimization**

479 Following the same procedure as for the $B \rightarrow \Lambda_c$ analysis, the optimized selection cuts
480 obtained for the event based ratio of the 2-nd to the 0-th order Fox-Wolfram moments,
481 the B_{tag} signal probability and the momentum of the D^0 candidates in the center of mass
482 system are:

- 483 • $foxWolframR2 < 0.3$
484 • $SignalProbability > 0.004$

- 485 • $p_{CMS}^{D^0} > 1 \text{ GeV}/c^2$

486 Figure Fig. 43 shows the distributions of M_{bc} and invariant mass in the signal region
 487 for the $B^- \rightarrow D^0 X$ reconstructed events after the selection cuts were applied.

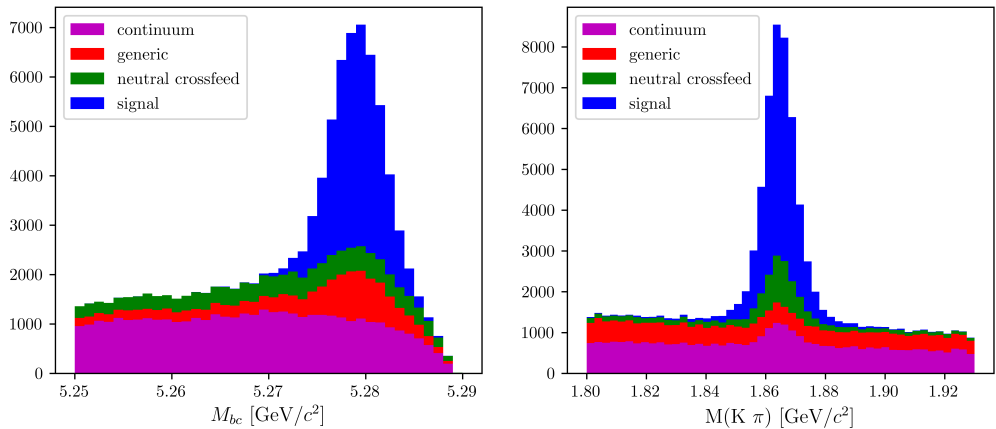


Figure (43) Distribution of M_{bc} (left) and invariant mass of charged correlated D^0 candidates (right), in the signal region after the above mentioned selection cuts.

488 **5.4 Probability Density Functions (PDFs) for two dimensional
 489 fit**

490 As already seen for the $B \rightarrow \Lambda_c$ decays, the signal total 2D PDF is a sum of a "peaking"
 491 and a "flat" component. The peaking events in M_{bc} are fitted with a Crystal Ball. The
 492 flat component in M_{bc} is fitted with a Novosibirsk function. Both "peaking" and "flat"
 493 component have a correspondent peak in the D^0 mass which is fitted with a sum of
 494 three gaussians with a common mean. The fitted distribution of M_{bc} and $M(\pi K)$ are
 495 shown in Fig. 44 with signal MC sample. The "peaking" and "flat" components can be
 496 distinguished by the different colors used. The "flat" component will be from now on
 497 denoted as misreconstructed signal component, as it is relative to signal events where the
 498 tagged B meson is not correctly reconstructed.

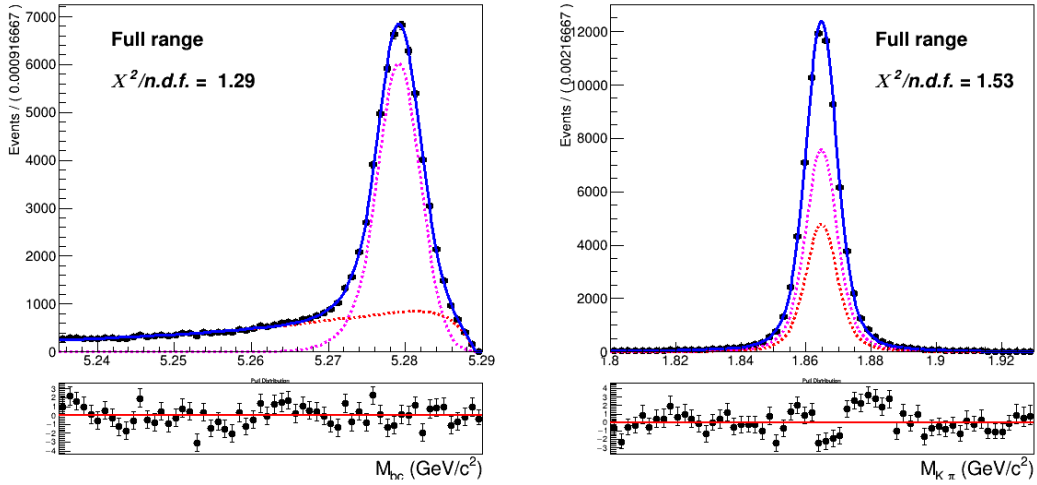


Figure (44) Two dimensional fit of total signal events in M_{bc} and $M(pK\pi)$

499 The generic background deriving from other B^+B^- events presents a similar shape in
500 M_{bc} : it is fitted again with a sum of Crystal Ball and Novosibirsk function. Instead the
501 distribution in the D^0 mass is fitted with a sum of first order Polynomial function and a
502 small gaussian peak, which is due to the small amount of flavor anti-correlated $B^+ \rightarrow D^0$
503 reconstructed events (see Fig. 45). The total two-dimensional PDF is a product of the
504 one-dimensional PDFs in M_{bc} and D^0 mass:

$$P_{B,D^0}^{GenBkg}(M_{bc}, M(K\pi)) = [\Gamma_{CB}(M_{bc}) + \Gamma_{Nov}(M_{bc})] \times [\rho_{pol1}(M(K\pi)) + \rho_G(M(K\pi)) \quad (8)$$

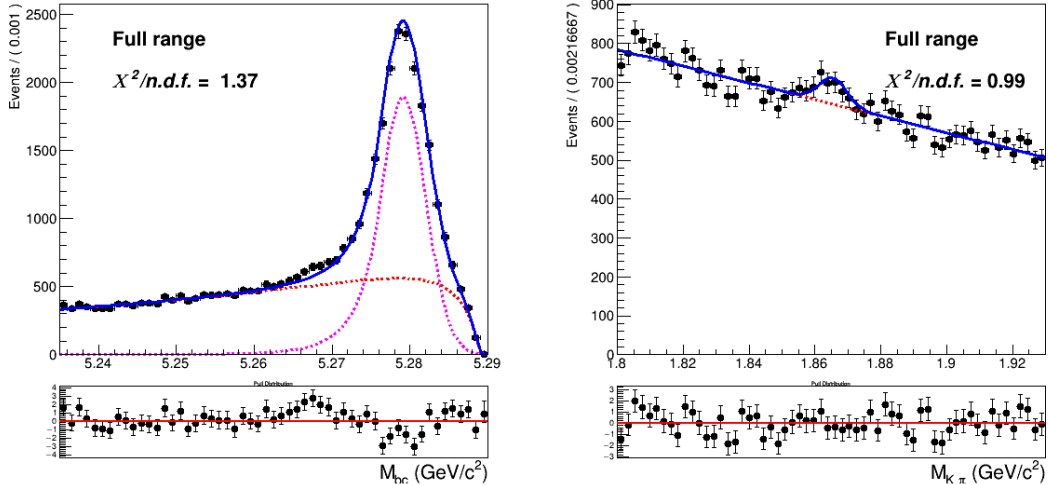


Figure (45) Two dimensional fit of generic (B^+B^-) background events in M_{bc} and $M(K\pi)$.

505 The crossfeed background deriving from $B^0\bar{B}^0$ events is shown in Fig. 46. The M_{bc}
506 distribution is fitted with a sum of Novosibirsk and Argus functions. The distribution in

507 the D^0 mass is fitted with a first order Chebyshev polynomial and the D^0 mass peak is
 508 fitted with the same sum of three gaussians used to describe the signal peak.

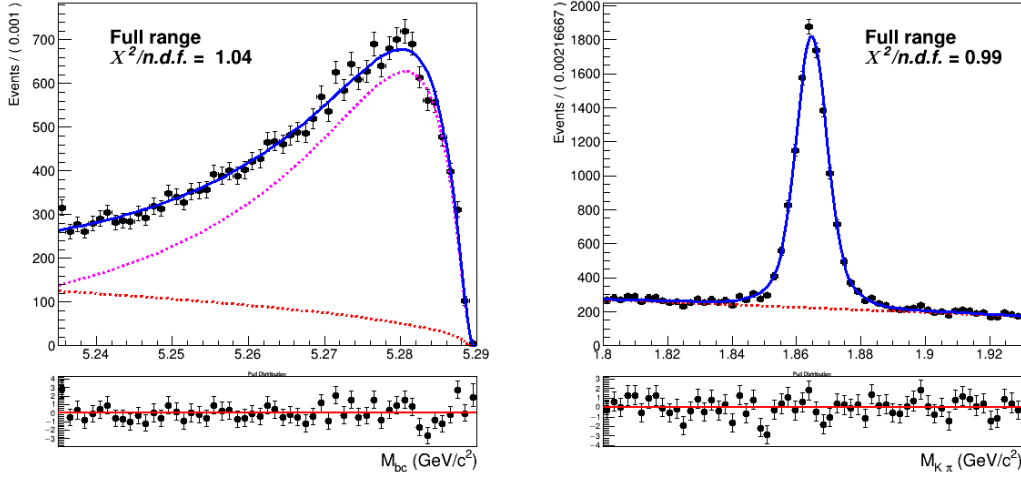


Figure (46) Two dimensional fit of crossfeed ($B^0\bar{B}^0$) events in M_{bc} and $M(K\pi)$.

509 The procedure adopted to model the continuum background is the same used for the
 510 $B \rightarrow \Lambda_c$ decays. Though for this control channel the available statistics is enough to
 511 perform the scaling with all the selection cuts also in the case of the two-dimensional fit.

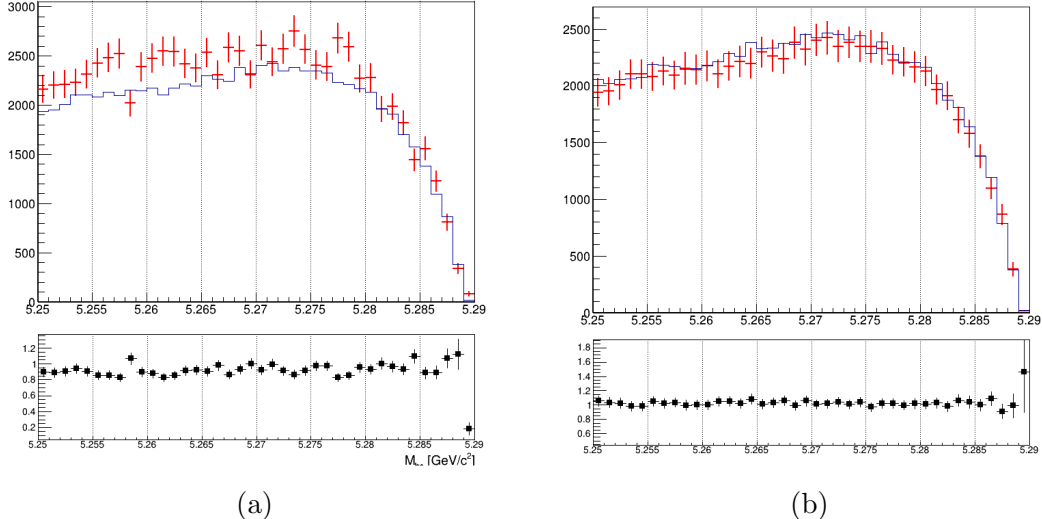


Figure (47) In Fig. 47a M_{bc} distributions of the MC (scaled) off-resonance sample (in red) and on-resonance (in blue). In Fig. 47b M_{bc} distributions of the corrected scaled off-resonance and on-resonance MC continuum.

512 For each bin a correction factor is calculated, in order to have a reasonable match
 513 with the expected continuum background. Fig. 47b shows the applied correction on an

514 independent MC sample. As in the case of $B \rightarrow \Lambda_c$ analysis, then the resulting M_{bc}
 515 distribution is fitted with a Novosibirsk function , whereas the D^0 mass distribution is
 516 fitted with a sum of first order Chebyshev polynomial and the sum of three gaussians used
 517 to describe the signal peak, to describe the peak. The fraction of events in the peak is the
 518 same in on- and off-resonance MC. This method is applied also to scale the off-resonance
 519 data.

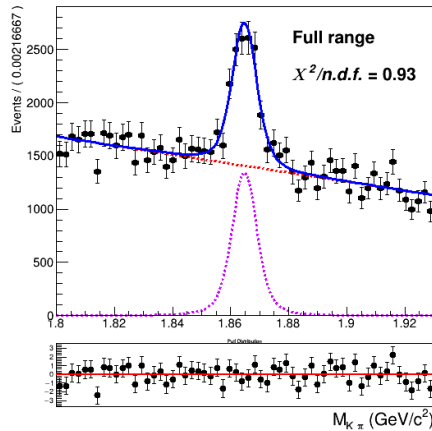


Figure (48) D^0 mass fit of scaled off-resonance Monte Carlo

520 5.5 2D Fit on Monte Carlo simulated data

521 As in the $B \rightarrow \Lambda_c$ study, five streams of Monte Carlo simulated data have been used to
 522 get values for the shaping parameters for the individual components described in the
 523 previous section and the fit model is tested on an independent stream.

524 For the six fits, the exact same conditions (floated parameters and fixed width ratios)
 525 were applied as to the two dimensional fit in the case of the $B \rightarrow \Lambda_c$ study. Exemplary, the
 526 distributions of stream 0 overlaid by the fitted PDF are depicted in Fig. 49 (see Appendix
 527 .2 for the projections of signal regions and sidebands).

528 In Table 6 the yields for reconstructed and misreconstructed signal are listed for each
 529 stream.

530

stream	0	1	2	3	4	5
NrecSig	56986 ± 400	57766 ± 437	55607 ± 426	57068 ± 372	58385 ± 369	57501 ± 437
NmisSig	31453 ± 321	30513 ± 350	32580 ± 350	33340 ± 399	29966 ± 390	32012 ± 355

Table (6) reconstructed and misreconstructed signal yields obtained fitting 6 independent streams

531 To be sure that the PDFs enables us to extract the signal yield in an unbiased way,
 532 the sum of reconstructed and misreconstructed signal yields, i.e. total signal, from the fits
 533 are compared to the true values of each stream (Table 7). There are quite some differences

534 between the fitted signal yield and the true values in individual streams. However, all
 535 these deviations are within statistical expectations.

536

streams	fit	MC truth	fit - MC truth
stream 0	88439 ± 340	88144	+ 295 (+0.33%)
stream 1	88279 ± 361	88551	-272 (-0.31%)
stream 2	88187 ± 360	88487	-300 (-0.34%)
stream 3	90408 ± 372	90149	+ 259 (+0.29%)
stream 4	88351 ± 383	87981	+ 370 (+0.42%)
stream 5	89513 ± 366	89710	-197 (-0.22%)
sum	533177	533022	+155 (+0.03%)

Table (7) Comparison of fitted and truth-matched total signal events in each stream.

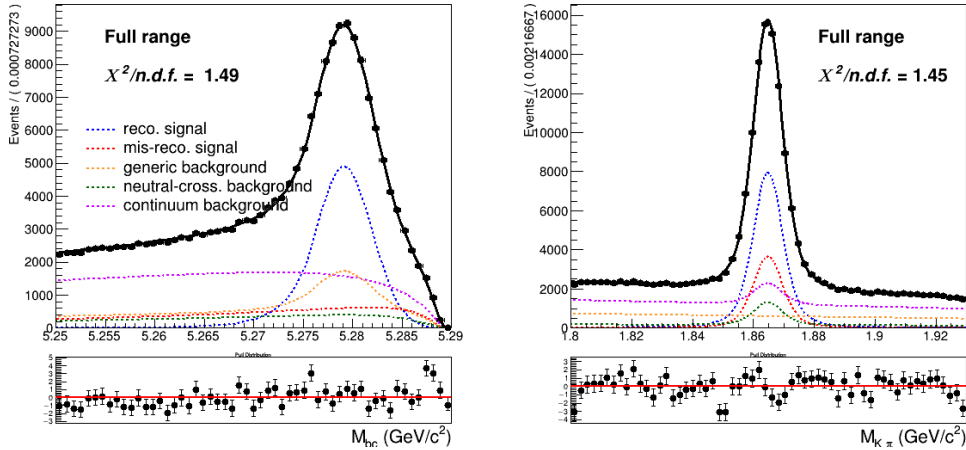


Figure (49) Two dimensional fit on stream 0 Monte Carlo simulated data.

537 5.6 2D Fit on data

538 After obtaining the model for the continuum background scaling and correcting the M_{bc}
 539 distribution of the off-resonance data, the model tested on Monte Carlo simulated data is
 540 applied on data with same free parameters and yields. Fig. 50 shows the projections of the
 541 two dimensional fit (see Appendix .2 for the projections of signal regions and sidebands).

542 Yields for the reconstructed and misreconstructed signal and for generic background
 543 are obtained from the fit:

NrecSig	36453 ± 367
NmisSig	23911 ± 309
Generic	27740 ± 408

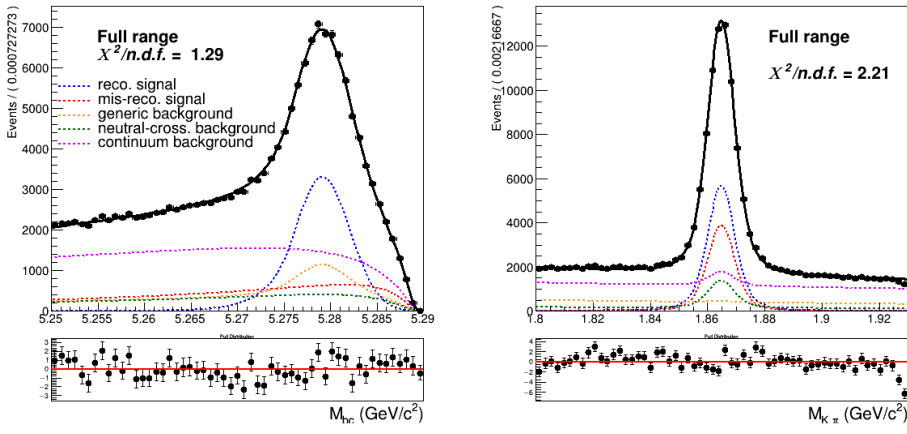


Figure (50) Two dimensional fit on Data

ratio	MC	DATA
NmisSig/NrecSig	0.56 ± 0.01	0.65 ± 0.01
NmisSig/Generic	0.90 ± 0.02	0.86 ± 0.02
Generic/NrecSig	0.62 ± 0.01	0.76 ± 0.02

Table (8) Comparison of ratios of yields from the two dimensional fits on Monte Carlo simulated data and on Data.

545 The total normalization from the fit is 174230 ± 407 (to be compared with the total
 546 data events: 173964).

547

548 5.7 Probability Density Functions (PDFs) for the B_{tag}

549 Like for the signal model in the 2D fit the M_{bc} distribution of the tagged charged B
 550 mesons is fitted with a Crystal Ball as for the reconstructed signal component, whereas
 551 the misreconstructed signal component is fitted with a Novosibirsk function (Fig. 51a).

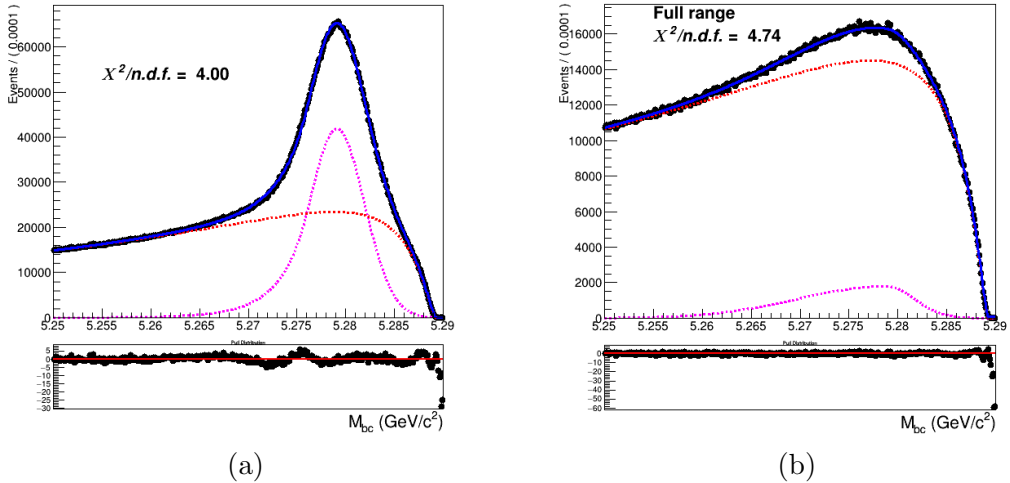


Figure (51) On the left: fitted distribution of tagged charged B mesons, reconstructed signal events (magenta) are described by a Crystal Ball whereas the misreconstructed signal events (red) are described by a Novosibirsk function. On the right: Crossfeed distribution fitted with a sum of Novosibirsk (red) and asymmetric Gaussian PDF (magenta)

552 The crossfeed background is fitted instead with a sum of a Novosibirsk and an asymmetric
 553 Gaussian PDF (Fig. 51b).

554

555 Regarding the continuum background component, same procedure used for the 2D fit was
 556 applied to the M_{bc} distribution of the continuum background in this case.

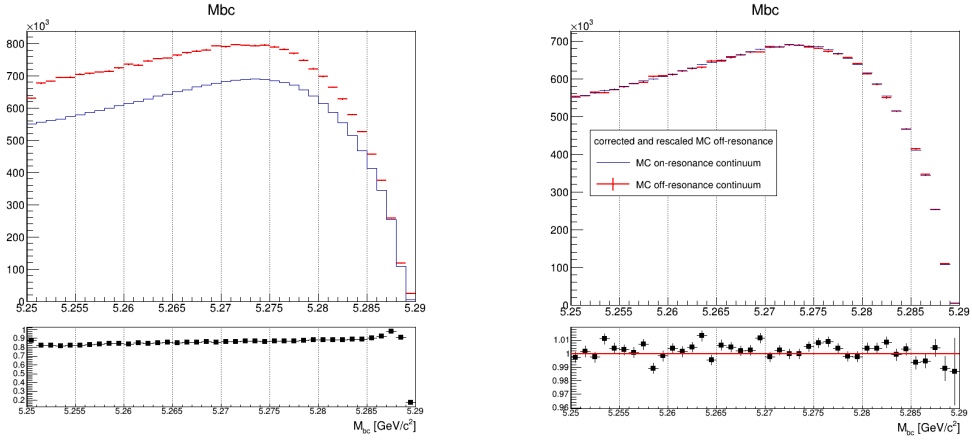


Figure (52) On the left: M_{bc} distributions of the MC off-resonance sample and the MC continuum sample. On the right: M_{bc} distributions of the corrected scaled MC off-resonance and on-resonance MC continuum.

557 5.8 B_{tag} Fit on Monte Carlo simulated data

558 An independent Monte Carlo stream was used to test the total fit model on tagged B
 559 mesons candidates. The usual condition is applied to the crossfeed background events:
 560 the ratio between its contribution and misreconstructed signal events is fixed from the
 561 other Monte Carlo stream.
 562 In this fit the shaping parameters that are not kept fixed are the Crystal Ball width (σ_{CB})
 563 and the width of the Novosibirsk function describing the misreconstructed signal events.
 564 As in the case of B_{tag} fit in Sec. 4 the range for the fit is restricted to values between
 565 5.250 and 5.287 GeV/c^2 .

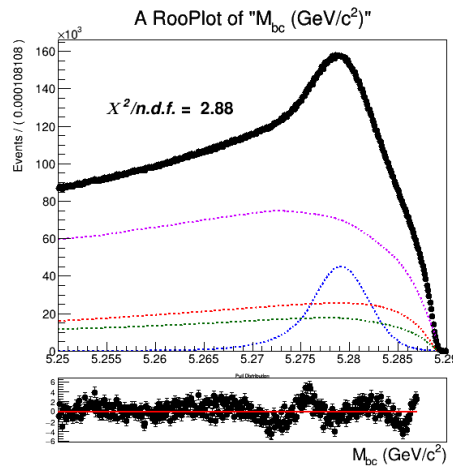


Figure (53) Total fit of tagged B mesons

566 Yields for the reconstructed and misreconstructed signal are obtained from the fit:

NrecSig	$3.25110 \cdot 10^6 \pm 6759$
NmisSig	$7.41107 \cdot 10^6 \pm 5341$

568 One can then compare the sum NrecSig+NmisSig (the so called total signal) with the
 569 true value known from the Monte Carlo and the same for the total number of events in
 570 this particular stream:

	fit	MC value
Total Signal	$10.662 \cdot 10^6 \pm 5249$	$10.671 \cdot 10^6$
Total events	$38.601 \cdot 10^6 \pm 6886$	$38.610 \cdot 10^6$

573 **5.9 B_{tag} Fit on data**

574 The fit model tested on Monte Carlo simulated data is then applied with the same method
 575 on data Fig. 54.

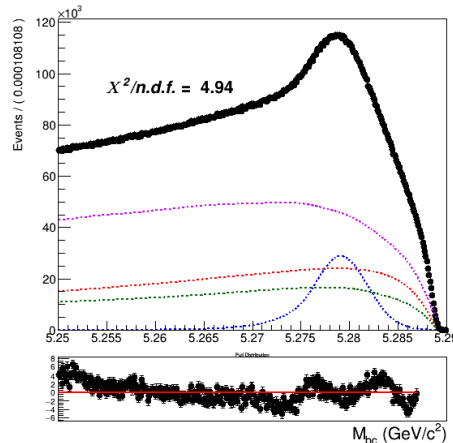


Figure (54) Total fit of tagged B^+ mesons candidates on data

576 Yields for the reconstructed and misreconstructed signal are obtained from the fit:

NrecSig	$2.011 \cdot 10^6 \pm 5858$
NmisSig	$6.975 \cdot 10^6 \pm 4667$
Total Signal	$8.982 \cdot 10^6 \pm 4587$

ratio	MC	DATA
NmisSig/NrecSig	2.28 ± 0.01	3.47 ± 0.01

Table (9) Comparison of ratios of yields from the tagged B mesons fits on Monte Carlo simulated data and on Data.

578 **5.10 PID efficiency correction**

579 The kaon identification efficiency was studied in detail Belle Note 779
 580 (http://belle.kek.jp/secured/belle_note/gn779/bn779.ps.gz). The decay
 581 $D^{*+} \rightarrow D^0\pi^+$ followed by $D^0 \rightarrow K^-\pi^+$, was used to examine the Kaon identification
 582 efficiency difference between data and MC in *Belle*. The efficiency ratio dependence on
 583 Kaon charge, momentum and polar angle is considered. The Kaon ID efficiency is defined as
 584

585
$$\epsilon_{KID} = \frac{\text{number of } K \text{ tracks identified as } K}{\text{number of } K \text{ tracks}}$$

586

587 and the comparison between MC efficiency and data efficiency by a double ratio
 588 defined as

589
$$R = \epsilon^{data}/\epsilon^{MC}$$

591

592 The average Kaon ID correction is estimated to be $R = 0.976 \pm 0.008$.

593 **5.11 D^0 and FEI efficiency**

594 The efficiency in reconstructing the D^0 after correctly tagging the charged B meson, can
 595 be estimated from the 2D fit on Monte Carlo simulated data, using the reconstructed
 596 signal yield and from a sample of B_{tag} candidates reconstructed in signal events in the
 597 Monte Carlo: where from B^+B^- at least a D^0 decaying into πK is produced.

598 For the latter a fit is performed to extract the yield of correctly tagged B mesons (Fig.
 599 55)

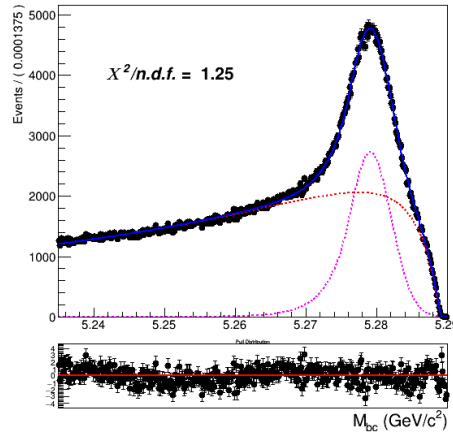


Figure (55) Fit of tagged B mesons in the "signal events" sample

600 Yields for the reconstructed and misreconstructed signal :

NrecSig	$1.46779 \cdot 10^5 \pm 767$
NmisSig	$6.16717 \cdot 10^5 \pm 1028$

602 From this and the results listed in Sec. 5.5 the efficiency to reconstruct D^0 is obtained :

603

$$604 \quad \epsilon_{D^0} = \frac{N_{recSig}(2D)}{N_{recSig}((B_{tag}^{sig})} = 39.1 \pm 0.4\%^2 \quad (\text{KID efficiency corrected value for data: } 38.2\%)$$

605

606 The results from the fit shown in (Fig. 55) can be used also to calculate the FEI tag-side
 607 efficiency for signal events, i.e. the efficiency to tag the B meson accompanying a B_{sig}
 608 decaying into a D^0 on the signal side. Whereas results from the fit of charged B_{tag} shown
 609 in Fig. 51a can be used to calculate the hadronic tag-side efficiency in the generic B^+B^-
 610 events case.

611 The ratio of the two efficiencies is found to be: $\frac{\epsilon_{FEI,sig}^+}{\epsilon_{FEI}^+} = 1.50 \pm 0.01$

612

613 5.12 Measured $B^+ \rightarrow \bar{D}^0 X$ inclusive Branching Fraction

614 The inclusive branching fraction of $B^+ \rightarrow \bar{D}^0 X$ can be determined by:

$$Br(B^+ \rightarrow \bar{D}^0) = \frac{r \cdot \epsilon_{FEI}^+}{Br(D^0 \rightarrow K^+\pi^-)\epsilon_{D^0}\epsilon_{FEI,sig}^+} \quad (9)$$

615 Where

- 616 • $r = \frac{N_{tag,D^0}}{N_{tag}}$ is the ratio of reconstructed signal yield in the two dimensional fit and in
 617 the M_{bc} fit of the tagged B mesons.
- 618 • ϵ_{D^0} is the D^0 reconstruction efficiency calculated as fraction of reconstructed signal
 619 events with correct tag of which then also a correctly reconstructed D^0 is recon-
 620 structed in the signal side.
- 621 • ϵ_{FEI}^+ represents the hadronic tag-side efficiency for generic B^+B^- events
- 622 • $\epsilon_{FEI,sig}^+$ represents the hadronic tag-side efficiency for B^+B^- events where one of the
 623 two B mesons decays inclusively into the signal channel ($D^0 \rightarrow K^+\pi^-$)
- 624 • $Br(D^0 \rightarrow K^+\pi^-) = 3.8\%$ in Belle DECAY.DEC table, $Br(D^0 \rightarrow K^+\pi^-) = 3.95\%$
 625 in PDG.

626 In Monte Carlo: $Br(B^+ \rightarrow \bar{D}^0) = 79.4 \pm 0.6^{(stat.)}\%$ (true MC value: 79.1%) In

627 Data: $Br(B^+ \rightarrow \bar{D}^0) = 78.2 \pm 0.82^{(stat.)}\%$

628

²the error reflects the limited Monte Carlo statistics

629 KID efficiency corrected: $Br(B^+ \rightarrow \bar{D}^0) = 80.1 \pm 0.8^{(stat.)}\%$ (PDG value: $79 \pm 4\%$)

630

631 The systematic uncertainties were estimated to be almost equivalent to the statistical
632 uncertainty. Sec. 5.12 lists the contribution of the various sources of systematics.

633

PID	0.5 %
ϵ_{D^0}	0.8 %
FEI efficiency	0.5 %
continuum background modelling	0.2 %
Total	1.1 %

Table (10) Sources of systematic uncertainties.

634 **6 $B^- \rightarrow \bar{\Lambda}_c^-$ decays**

635 Applying the same procedure already illustrated in Sec. 4, the optimized selection cuts for
 636 the charged flavor-anticorrelated decays are:

- 637 • $\text{foxWolframR2} < 0.3$
 638 • SignalProbability > 0.1
 639 • $p_{CMS}^{\Lambda_c} < 1.5 \text{ GeV}/c$

640 **6.1 Probability Density Functions (PDFs) for the two dimensional fit**

642 The PDFs used to describe the signal distributions are the same already used in Sec. 4.1
 643 (only the shaping parameters differ) and an example of the 2D fit is shown in Fig. 56.
 644 Also the generic background deriving from other B^+B^- events presents similar shapes of
 645 the distributions as shown already in Sec. 4.1, therefore the probability density functions
 646 used are the same (fit is shown in Fig. 57).

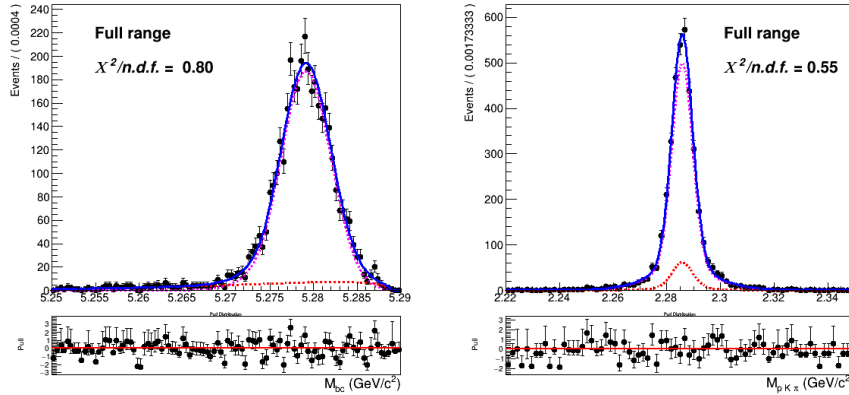


Figure (56) Two dimensional fit of total signal events in M_{bc} and $M(pK\pi)$.

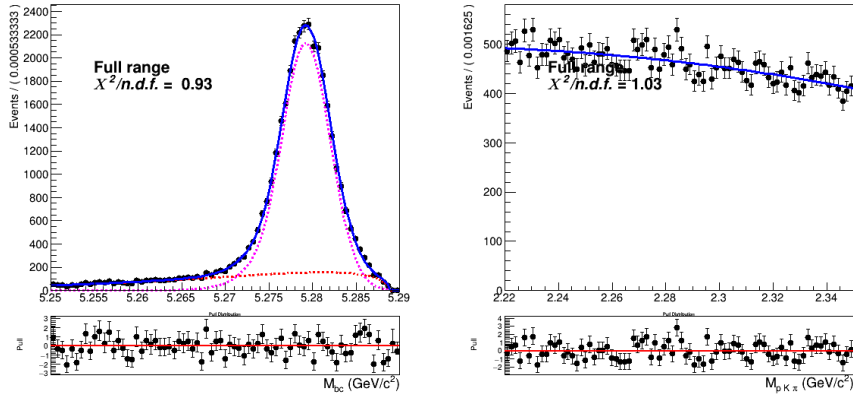


Figure (57) Two dimensional fit of generic (B^+B^-) events in M_{bc} and $M(pK\pi)$.

647 The same can be said about the misreconstructed B^0 events (Fig. 58)

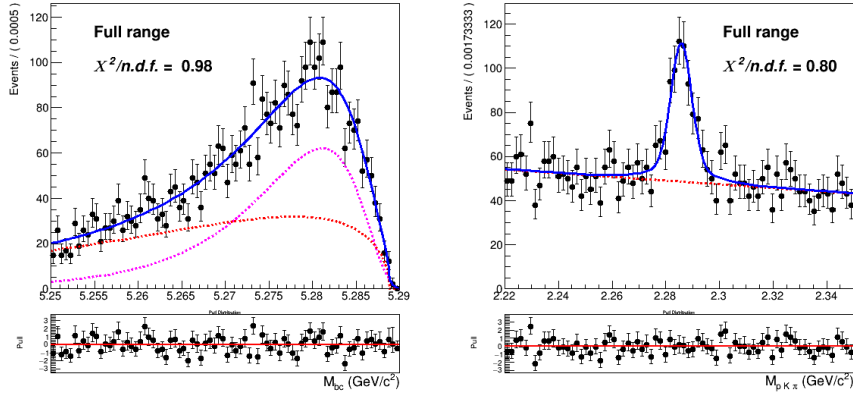


Figure (58) Two dimensional fit of crossfeed ($B^0\bar{B}^0$) events in M_{bc} and $M(pK\pi)$.

648 To check that the shapes determined using 5 streams of Monte Carlo are describing with
 649 reasonable accuracy the 2D distribution, the projections of the fit of the two-dimensional
 650 distributions in the signal and sideband regions are plotted (Fig. 60 - Fig. 62). One can see
 651 the same tendencies of undershooting/overshooting the Λ_c invariant mass peak, as in the
 652 case of charged correlated decays (Figures 15 - 16). But when examining the independent
 653 Monte Carlo stream distribution overlaid by the determined PDF in the very same regions
 654 (see Figures 63 - 65) those effects are so much diminished, according to the statistics, that
 655 the effects are within statistical fluctuations and therefore negligible, contrary to the case
 656 of charged flavor-correlated decays.

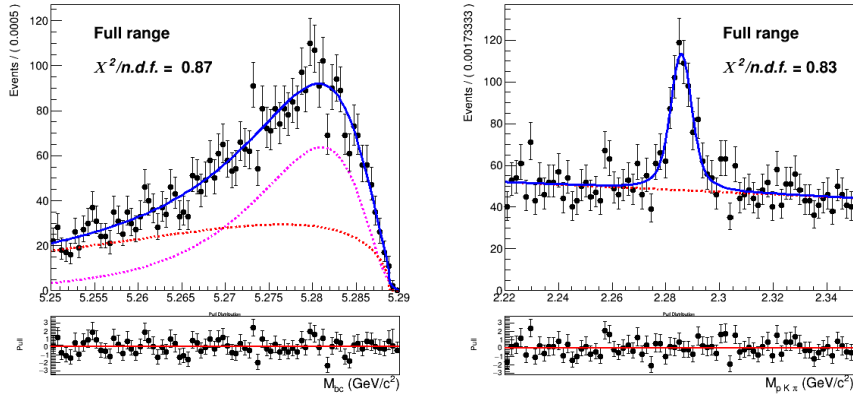


Figure (59) Two dimensional fit of crossfeed ($B^0 \bar{B}^0$) events in M_{bc} and $M(pK\pi)$.

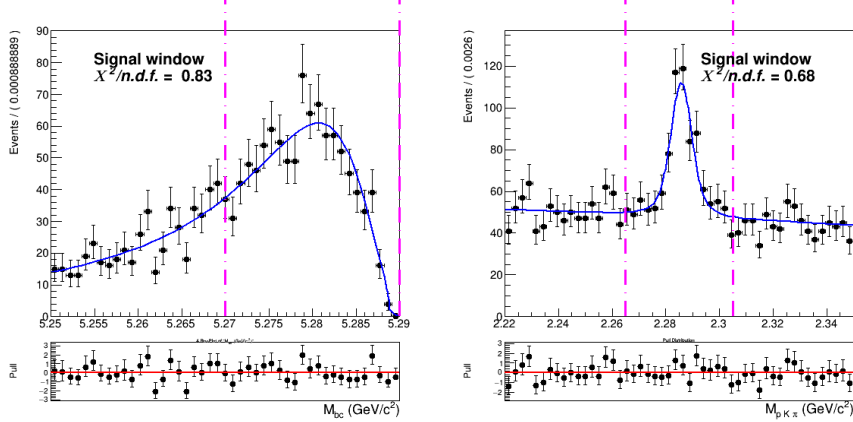


Figure (60) Signal region projections in M_{bc} and $M(pK\pi)$ of the fit of crossfeed events.

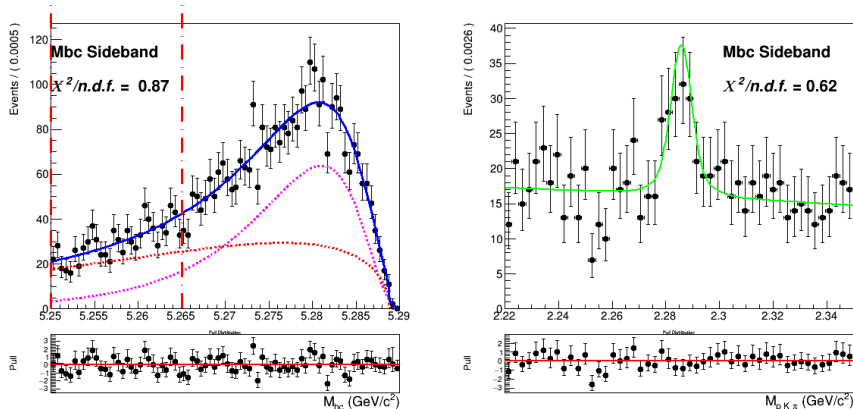


Figure (61) M_{bc} sideband region projection of the fit of crossfeed events in $M(pK\pi)$.

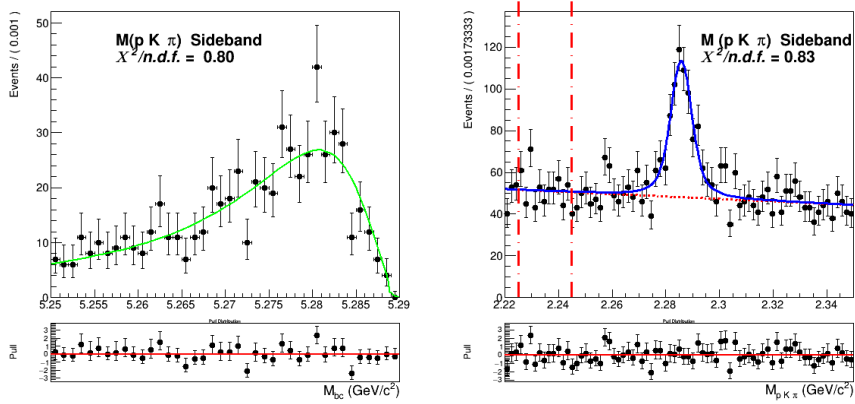


Figure (62) $M(pK\pi)$ sideband region projection of the fit of crossfeed events in M_{bc} .

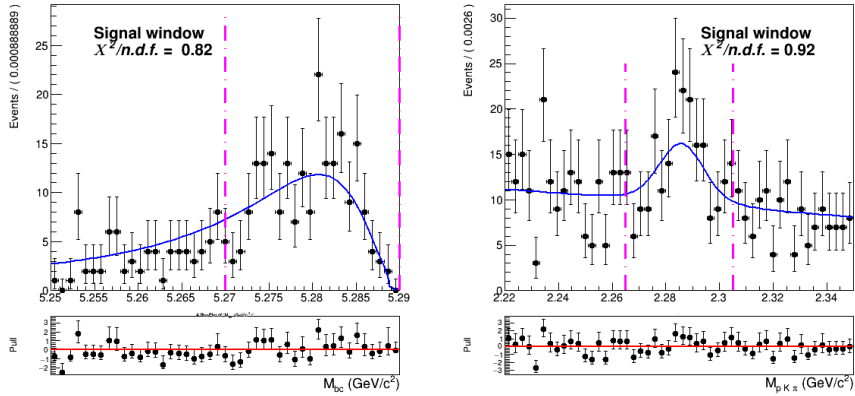


Figure (63) Signal region projections in M_{bc} and $M(pK\pi)$ of the fit of crossfeed events.

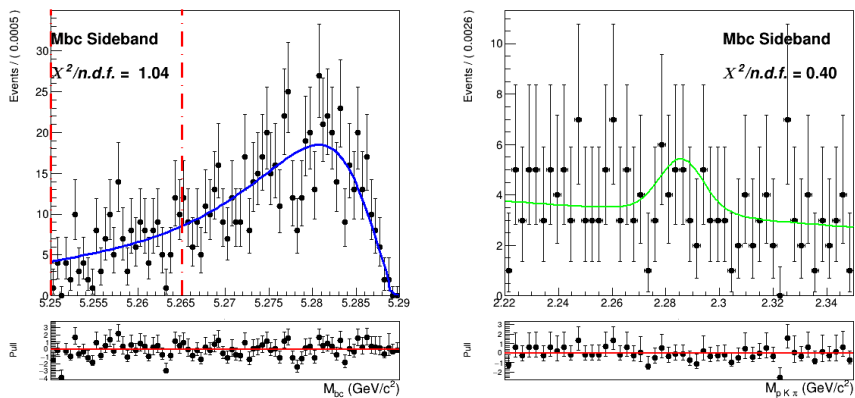


Figure (64) Two dimensional fit of crossfeed ($B^0\bar{B}^0$) events in M_{bc} and $M(pK\pi)$.

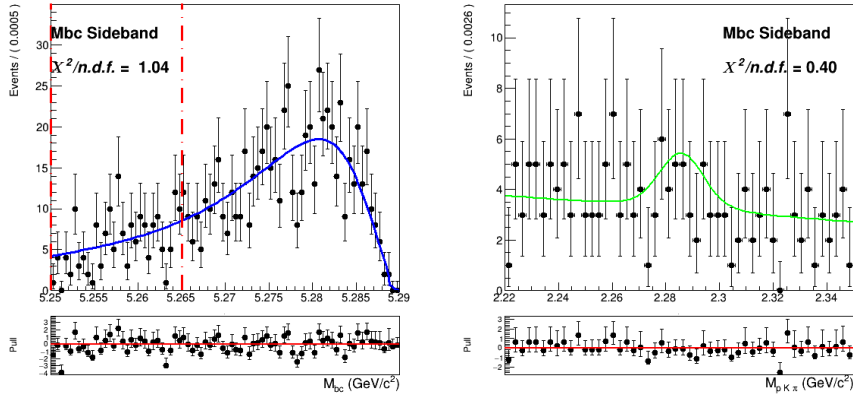


Figure (65) Two dimensional fit of crossfeed ($B^0 \bar{B}^0$) events in M_{bc} and $M(pK\pi)$.

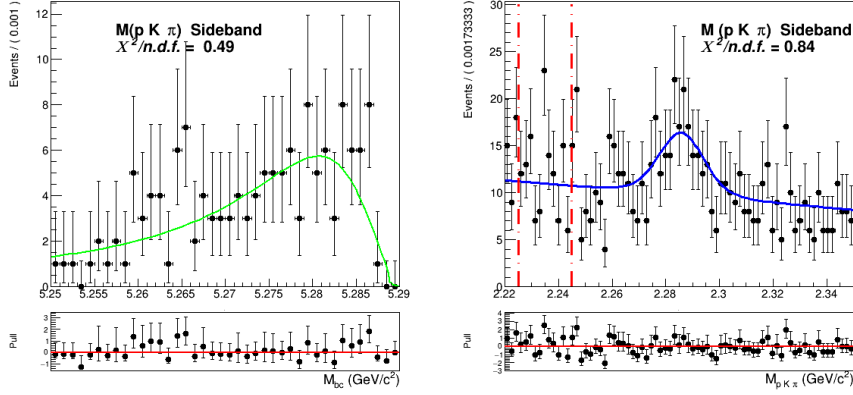


Figure (66) Two dimensional fit of crossfeed ($B^0 \bar{B}^0$) events in M_{bc} and $M(pK\pi)$.

657 The procedure adopted to model the continuum background is the same used for the
 658 charged correlated $B \rightarrow \Lambda_c$ decays. To obtain the shape that can describe the continuum
 659 background M_{bc} distribution, the continuum suppression is not applied on the off-resonance
 660 continuum sample in order to acquire more statistics. It is then scaled and corrected for
 661 the *SignalProbability* correlated effects. The scaling and bin-correction procedure was

662 carried out on a sample of five streams of on- and off-resonance MC. From a ratio plot,
 663 like the one in Fig. 67a, showing the continuum on-resonance distribution in M_{bc} and the
 664 scaled continuum on-resonance distribution without the continuum suppression applied,
 665 the bin-correction is obtained to correct the off-resonance data in the scaling procedure.
 666 The validity of this procedure is first tested on the sixth independent MC sample: Fig. 67b
 667 shows the scaled and bin-corrected off-resonance continuum histogram compared with the
 668 continuum on-resonance distribution of the independent stream. Compared to the charged
 669 correlated decays one can notice larger statistical fluctuations but the overall result looks
 670 still fairly reasonable, in order to obtain the PDF describing the distribution by fitting its
 671 histogram (see Fig. 68a), i.e. with a Novosibirsk function.
 672 Since in the Λ_c invariant mass one doesn't expect correlation effects, one can fit directly the
 673 properly scaled distribution with a first order polynomial (see Fig. 68b) It is possible then
 674 to check the validity of the whole procedure on the on-resonance Monte Carlo independent
 675 stream (Fig. 69)

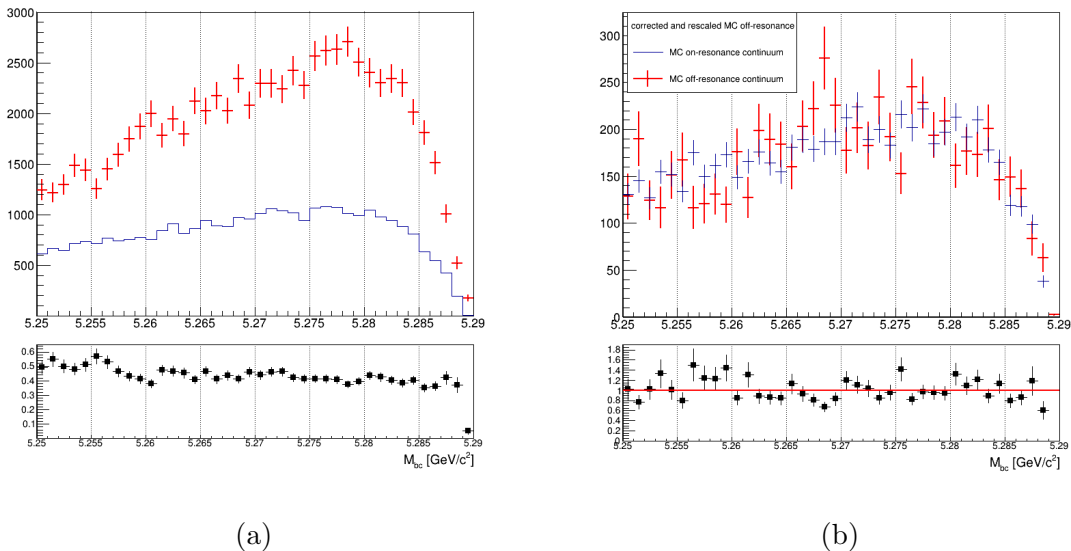


Figure (67) On the left: M_{bc} distributions of the MC off-resonance sample without continuum suppression and the MC continuum sample with applied continuum suppression (5 streams). On the right: M_{bc} distributions of the corrected scaled MC off-resonance and on-resonance MC continuum (independent stream).

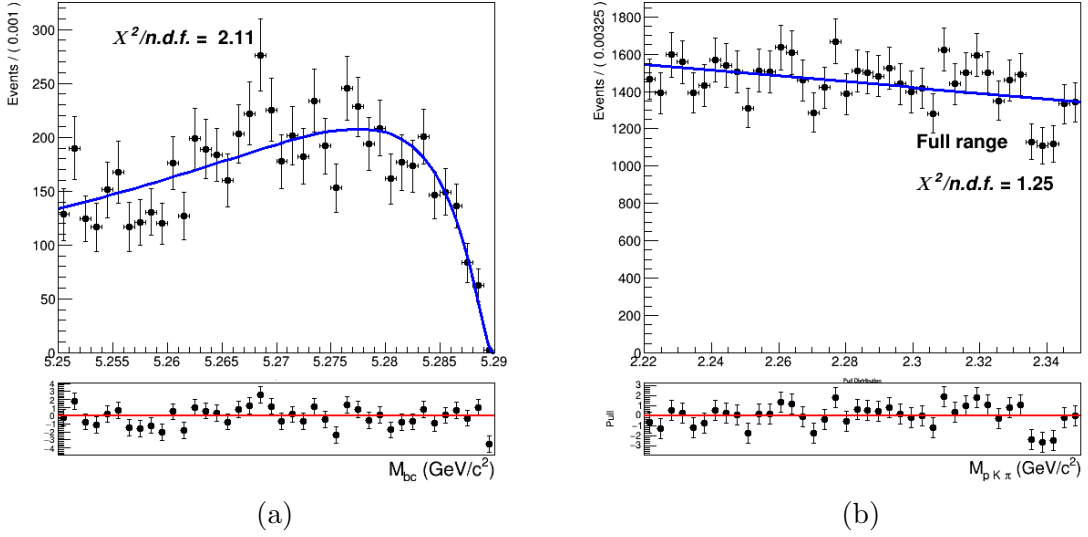


Figure (68) On the left: fit of the M_{bc} distribution MC (scaled and corrected) off-resonance continuum (one stream). On the right: fit of the Λ_c invariant mass distribution of five stream scaled off-resonance continuum.

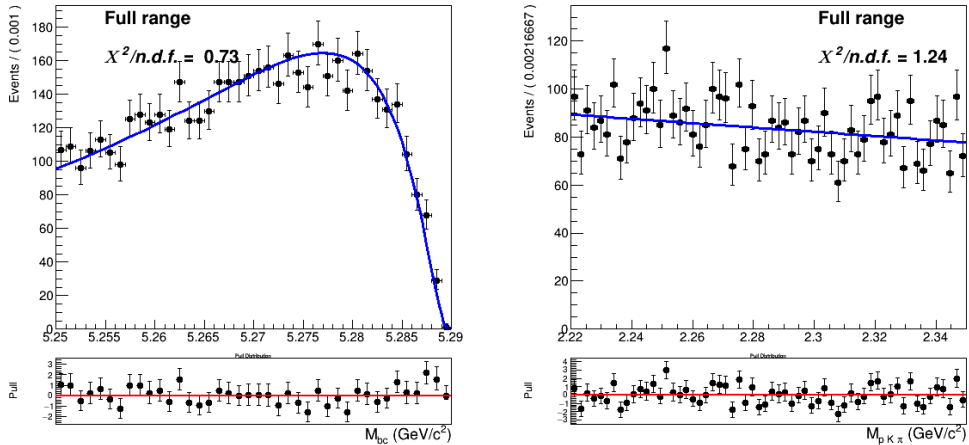


Figure (69) Continuum M_{bc} and $M(pK\pi)$ distributions overlaid by the PDFs obtained in fits shown in Figures 68a - 68b

676 6.2 Two dimensional fit

677 After obtaining the PDFs describing the various signal/background components using five
 678 streams statistics, the fit model is tested with six fits on the six independent Monte Carlo
 679 streams. The conditions for these six two dimensional fits are again the same used for
 680 the charged correlated decays (see Sec. 4.2). Exemplary, the distributions of stream 0

681 overlaid by the fitted PDF are depicted in Fig. 70 (see for the projections in signal and
 682 sideband regions). In Table 1 the signal yields of the fits (**Reconstructed Signal**) to
 683 the two dimensional distributions for the six streams of $B^- \rightarrow \bar{\Lambda}_c^-$ flavor-anticorrelated
 684 decays are listed and compared to the expected yields of reconstructed signal, and fitted
 685 and truth-matched total signal events are also compared, together with their deviations.

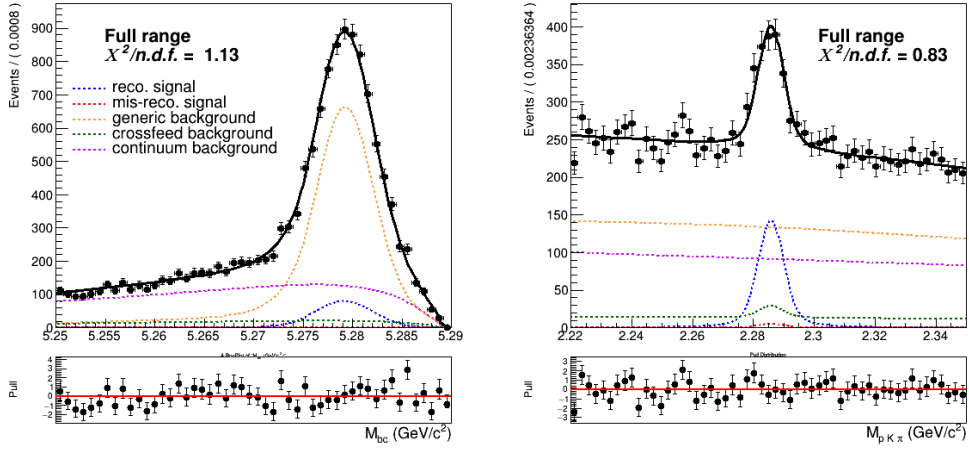


Figure (70)

	Reconstructed Signal		Total Signal			
	fit	expected	fit	MC truth	fit - MC truth	
stream 0	729 ± 63	660 ± 21	810 ± 63	765	45	5.9 %
stream 1	729 ± 61	698 ± 29	791 ± 61	785	6	0.8%
stream 2	760 ± 66	718 ± 29	800 ± 65	797	3	0.4%
stream 3	719 ± 68	702 ± 29	764 ± 65	802	-38	-4.7%
stream 4	830 ± 71	710 ± 29	810 ± 71	804	6	0.7%
stream 5	640 ± 54	675 ± 29	699 ± 59	765	-66	-8.6%
sum	4407	4163	4674	4718	-44	-0.9%

Table (11) Comparison of fitted and expected signal yields, fitted and truth-matched total signal for six streams of Belle generic MC when fitting the two dimensional distributions of M_{bc} and $M(pK\pi)$.

686 Except for stream 4 all the fits show values of reconstructed signal within the 1σ uncer-
 687 tainties in agreement with the expected ones, but as already encountered in Sec. 4.2 a
 688 tendency of overestimation can be seen also in these fits, confirmed by the fit shown in Fig
 689 72. Again this small, but not negligible, bias has to be taken into account while fitting the
 690 data.

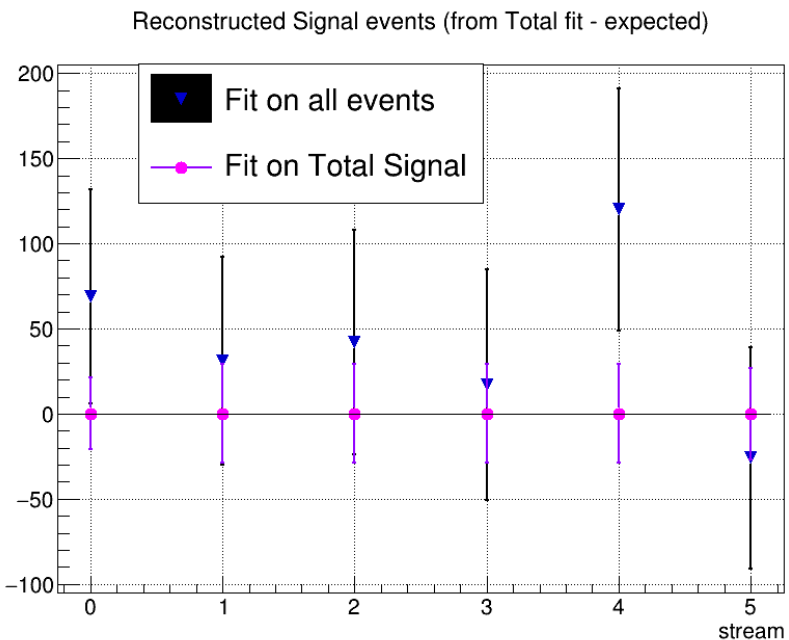


Figure (71) Differences between results from the fits and "expected" values for signal yields as reported in the first columns on Table 11 .

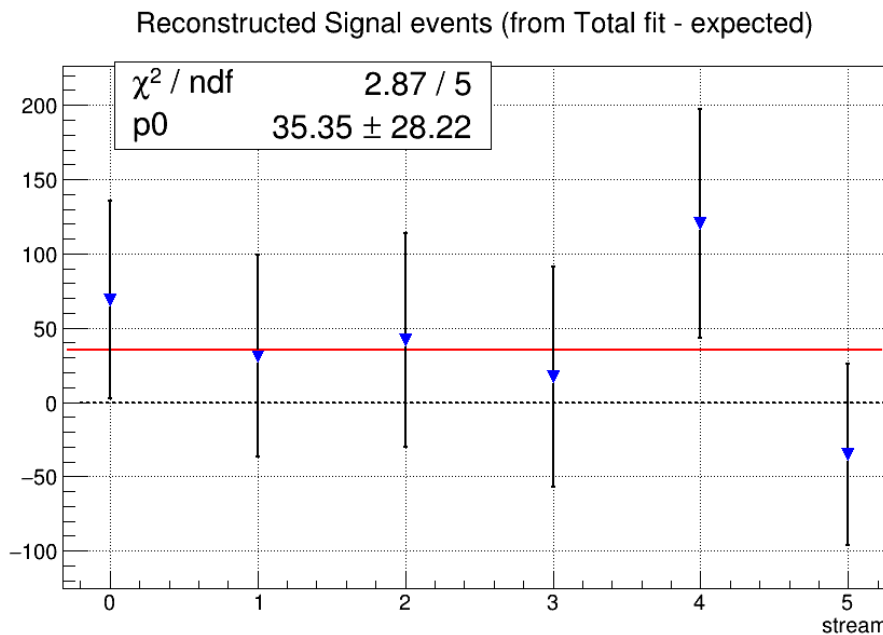


Figure (72)

691 Also the behaviour for different signal-to-background ratio was investigated using five
 692 independent streams. The amount of total signal is varied between 50% and 150% of the

693 nominal values. The amount of background varies according to poissonian fluctuations,
 694 as it is taken from the five independent streams. The plot in Fig. 73 shows the values
 695 of reconstructed signal obtained in the total fits versus those expected by the fits on
 696 total signal events. The performed linear fit suggests a compatibility with a 1:1 relation,
 697 although the points are located above the bisector line (dotted blue line).

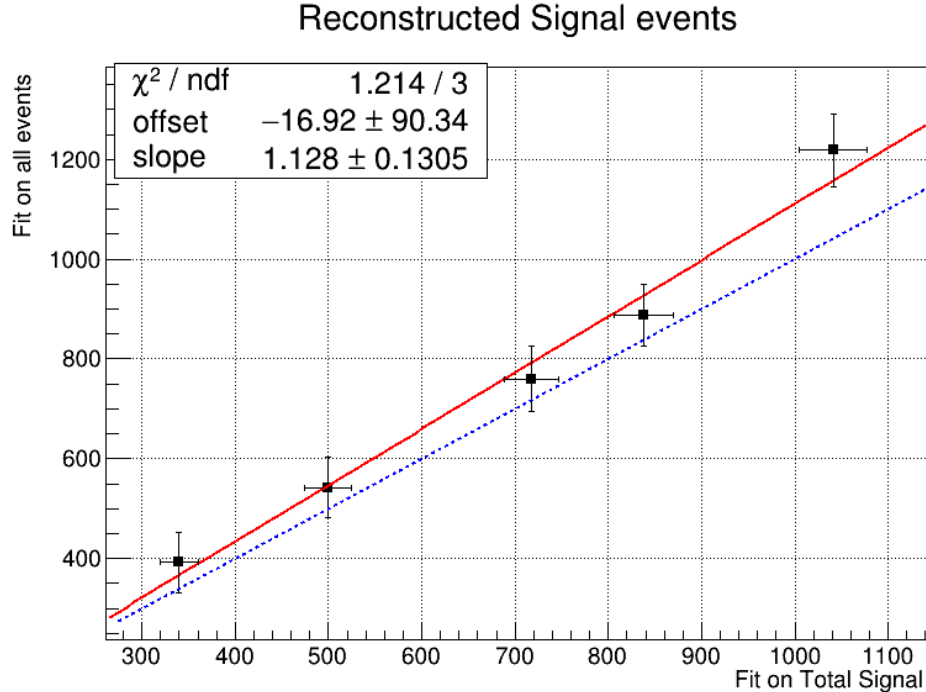


Figure (73) Linearity test: on the x-axis the obtained reconstructed signal yields from fits on different amounts of total signal; on y-axis the yields of reconstructed signal obtained fitting all events. The values are fitted with a red continuous line, whereas the blue dotted line corresponds to a 1:1 linear dependence.

698 Toy MC pseudo-experiments were performed as well (see Appendix).

699 6.3 Probability Density Functions (PDFs) for the B_{tag}

700 The M_{bc} distribution of the tagged B mesons is fitted with a Crystal Ball as for the
 701 "peaking" component and the "flat" component is fitted with a Argus function (Fig. 74a).
 702 The crossfeed background, consisting of neutral B mesons tagged as charged B , is fitted
 703 instead with a sum of a Novosibirsk and an asymmetric Gaussian PDF (Fig. 74b).

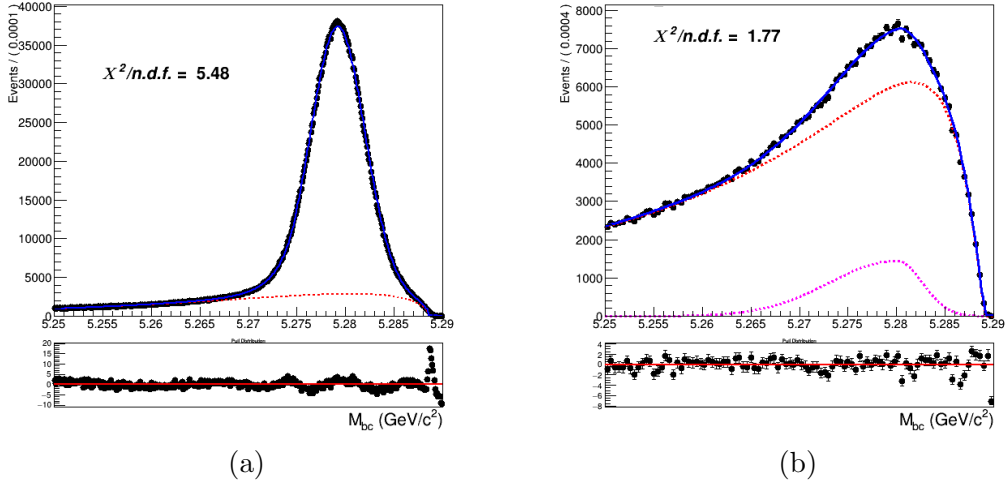


Figure (74) On the left: fitted distribution of tagged charged B mesons, reconstructed signal events (magenta) are described by a Crystal Ball whereas the misreconstructed signal events (red) are described by an Argus function. On the right: Crossfeed distribution fitted with a sum of Novosibirsk (red) and asymmetric Gaussian PDF (magenta)

704 As for the continuum background, same procedure as the one in the case of charged
 705 flavor-correlated decays is adopted:

- 706 • first the off-resonance sample is scaled accordingly with all the included cuts.
- 707 • the ratio between the scaled off-resonance and the on-resonance in MC is calculated
 708 in each bin (see Fig. 75a)
- 709 • the bin-correction is applied on an independent stream and the scaled and bin-
 710 corrected M_{bc} distribution is compared with the on-resonance distribution as shown
 711 in Fig. 75b

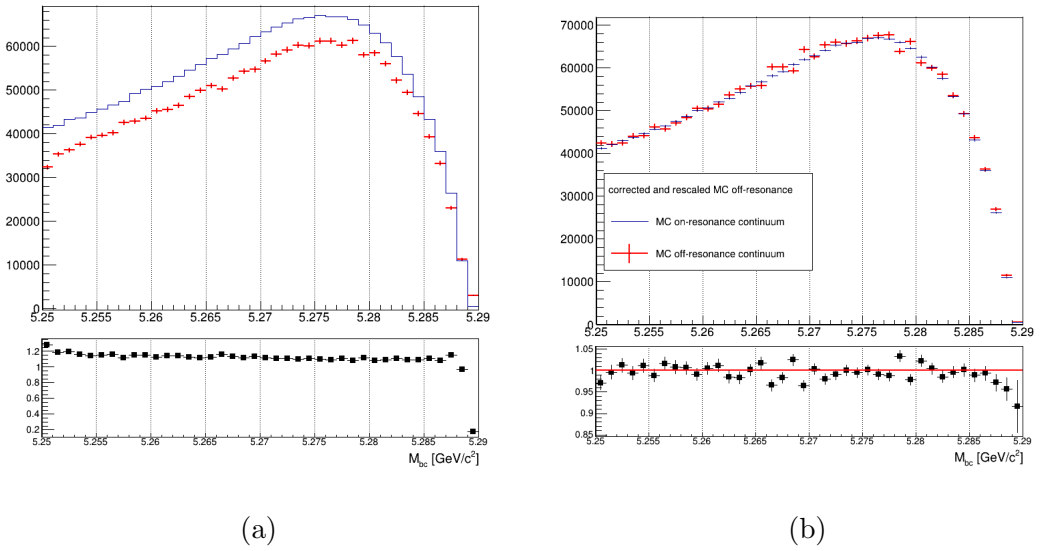


Figure (75) On the left: M_{bc} distributions of the MC off-resonance sample and the MC continuum sample with applied continuum suppression. On the right: M_{bc} distributions of the corrected scaled MC off-resonance and on-resonance MC continuum.

712 **6.4 B_{tag} fit**

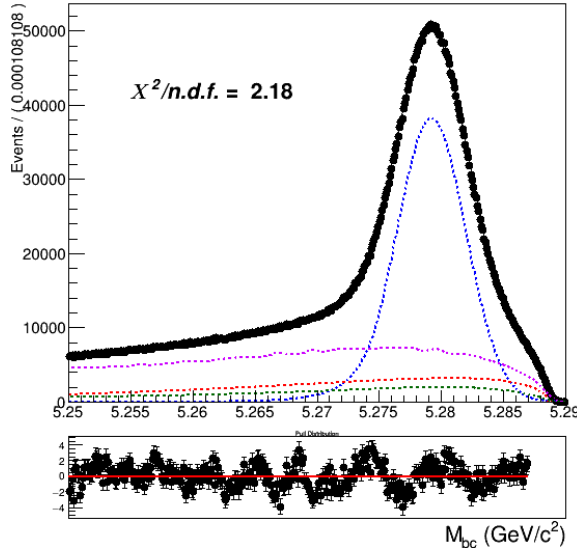


Figure (76) Total fit of tagged B mesons on Monte Carlo simulated data.

713 An independent Monte Carlo stream was used to test the total fit model on tagged B
 714 meson candidates. As in the 2D fit, the parameter for the width, σ_{CB} , of the Crystal Ball is
 715 floated and the ratio between expected crossfeed background events and misreconstructed
 716 signal events is fixed from the MC. The Argus function describing the misreconstructed
 717 signal is also not fully constrained: the parameter describing the tail is free. As in the
 718 previous B_{tag} fits, the range for the fit is restricted to values between 5.250 and 5.287
 719 GeV/c^2 . Yields for the reconstructed and misreconstructed signal are obtained from the
 720 fit:

721

NrecSig	$2.5099 \cdot 10^6 \pm 4408$
NmisSig	$7.82307 \cdot 10^5 \pm 2936$

723 The Total Signal (the sum NrecSig+NmisSig) is 3292168 ± 2423 (to be compared with
 724 3299629 from the Monte Carlo), which means a $\sim 3\sigma$ underestimation. As in the case of
 725 charged flavor-correlated decays, this can produce some systematic effect which needs to
 726 be taken into account. In fact, a slight underestimation of the Total Signal is found also
 727 in the result of the toy Monte Carlo study³: Fig. 77 shows the results for the Total Signal
 728 events and one can notice a mean value for the pulls consistently below zero.

³as usual performed with 3×10^3 pseudo-datasets

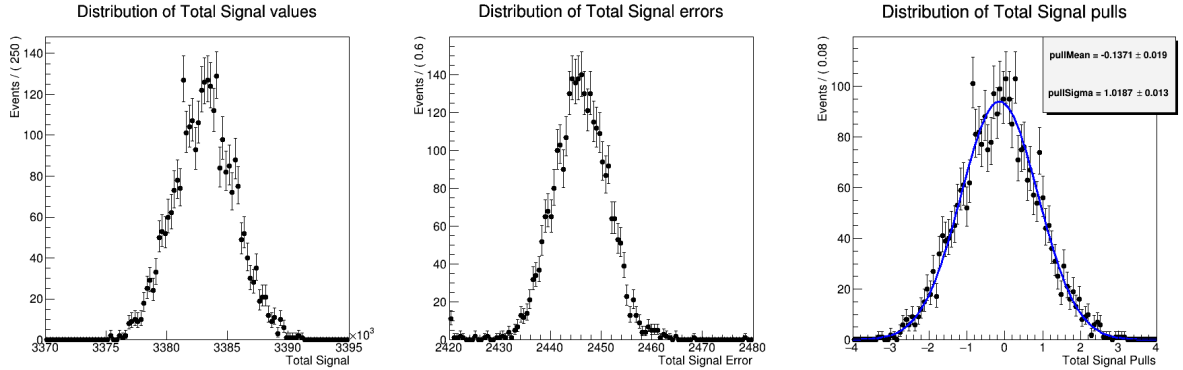


Figure (77) Toy MC fits of pseudo-data showing the Total Signal yield (left), Total Signal yield errors (center) and the pull distribution of the Total Signal (right).

729 6.5 Λ_c and FEI efficiency

730 The efficiency in reconstructing the Λ_c baryon after correctly tagging the charged B meson,
 731 is as usual estimated as the ratio:

$$\frac{N_{recSig}(B_{tag}, \Lambda_c)}{N_{recSig}(B_{tag}^{sig})} \quad (10)$$

732 where $N_{recSig}(B_{tag}, \Lambda_c)$ are the yields of reconstructed signal from the two dimensional fits
 733 (reported in Table 11) and $N_{recSig}(B_{tag}^{sig})$ are the yields of correctly reconstructed signal in
 734 a fit of B mesons tagged in events where one of the two mesons decayed hadronically and
 735 inclusively into a Λ_c baryon (see Fig 39). This ratio was calculated upon six streams of
 736 Monte Carlo simulated data.

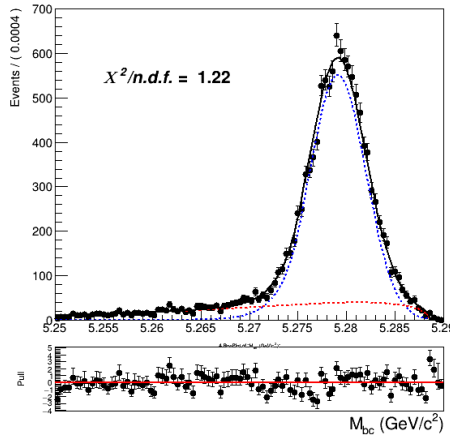


Figure (78) Fit of tagged B mesons in the "signal events" sample

From this and the results listed in Sec. 6.2 the efficiency to reconstruct Λ_c is obtained :

$$\epsilon_{\Lambda_c} = \frac{N_{recSig}(B_{tag}, \Lambda_c)}{N_{recSig}(B_{tag})} = 39.84 \pm 1.77\%$$

The yields from the fit shown in Fig. 78) are then used to calculate the FEI tag-side efficiency for signal events, the yields from the fit of charged B_{tag} shown in Fig. 74a can be used to calculate the hadronic tag-side efficiency in the generic B^+B^- events case.

The ratio between the two efficiencies is calculated: $\frac{\epsilon_{FEI,sig}^+}{\epsilon_{FEI}^+} = 0.973 \pm 0.009$

744

6.6 Studies of Systematic Effects

In Table 2 the systematic uncertainties of the various considered sources are summarized. Their individual calculation is outlined in the subsequent subsections

source	%
Continuum modeling	0.04
Crossfeed fraction	0.13
$\epsilon_{FEI,sig}^+/\epsilon_{FEI}^+$	0.01
ϵ_{Λ_c}	0.05
Fit bias	0.05
Total	0.15

Table (12) Systematic uncertainties in the determination of the $B^- \rightarrow \bar{\Lambda}_c^- X$ branching fractions in %.

6.7 Continuum background modeling

As already done in the case of charged flavor-correlated decays, to estimate the systematic uncertainty deriving from statistical uncertainties two-dimensional fits were performed where the parameters' values have been varied by their uncertainties (once with +err and then with -err). Whereas the impact of statistical uncertainties in the case of the B_{tag} was estimated varying the nominal number of events described with the histogram PDF by Poissonian variation.

Exemplary, fits used to estimate the impact of these uncertainties are shown here in Figures 79 - 80. Mean deviation values are then obtained for both the two-dimensional fit and the B_{tag} fit.

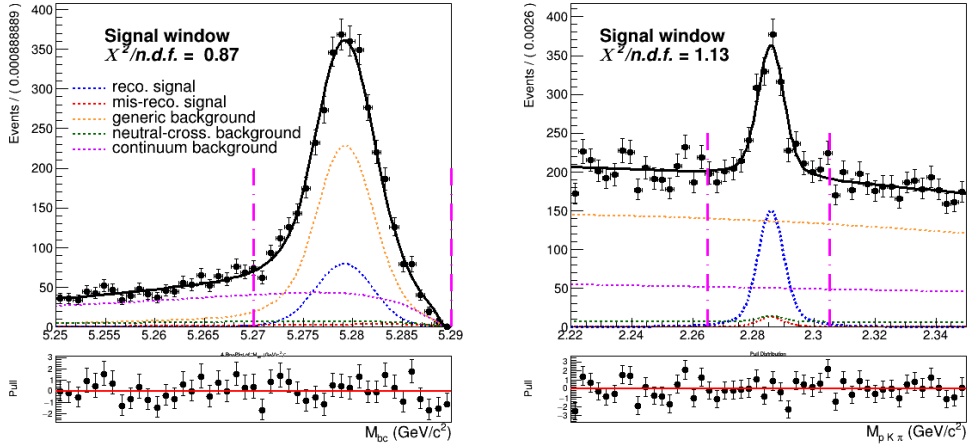


Figure (79) Signal window projections of a two dimensional fit on Monte Carlo simulated data where the shaping parameters were varied of their uncertainties.

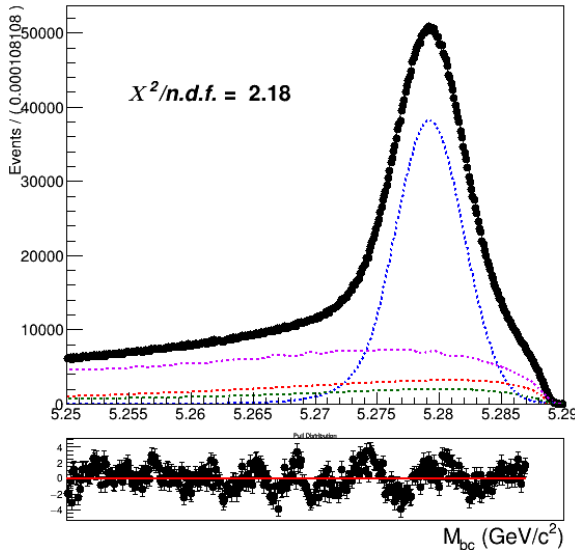


Figure (80) Fit of tagged B meson candidates on Monte Carlo simulated data where the shaping parameters were varied of their uncertainties.

Fit	$-\sigma$	$+\sigma$	$\pm\bar{\sigma}$
2D	21	22	22
B_{tag}	5800	5800	5800

759 The estimated systematic uncertainty on Br value from this source is 0.04%.

760 The continuum suppression cut is found to reject about 68% of the continuum back-
761 ground in data, whereas it rejects 64% of the continuum background in MC (66.5% in
762 on-resonance MC). This means that in data one can expect about 1.4% less continuum

background events. The statistical uncertainty on this fraction of events can be also be taken into account as systematics. But again, as already seen in the case of charged flavor-correlated decays, the statistical uncertainty on the on-resonance continuum background events in MC originates a much larger systematic uncertainty: the relative systematic uncertainty deriving from the different impact on data of the continuum suppression would account for just 0.004% on the BR value (one order of magnitude smaller than systematics deriving from the statistical uncertainties). This second source is again consequently neglected.

6.8 Crossfeed background modeling

This source of systematic uncertainty is again estimated performing the fits varying the parameters of the Crossfeed PDFs by their uncertainties (see the table below for the deviations in terms of signal yields). The resulting absolute systematic uncertainty is about 0.003% on the BR value, which is negligible compared to the other systematic effectes.

Fit	$-\sigma$	$+\sigma$	$\pm\bar{\sigma}$
2D	2	1	2
B_{tag}	1500	1100	1300

Table (13) Offsets on the signal yields obtained varying the parameters of crossfeed background PDFs within their uncertainties in the two dimensional and B_{tag} fit and mean deviations reported in the last column.

6.9 Crossfeed ratio

As already done for the charged flavor-correlated decays, the systematic uncertainty on the crossfeed/misreconstructed events' ratio is studied considering a plausible discrepancy of this value up to 20% between Monte Carlo and data (the procedure adopted is the same as illustrated in Sec. 4.9. (will check with $\pm 5\%$, $\pm 10\%$)

Fit	$-\sigma$	$+\sigma$	$\pm\bar{\sigma}$
2D	77	66	72
B_{tag}	9600	16200	12900

Table (14) Offsets on the signal yields obtained varying of $\pm 20\%$ the crossfeed/misreconstructed ratio in the two dimensional and B_{tag} fit and mean deviations reported in the last column.

The estimated systematic uncertainty on Br value from this source is 0.13%.

783 **6.10 Efficiencies**

784 The ratio between the two FEI efficiencies is: $\frac{\epsilon_{FEI,sig}^+}{\epsilon_{FEI}^+} = 0.973 \pm 0.009$

785 The uncertainty on this value originates a systematic uncertainty of 0.01% on the Br
786 value. The Λ_c reconstruction efficiency is determined to be $\epsilon_{\Lambda_c} = 39.84 \pm 1.77\%$. When
787 propagating its uncertainty, a systematic error of 0.07% on the Br value is calculated.

788 **6.11 Fit biases**

789 The small bias on the reconstructed signal seen in the two-dimensional fit model produces
790 a not negligible systematic uncertainty on the branching fraction. The discrepancy in the
791 amount of the total signal estimated by the B_{tag} fit needs to be included as well in the
792 systematic effects. Propagating the two sources of systematics in the branching fraction
793 calculation results in an additional 0.05% uncertainty on the branching fraction value.

794 **6.12 Measured $B^+ \rightarrow \Lambda_c^+$ inclusive Branching Fraction**

795 Using the results from the two dimensional fit performed on stream 5 and with all the
796 needed factors known, it's possible to examine the agreement between the the branching
797 ratio value used in MC generation and the measured one. Using the expected yields for
798 the two-dimensional fit on stream5 and the B_{tag} fit performed only on signal events, the
799 measured value is $(1.20 \pm 0.07^{stat.})\%$. Instead from the fit result on stream5 for the
800 two-dimensional fit and the result for the B_{tag} fit shown in Fig. 76, the measured value is
801 $(1.19 \pm 0.10^{stat.} \pm 0.15^{syst.})\%$.

802 The two measured values using Monte Carlo simulated data agree with each other
803 within statistical uncertainties as well as with the value set in the Belle MC: 1.22%.
804 Moreover as in the charged flavor-correlated decays the precision obtained on Monte Carlo
805 simulated data is improved by factors compared to the branching fraction measured by
806 BaBar experiment (see [?]).

807 **Appendices**

808 **.1 $B^- \rightarrow \Lambda_c^+$ decays: additional plots**

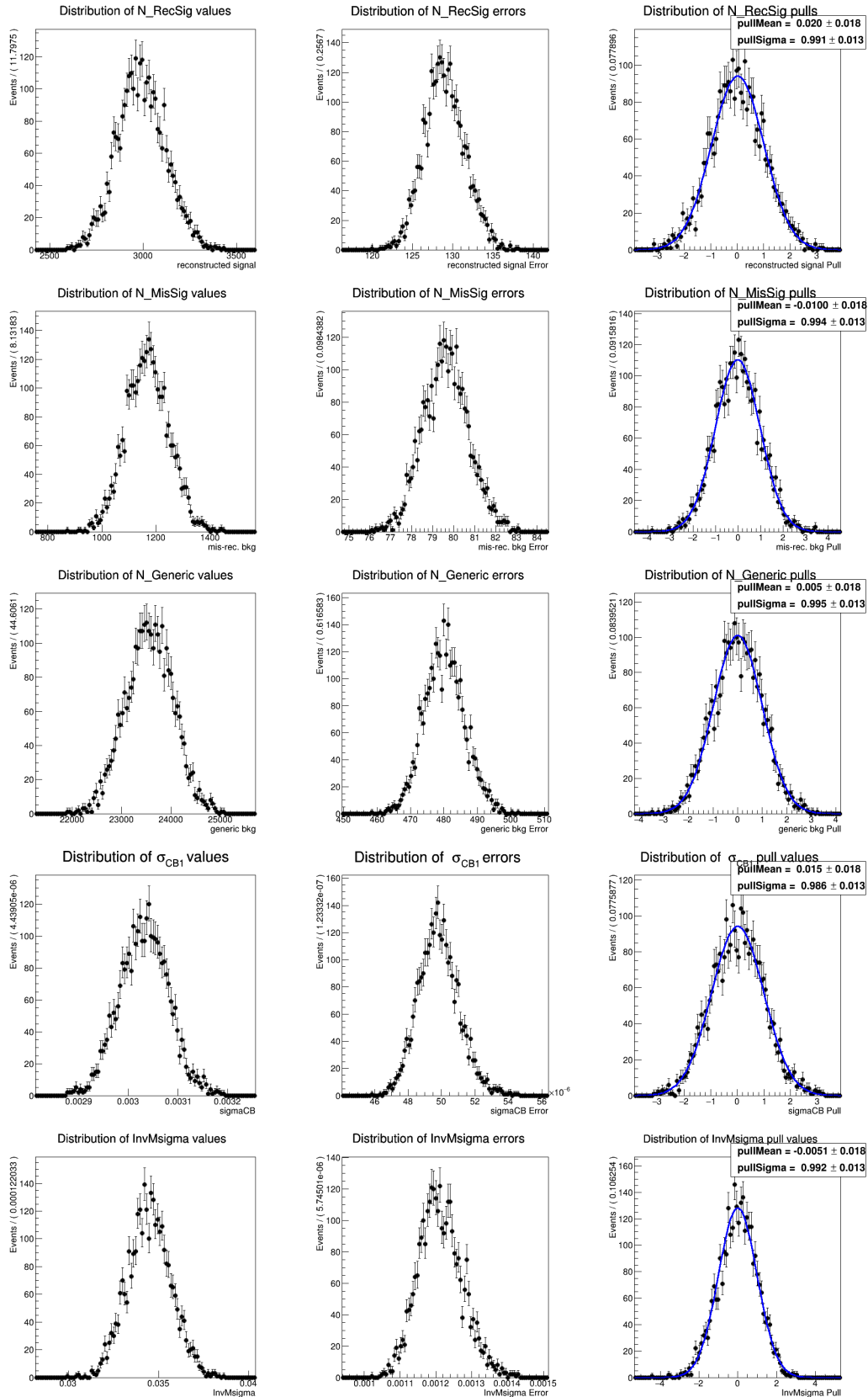


Figure (81) Toy MC study for the two dimensional fit model described in Sec. 4.2

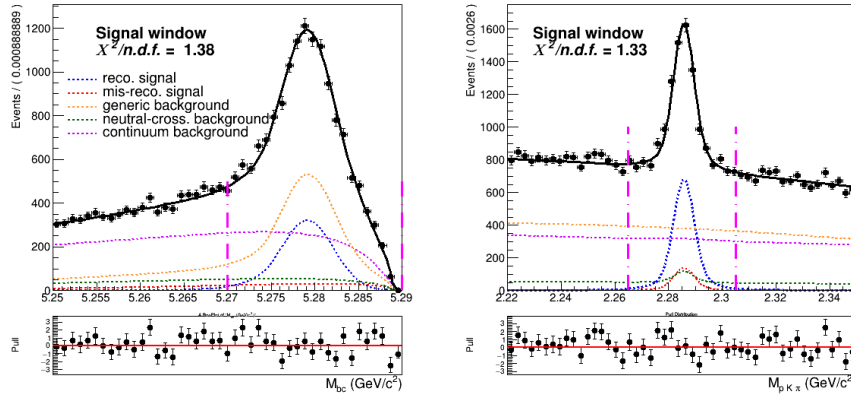


Figure (82) Signal region ($2.22 < M(pK\pi) < 2.35 \text{ GeV}/c^2$ and $5.27 < M_{bc} < 5.29 \text{ GeV}/c^2$) projections pf the dimensional fit on stream 0 Monte Carlo simulated data.

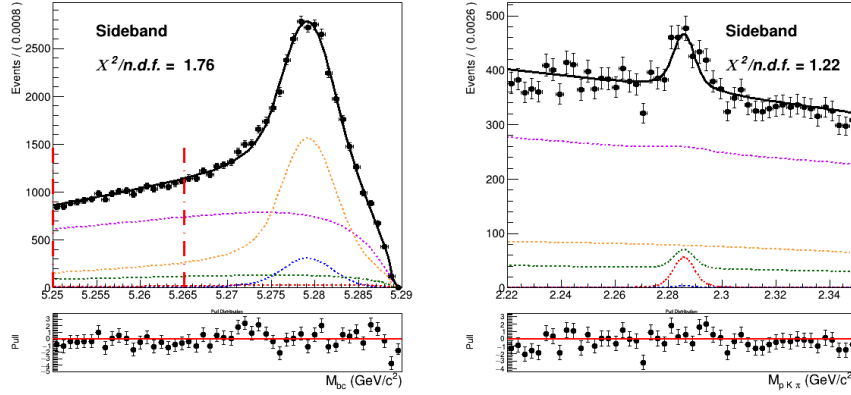


Figure (83) Sideband region of $5.25 < M_{bc} < 5.265 \text{ GeV}/c^2$ projection of the two dimensional fit on stream 0 Monte Carlo simulated data.

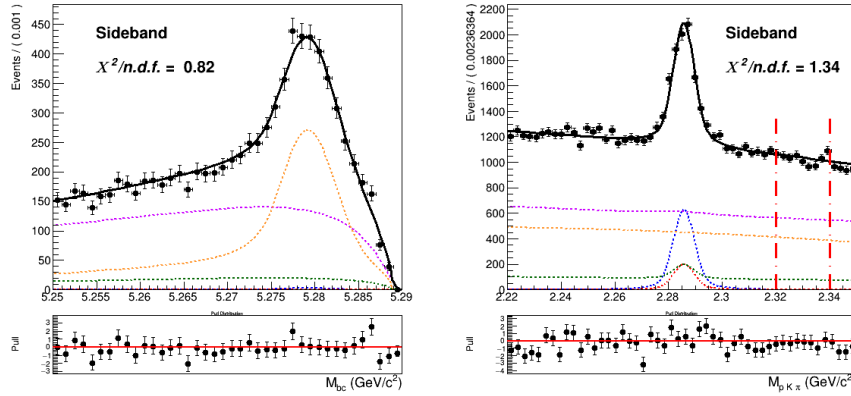


Figure (84) Sideband region of $2.22 < M(pK\pi) < 2.35 \text{ GeV}/c^2$ projection of the two dimensional fit on stream 0 Monte Carlo simulated data.

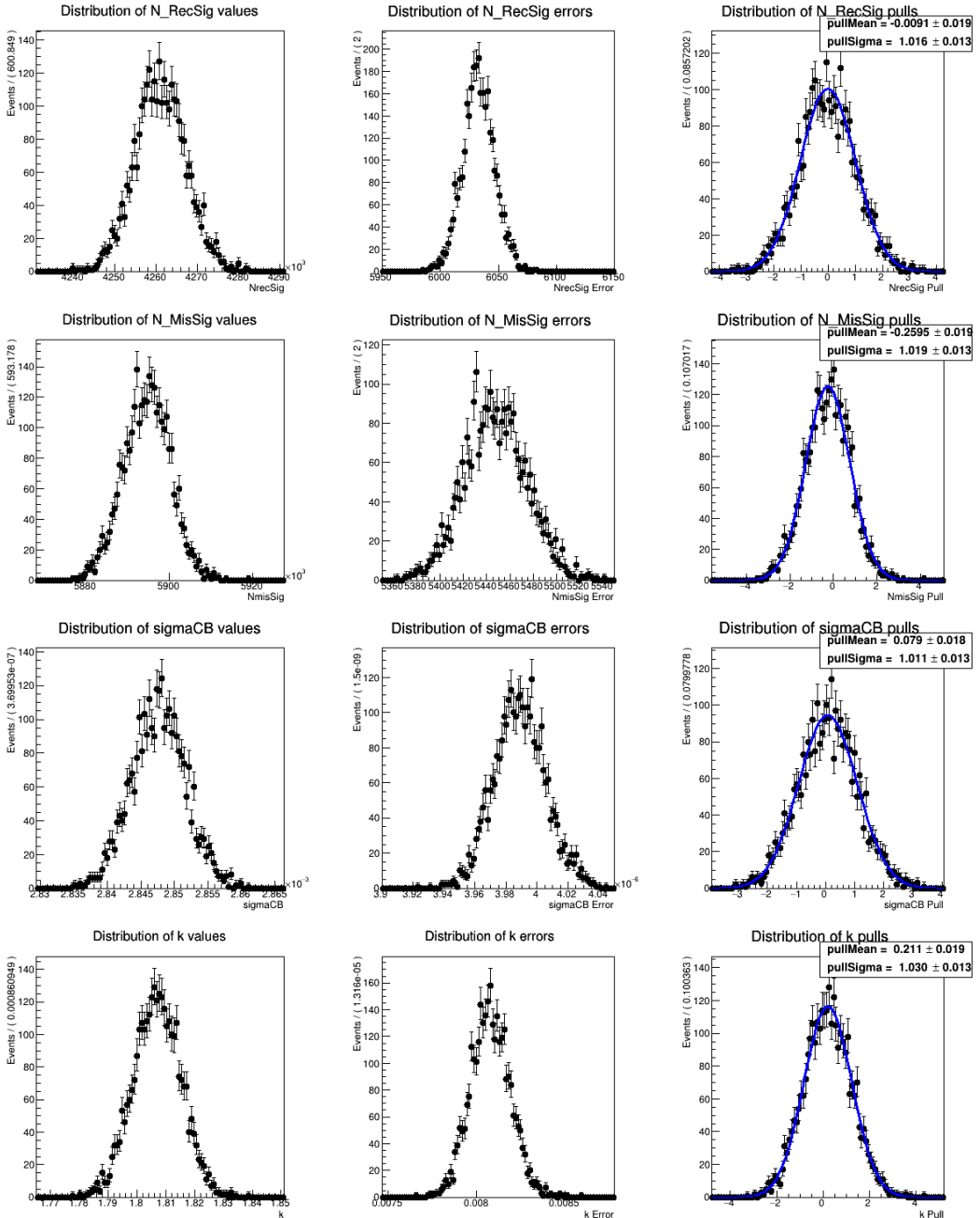


Figure (85) Toy MC study for the B_{tag} fit model described in Sec. 4.4

809 .2 $B^- \rightarrow D^0$ decays: additional plots

810 Figures 86-88 show the projections of signal regions and sidebands in M_{bc} and in the D^0
 811 invariant mass of the two dimensional fit on stream 0.

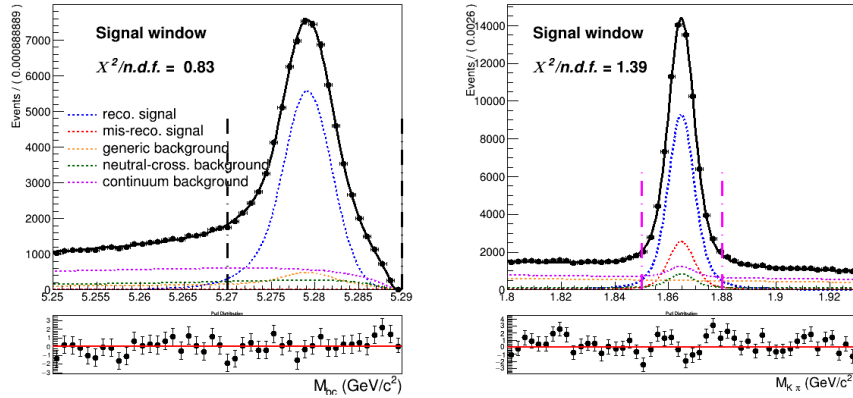


Figure (86) Signal region ($1.85 < M(\pi K) < 1.88 \text{ GeV}/c^2$ and $5.27 < M_{bc} < 5.29 \text{ GeV}/c^2$) projections of the two dimensional fit on stream0 (Fig. 49).

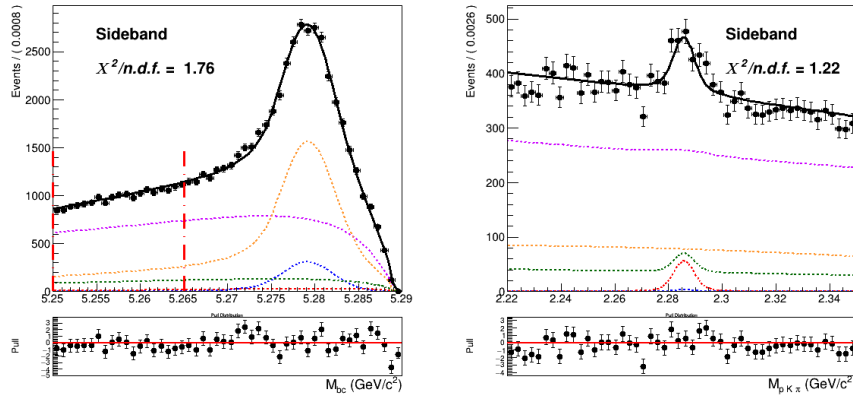


Figure (87) Sideband region of $5.25 < M_{bc} < 5.265 \text{ GeV}/c^2$ projection in $M(\pi K)$ of the two dimensional fit on stream 0.

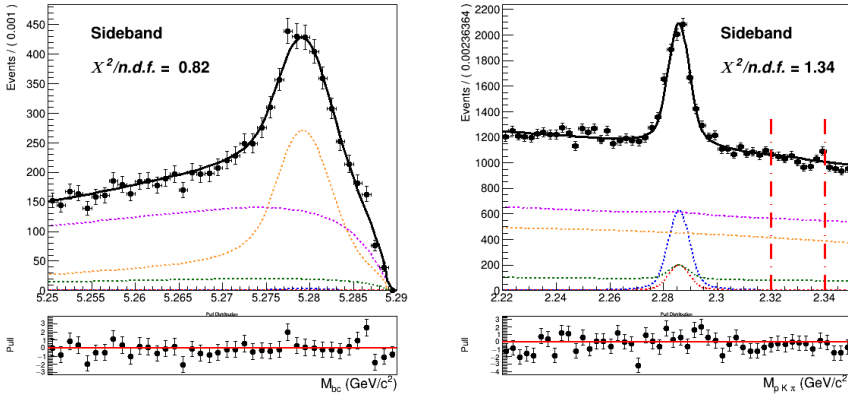


Figure (88) Sideband region of $1.8 < M(\pi K) < 1.84 \text{ GeV}/c^2$ projection in M_{bc} of the two dimensional fit on stream 0.

812 Figs. 89 to 91 show the projections in M_{bc} and in the D^0 invariant mass of the two
813 dimensional fit on data.

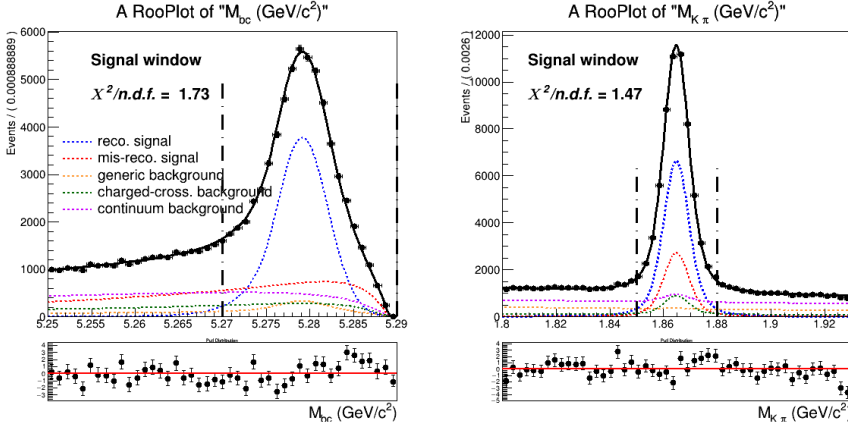


Figure (89) Signal region ($1.85 < M(\pi K) < 1.88 \text{ GeV}/c^2$ and $5.27 < M_{bc} < 5.29 \text{ GeV}/c^2$) projections of the two dimensional fit on data described in Sec. 5.6

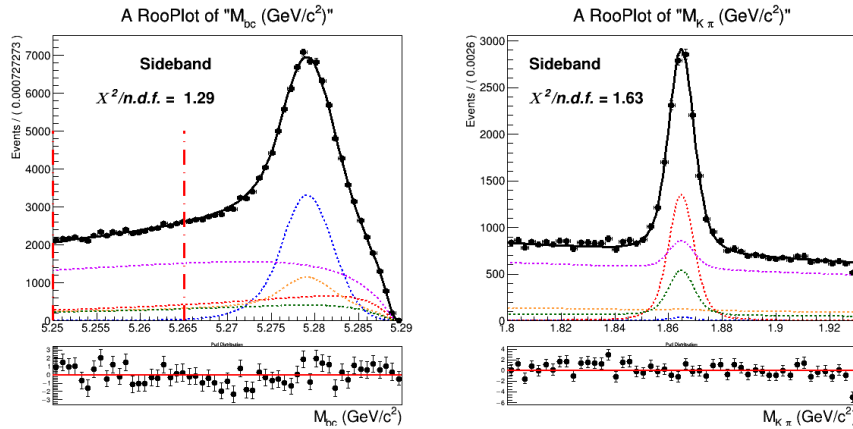


Figure (90) Sideband region of $5.25 < M_{bc} < 5.265 \text{ GeV}/c^2$ projection in $M(\pi K)$ of the two dimensional fit on data

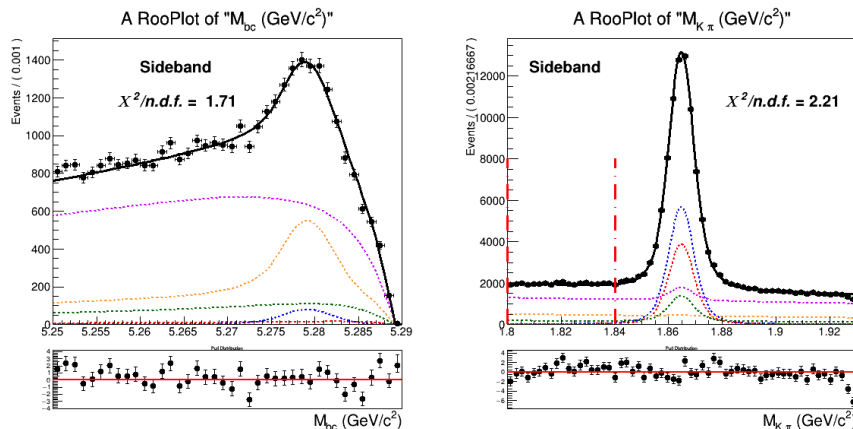


Figure (91) Sideband region of $1.8 < M(\pi K) < 1.84 \text{ GeV}/c^2$ projection in M_{bc} of the two dimensional fit on data.

.3 $B^- \rightarrow \bar{\Lambda}_c^-$ decays: additional plots

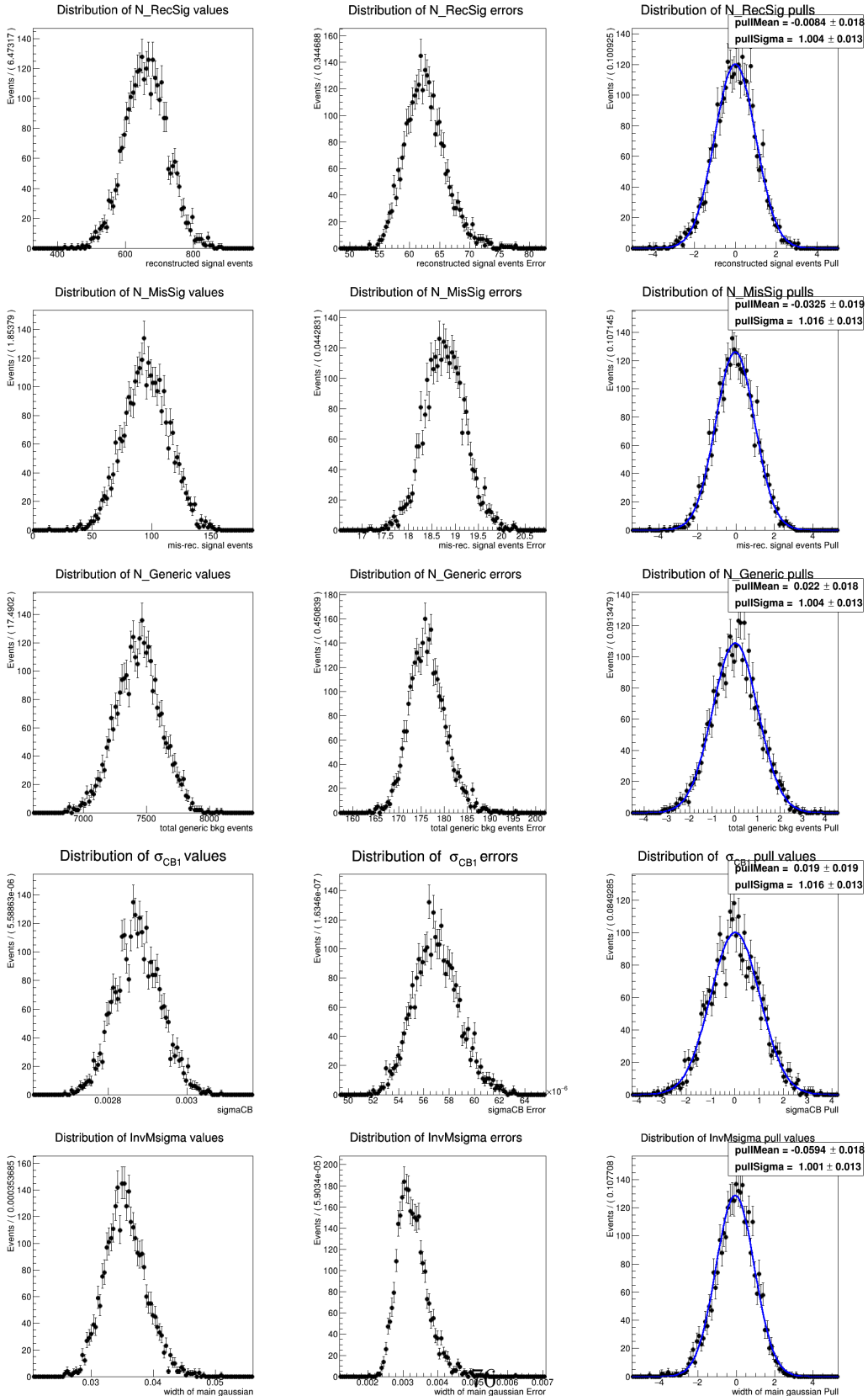


Figure (92) Toy MC study for the two dimensional fit model described in Sec. 6.2

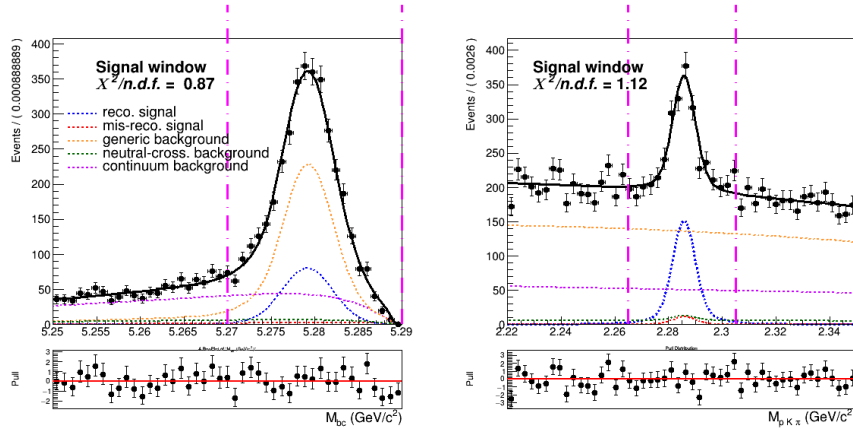


Figure (93) Signal region ($2.22 < M(pK\pi) < 2.35 \text{ GeV}/c^2$ and $5.27 < M_{bc} < 5.29 \text{ GeV}/c^2$) projections of the dimensional fit on stream 0 Monte Carlo simulated data.

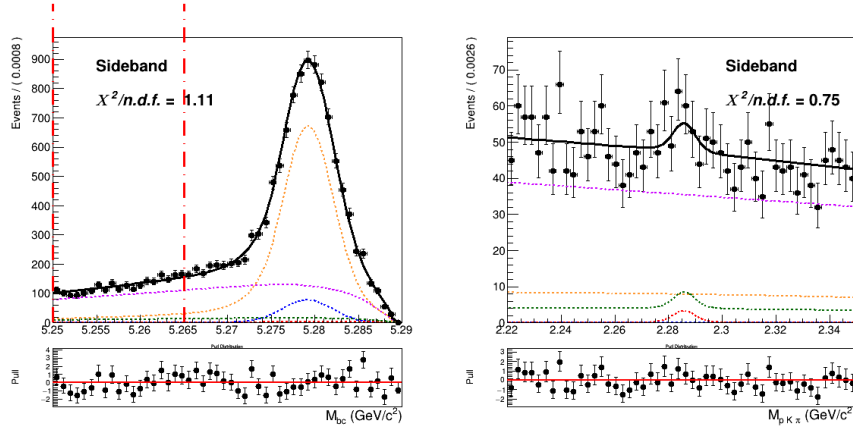


Figure (94) Sideband region of $5.25 < M_{bc} < 5.265 \text{ GeV}/c^2$ projection of the two dimensional fit on stream 0 Monte Carlo simulated data.

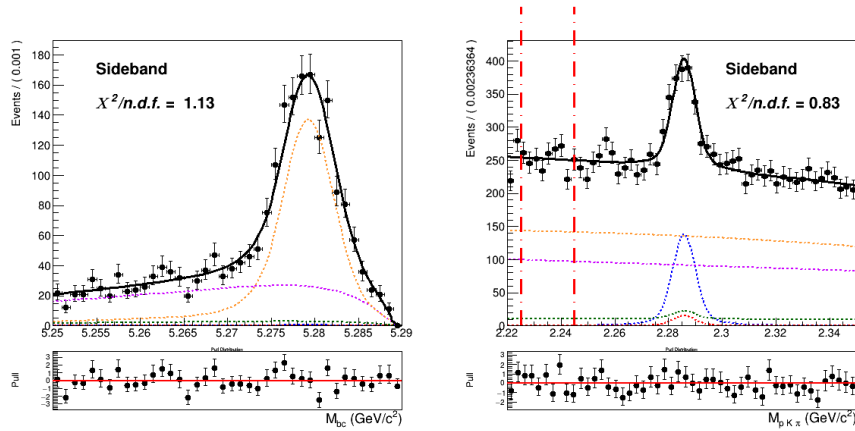


Figure (95) Sideband region of $2.22 < M(pK\pi) < 2.35 \text{ GeV}/c^2$ projection of the two dimensional fit on stream 0 Monte Carlo simulated data.

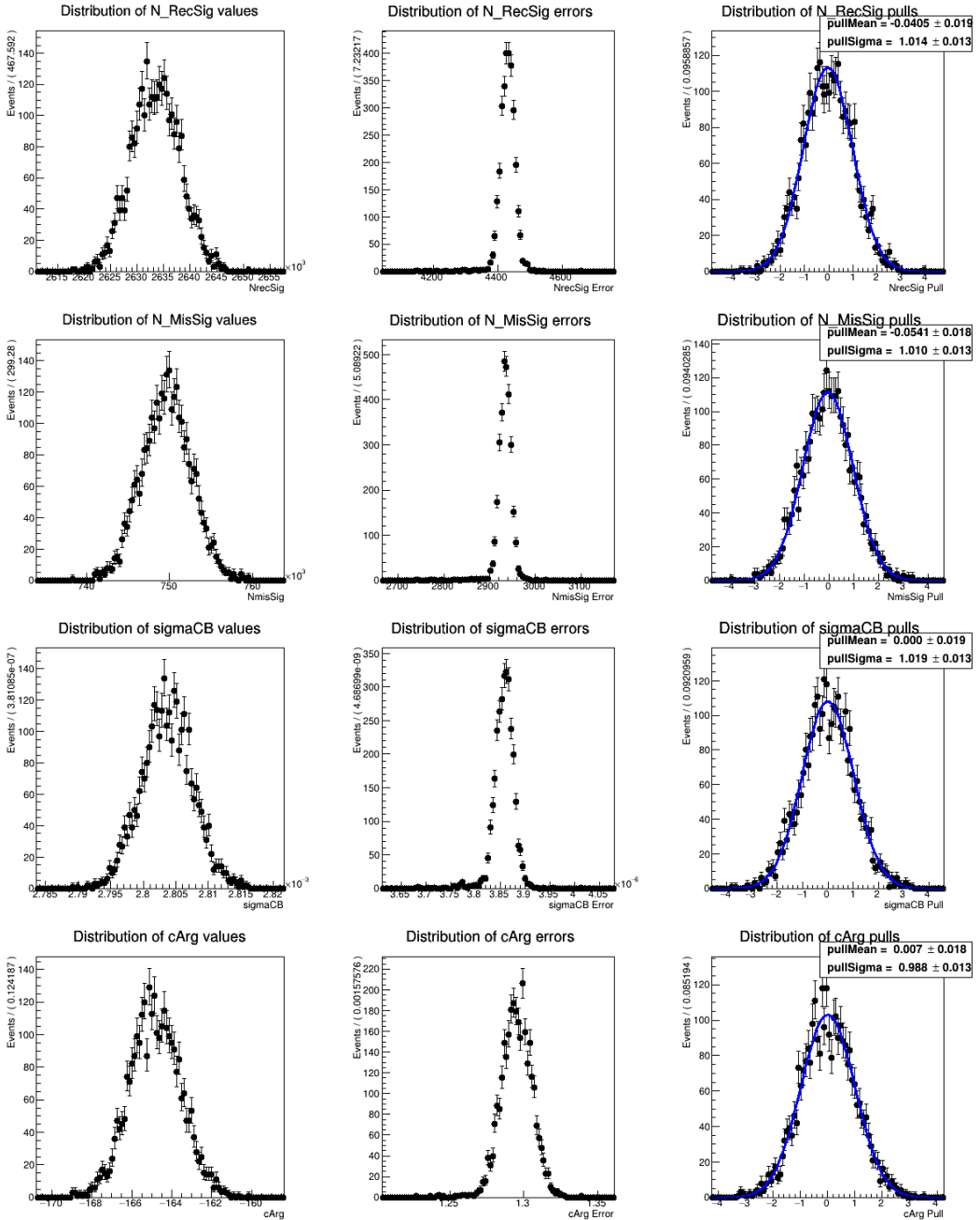


Figure (96) Toy MC study for the B_{tag} fit model described in Sec. 6.4